2014

Investigation of negative moment reinforcing steel in pre-cast pre-stressed concrete beam bridge decks

Sameera Tharanga Jayathilaka
Iowa State University

Investigation of negative moment reinforcing steel in pre-cast pre-stressed concrete beam bridge decks

by

Sameera Tharanga Jayathilaka

A thesis submitted to the graduate faculty

in partial fulfillment of the requirements for the degree of

MASTER OF SCIENCE

Major: Civil Engineering (Structural Engineering)

Program of Study Committee:
Brent M. Phares, Major Professor
Terry J. Wipf
Kejin Wang

Iowa State University

Ames, Iowa

2014

TABLE OF CONTENTS

LIST OF FIGURES

LIST OF TABLES

ACKNOWLEDGEMENT

Firstly I would like to thank Dr. Brent M. Phares, my major Professor. I appreciate the freedom, guidance and support which he has given me throughout the course of this research. I would also like to thank Dr. Terry J. Wipf and Dr. Kejin Wang for being a part of my master's committee. I would like to thank Dr. Lowell Greimann, my project supervisor, and his wife Jennie Greimann, for the endless hours of patience and help. Without them this work would have been far from complete. I am grateful to Bridge Engineering Center (BEC) and Iowa DOT (Department of Transportation) which have funded my project and also its several engineers, who have helped in various aspects of the project. I would also like to acknowledge the Department of Civil Construction and Environmental Engineering of Iowa State University and all its professors for molding my mind into what it is today. Finally I would like to thank my family, friends for all their help, encouragement and their valuable company. Thank You.

ABSTRACT

Multi-span Pre-tensioned Pre-stressed Concrete Beam (PPCB) bridges made continuous usually experience a negative live load moment region over the intermediate support. Conventional thinking dictates that sufficient reinforcement must be provided in this region to satisfy the strength and serviceability requirements associated with the tensile stresses in the deck. The AASHTO LRFD bridge design manual recommends negative moment reinforcement be extended beyond the inflection point. Based upon satisfactory previous performance and judgment, the Iowa DOT OBS currently terminates b2 reinforcement at 1/8 of the span length. Although the Iowa DOT policy results in approximately 50% shorter b2 reinforcement than the AASHTO LRFD specifications, the Iowa DOT has not experienced any significant deck cracking over the intermediate supports.

The primary objective of this project is to investigate the Iowa DOT OBS policy regarding the required amount of b2 reinforcement to provide the continuity over bridge deck. Other parameters, such as termination length, termination pattern and effects of the secondary moments were also studied. Live load tests on five bridges were carried out. The data were used to calibrate three-dimensional finite element models of two bridges. A parametric study was conducted on the bridges with uncracked deck, a cracked deck, and a cracked deck with cracked diaphragm. The general conclusions were as follows.

- The parametric study results show an increased area of the b2 reinforcement slightly reduces the strain over the pier. Whereas, increased length and staggered reinforcement pattern slightly reduce the strains of the deck at 1/8 of the span length.
- Secondary moments affect the behavior in the negative moment region. The impact may be significant enough that the deck over piers may never experience a tensile stress.
- Finite element results suggested that the transverse field cracks over the pier and at 1/8 of the span length, are mainly due to the deck shrinkage.
- Bridges with higher skew angles have lower strains over the intermediate supports.

CHAPTER 1. INTRODUCTION

1.1 Background

For design, multi-span Pre-tensioned Pre-stressed Concrete Beam (PPCB) bridges are usually assumed to experience two different stages of behavior. During the first stage, the PPCB girders are placed on supports, and are assumed to behave as a simply-supported span to resist the self-weight of the structure. After the concrete deck is placed and fully cured, the bridge moves to the second stage, during which it behaves like a fully continuous structure over the intermediate support to resist the live loads and superimposed dead loads of the post deck construction.

During the second stage, the structure will experience negative moments over the intermediate supports and as a result reinforcement must be provided to satisfy the strength and serviceability requirements within the negative moment region. According to the Iowa Department of Transportation (DOT) Office of Bridges and Structures (OBS) bridge design manual, continuous longitudinal reinforcement (b1 reinforcement) is provided over the top and bottom of the entire deck. In addition to the b1 reinforcement, negative moment reinforcement (b2 reinforcement) is provided for strength over the intermediate supports and to control the cracks due to negative moments.

The amount of b2 reinforcement is designed based on the negative moments at the intermediate supports due to the live load and superimposed dead load. However, current OBS policy regarding the termination of the b2 reinforcement is, in many cases, based upon anecdotal evidence of previous satisfactory previous performance. As per Iowa DOT OBS bridge design manual 5.4.2.4.1.7, the b2 reinforcement is terminated at 1/8 of the span length, which, perhaps not coincidentally, is also generally the location of allowable deck construction joints. However, AASHTO 5.14.1.4.8 states that, “Longitudinal reinforcement used for the negative moment connection over an interior pier shall be anchored in regions of the slab that are in compression at strength limit state and shall satisfy the requirements of AASHTO 5.11.1.2.3. The termination of this reinforcement shall be staggered.” [1]. AASHTO 5.11.1.2.3 further describes the development length of b2 reinforcement as, “At least one third of the total reinforcement provided for the negative moment at a support shall have an embedment length beyond the point of inflection not

less than, (1) The effective depth of the member (2) 12.0 times of the nominal diameter of bar (3) 0.0625 times the clear span" [1].

The distance to the inflection point of a two-span continuous beam under uniformly distributed load is about 1/4 of the span, which is about twice the length prescribed by the Iowa DOT. Although the Iowa DOT policy results in shorter b2 reinforcement than the AASHTO LRFD specifications, the Iowa DOT has not experienced any significant deck cracking in the negative moment regions of PPCB bridges.

1.2 Objectives of the Research

Because the Iowa DOT OBS has observed satisfactory historical performance of PPCB bridges there is a desire to provide research evidence as to appropriateness of current OBS policy. Further, there is a desire to potentially modify current OBS policy if one is justified. The objectives of this work are to:

- Investigate the Iowa DOT OBS policy regarding the required amount of b2 reinforcement to provide the continuity over bridge deck.
- Investigate OBS policy regarding the termination length of b2 reinforcement at the 1/8 span location.
- Investigate the impact of the termination pattern of the b2 reinforcement.
- Investigate the effect of secondary moments on the performance of the PPCB bridges.

1.3 Research Plan

To achieve the research objectives a total of four tasks were undertaken. Each task was molded based on lessons learned from each previous task.

- Task 1 – Information gathering

A literature search was conducted to collect information on the design of negative moment reinforcement for PPCB bridges. The current domestic state-of-the-practice with regard to continuity and associated design of b2 reinforcement and termination were also collected through a web based survey.

- Task 2 – Field test and inspection

Field tests and inspections were conducted on five bridges with diverse geometric properties as width, length, skew angle, girder type, number of spans and number of girders

to study the actual behavior of typical PPCBs. Strain gauges were installed on the deck and girders at several transverse sections. A known truck then crossed the bridge along several longitudinal paths, generating longitudinal strain profiles. Strain profiles were used to study general bridge performance and, later, to calibrate the analytical models.

- Task 3 – Analytical modeling

Based on the field test observations, two bridges were selected for finite element modeling. Finite element models were highly discretized in such a way that the behavior of an individual b2 reinforcement could be evaluated. Finite element models calibrated from the live load were then used to conduct a parametric study.

- Task 4 – Reporting the recommendations

A final report was developed to present all the observations, conclusions and recommendations on the design of negative bending moment b2 reinforcement of the multi-span continuous PPCB bridges.

CHAPTER 2. LITERATURE REVIEW

2.1 Introduction to Transverse Cracks on Bridge Decks

Most concrete bridge decks develop transverse cracks at an early stage. According to the literature, the predominant mode of deck cracking is transverse cracking, which usually occurs over the transverse reinforcement. It has been estimated that more than 100,000 bridges in the United States have transverse cracks on their decks.

These cracks accelerate the corrosion of the reinforcement, especially where deicing chemicals are applied, and then reduce the service life of the structure, while increasing the maintenance costs. Freeze-thaw cycles of water inside the cracks also reduce the service life of the structure.

Although transverse cracks in bridge decks are a concern among designers and researchers, the effects of numerous contributing factors and mitigation procedures are not yet fully understood. The material and mix design, construction practices and environmental conditions and structural design factors are the primary causes of the transverse cracks. Additional factors are listed in Table 1 [2].

Table 1. Cause of transverse cracks on bridge decks [2]

Material and mix design	Construction practices and environmental conditions	Structural design factors
Aggregates	Weather condition and concrete temperature	Girder type, boundary conditions and spacing
Water content	Curing	Shear studs configuration and properties
Cement type	Pour length and sequence	Concrete cover
Cement content	Time of casting	Deck thickness
Water/Cement ratio	Finishing	Reinforcement type, spacing, size and distribution
Concrete strength	Vibration of fresh concrete	Section stiffness
Slump	Construction loads	Vibration and impact characteristics
Air content	Form type	Traffic

2.1.1 Material and Mix Design

Most research work has been conducted on material and mix design to determine why transverse cracks occur on bridge decks. Several researchers found that the aggregates in the concrete lead to deck cracking [3]. Suggestions showed that the larger size of aggregates with high specific gravity and low shrinkage aggregates may minimize the deck cracking.

Babaei et al. [3] suggested the maximum water content as 12 lb/ft^3. Higher cement content induces higher temperature throughout the hydration processes and leads to drying shrinkage and thereby cracks in the concrete deck. French et al. [4] and Babaei et al. [3] provided an acceptable cement content range of 22 lb/ft^3 to 28 lb/ft^3 to minimize the concrete deck cracking. Schmitt et al. [5] found that an increase in water content increases deck cracking and recommended to not exceed 27% of both water and cement content of the total concrete volume. Reduction in the water/cement ratio reduces the shrinkage. Schmitt et al. [5] suggested a water/cement ratio of 0.40 to 0.48 to minimize the deck cracking.

The compressive strength of the concrete is another factor that is thought to affect deck cracking. However, there is no general conclusion among the researchers on this factor. Schmitt et al. [5] observed an increase in deck cracking due to an increase in compressive strength. Krauss et al. [6] proposed to use low early strength concrete to minimize deck cracking. The slump of a concrete mix is also a factor which leads to concrete cracking. Among different conclusions on the effect of the slump, most of the researchers noticed that the higher the slump level, the more deck cracks [7].

Cheng et al. [8] and Schmitt et al. [5] observed deck cracking can be reduced by increasing the air content of the concrete. Schmitt et al. [5] proposed to use at least 6% air content. Similarly, Babaei et al. [3] proposed 5.5% - 6.0% air content to minimize cracking.

2.1.2 Construction Practices and Environmental Conditions

The temperature of the concrete is an important factor that affects cracking. After concrete placement, the temperature of the deck increases due to hydration. However, the temperature of the girders remains almost unchanged. The larger the temperature difference between the deck and the girders the greater the chance for deck cracking.

French et al. [4] suggested 40°F as the minimum temperature and 90°F as the maximum temperature for concrete deck placement. Babaei et al. [3] recommended to maintain the temperature difference between the deck and girders below 22°F for at least 24 hours to minimize the deck cracking.

High temperature with low humidity and high wind speed increase the evaporation of water from plastic concrete, which lead to the formation of plastic shrinkage cracks. Several researchers recommended that special attention be given when the evaporation rate exceeds 0.2 lb/ft^2/h for normal concrete and 0.1 lb/ft^2/h for concrete with low water/cement ratios [6].

Several studies showed that concrete placement length and sequence may have some effect on deck cracking. Kochanski et al. [9] suggested that concrete pour rates greater than 0.6 span length/hour minimize the cracking of the concrete deck. Based on an analytical study Issa [7] concluded that placing concrete first in the positive moment region will reduce the deck cracking. Ramey et al. [10] recommended a detailed procedure to minimize cracking.

Some studies illustrate the effect of form type on the deck cracking. Frosch et al. [11] showed that stay-in-place forms increase deck cracking and suggested other form types for deck construction.

2.1.3 Structural Design Factors

Very little research has been carried out on the effects of the structural design factors such as girder type, shear studs configuration, deck thickness, reinforcement size, type and vibrations on deck cracking.

Concrete has a lower thermal conductivity than steel. Therefore, bridges with steel girders experience more deck cracking than the concrete girder bridges due to the high temperature gradients [6]. Composite action is achieved through shear studs between the deck and the girders. However, these shear studs restrain the shrinkage of the concrete deck, which leads to cracking of the concrete deck. Although Krauss et al. [6] did not give any recommendations, they stated that the girder restraint and shear stud type can cause a

significant amount of cracking. French et al. [4] recommended fewer studs with smaller row length, but specific guidelines were not given.

Higher deck thicknesses decrease transverse cracking. This may be due to the increased deck/girder stiffness ratio [2]. Konchanski et al. [9] recommended to use 8.5in. to 9in. decks, whereas French et al. [4] suggested that deck thicknesses greater than 6.25in. perform well.

Several researchers have observed that reinforcement size, type and distribution affect deck concrete cracking. With the increase of bar size cracking will increase. Several researchers suggested the use of No.5 reinforcement as the maximum reinforcement size for the longitudinal reinforcement [9] [10]. However, Karuss et al. [6] recommended to use No. 4 bars as the largest reinforcement with 6in. spacing to minimize deck cracking. Ramey et al. [10] gave detailed guide lines for reinforcement detailing to decrease cracking tendency.

Researchers illustrated that the vibration and impact characteristics of the live loads on the super-structure effect deck cracking. Babaei et al. [3] suggested the use of vibrations with low amplitude and frequency to compact the concrete to minimize the deck cracking. Mckeel [12] observed that bridges carrying a large number of trucks at high speeds experience more deck cracking.

2.2 Transverse Cracks at the Intermediate Supports of PPCB Bridges

According to the literature, two primary concepts can be found related to the design of the reinforcement at the intermediate supports of PPCB bridges: design of continuity reinforcement at the bottom of the connection and design of continuity reinforcement at the top of the connection.

2.2.1 Design of the Reinforcement at the Bottom of the Continuity Connection

According to the Michael D McDonagh et al. [13], time dependent moments due to creep of the girders and differential shrinkage between the deck and the girders play an important role on the design of the reinforcement at the bottom of the continuity connection. Creep of the girders induces a positive secondary moment, whereas differential shrinkage generates a negative secondary moment at the bottom of the continuity

connection. A PCA report [14] showed that the positive secondary moments are usually greater than the negative secondary moments. Further, based on an experimental and analytical research on the behavior of joint less integral abutment bridges, Ralph G Oesterle et al. [15] concluded that the negative moment induced by the live load can be significantly reduced by the time dependent load effects.

Unfortunately, the time dependent secondary moments mentioned above cannot be calculated reliably. Several methods have been proposed to calculate these secondary moments. The Portland Cement Association (PCA) method [14] is the most popular method. Construction Technology Laboratory (CTL) method, NCHRP Report 322 guidelines and RMCALC software [13] by Washington DOT are also available to estimate the secondary moments..

The positive moment continuity connection varies from state to state. Makarand Hastak et al [16] conducted research to study the different types of positive moment connections used around the country and also to identify the possible potential problems associated with those connections. Charles D Newhouse [17] conducted research which involved a comparison of different methods used to calculate the secondary moments. The results were used to develop three different types of continuity connection details at the bottom of the intermediate support. Recently, Chebole [18] conducted research to investigate the accuracy of the calculation methods of the secondary moments. A program was developed to enhance the estimation accuracy of the secondary moments. Hyo-Gyoung Kwak et al. [19] developed an analytical model to simulate the time dependent effects of creep, shrinkage and concrete cracking of PPCB bridges. The model was calibrated experimentally. Researchers concluded that the positive reinforcing steel at the support has no significant effect on the resulting negative moment.

2.2.2 Design of the Reinforcement at the Top of the Continuity Connection

No research was found that addressed the design of reinforcement at the top of the continuity connection (b2 reinforcement). If fact, no guidelines on the design of reinforcement at the top of the continuity connection are given in the AASHTO LRFD design speciation. Iowa DOT designs the reinforcement by assuming a fully cracked

section as shown in Figure 1. With a detailed design example, W.G Wassef et al. [20] used this same design procedure to calculate the required negative moment reinforcement.

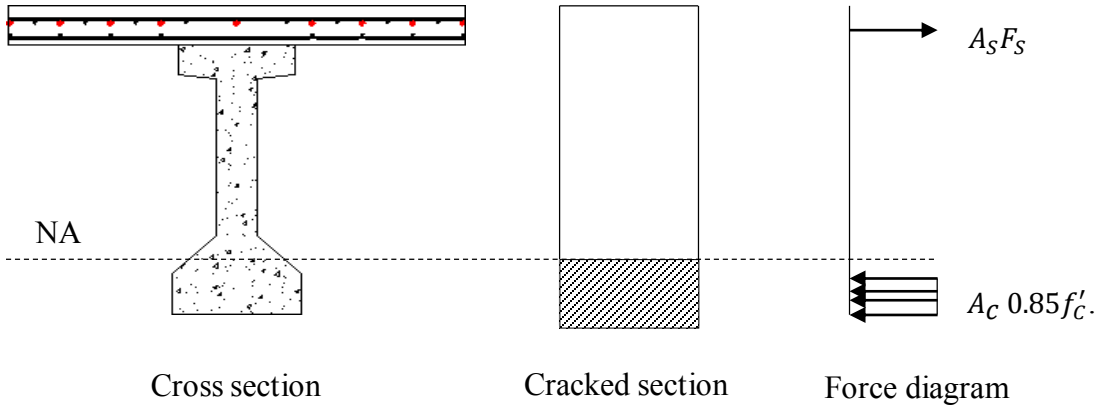

Figure 1. Force diagram at continuity connection

As mentioned in the CHAPTER 1, guidance is given in the AASHTO LRFD specification regarding the termination point and pattern of the b2 reinforcement. However, the Iowa DOT uses reinforcement approximately 50% less than the recommended length, without experiencing significant cracks. In the detailed design example, W.G Wassef et al. [20] do not provide any details regarding the termination of the b2 reinforcement.

2.3 State-of-Practice on Negative Moment Reinforcement Design

The Bridge Engineering Center (BEC) of Iowa State University in cooperation with the Iowa Highway Research Board conducted a web based survey to identify the state-of-practice on continuity considerations and negative moment reinforcement (b2 reinforcement), with emphasis on the design policies and practices associated with designing multi-span PPCB bridges. As a summary, around 45% of respondents assume that adjacent spans act as simple spans for non-composite dead loads and are continuous for composite dead and live loads in the design of the b2 reinforcement for multi-span PPCB bridges. Simple span for all dead loads and continuous for all live loads was assumed by 30% of respondents. Further, 20% respondents assumed simple spans for all loads. Extension of the bottom pre-stressing strands with the girder end embedded into the diaphragm plus additional negative moment reinforcement in the deck were the most commonly used continuity connection details. Different DOTs use various practices to terminate the b2 reinforcement. For example, in addition to the embedment length, North

Carolina DOT uses 1/3 the span for termination of the b2 reinforcement, whereas Kansas DOT uses 1/4 span, both near the point of inflection. Delaware DOT, Nevada DOT and several other DOTs follow the AASHTO LRFD guide lines to terminate the b2 reinforcement (CHAPTER 1). New Mexico DOT uses the lengths as per the CONSPAN bridge design software. Michigan DOT and Pennsylvania DOT use staggered b2 reinforcement pattern to minimize the transverse cracking.

CHAPTER 3. FIELD TEST

3.1 Introduction

Five bridges with different characteristics (Appendix) were selected for the field test as listed in Table 2. These bridges were selected because they have differing numbers of spans, span lengths, widths, skew angles, number of girders and girder types. However, the length of the negative moment b2 reinforcement (Figure 2) is approximately the same. As a result, it was anticipated that the field testing program would allow the research team to investigate the effects of bridge characteristics on the negative bending behavior. It is also worth noting that in addition to allowing one-to-one comparisons the field test results will also be used to calibrate the subsequently described finite element models.

Table 2. Bridge characteristics

Bridge #		1	2	3	4	5
Location	On	C50	I80	Meredith Drive	Mt Pleasant bypass	US20
	Over	US218	US65	I35/80	Big Creek	Whiskey Creek
Spans		2	2	2	3	3
Length / (ft)		277	316	270	215	203
Width / (ft)		47.2	76.5	82	42.5	43.2
Skew / (deg)		24	42	5	36	0
No: of girders		6	11	11	6	6
Type of girders		BTE	BTE	BTD	DM	LXD
Length of b2 / (ft)		35	39	36	30	29

3.2 Instrumentation

During testing strain gauges were installed at two general locations: on the top surface of the bridge deck in the negative bending region and on the girders. To study the effects of the b2 reinforcement and to generally aid in understanding bridge deck behavior, a set of strain gauges was placed on the deck top surface 1 ft inside and 1 ft outside the end

of the b2 reinforcement. Another set of strain gauges was located over the pier, which helped to capture the strain response over the pier.

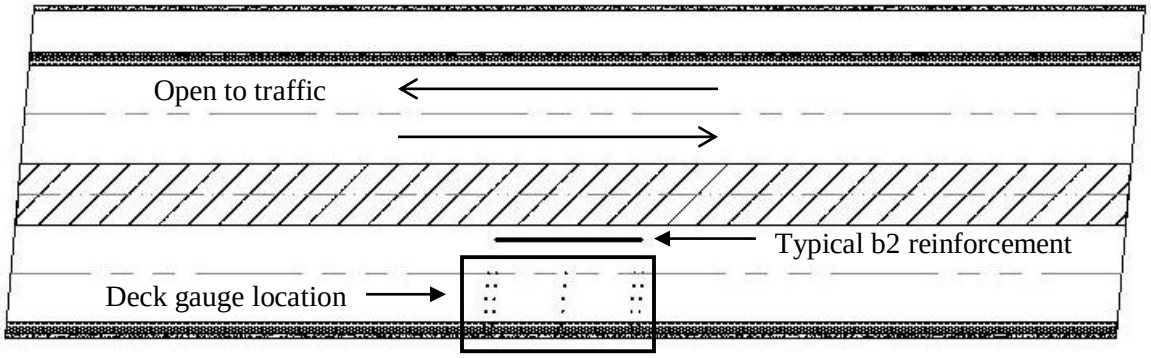

Figure 2. Typical deck gauge installation plan

Figure 3. Strain gauges end of the b2 bar

Figure 4. Cover plate to prevent damage

To investigate the behavior of the principal strains, several rosettes were also installed 1ft inside and 1ft outside at the end of the b2 reinforcement.

Figure 5. Rosette near b2 reinforcement

In addition to the sensors placed on the deck, several gauges were attached to the girders at the mid-span location and near one of the piers. As shown in Figure 6, gauges were attached to both top and bottom flanges.

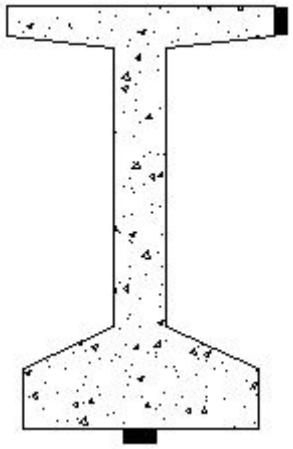

Figure 6. Typical girder gauge location

A summary of the number of deck gauges, girder gauges, dummy gauges and rosettes used in field tests on each bridge is listed in Table 3. Further, details of gauge location for each bridge is shown in Appendix.

Table 3. Summary of gauges

Bridge #	Total gauges attached		Rosettes	Dummy gauges
	On deck	On girders		
1	46	16	8	-
2	43	32	4	-
3	37	28	6	7
4	46	20	8	6
5	55	20	10	4

3.3 Loading of the Bridge

Once all the strain gauges were installed, standard snooper truck provided by the Iowa DOT (Figure 7) crossed the bridge along multiple transverse paths at a crawl speed. Details of the Load Cases (LC) for each bridge test are given in Appendix.

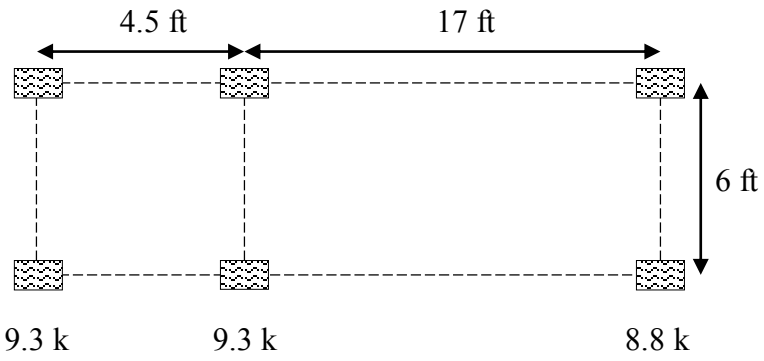

Figure 7. Details of the loading truck

3.4 Longitudinal Strain Profiles of Deck Gauges

According to the strain profiles of the deck gauges (Appendix), almost every gauge on the bridge deck showed an expected strain variation (Figure 8). It was found that the strain gauges at the outside of the b2 reinforcement show a little higher magnitude than the strain magnitude of the gauges in the inside of the b2 reinforcement. Even though the field

tests involved 5 bridges with different properties, the strain profiles of the deck gauges look similar in terms of pattern and sometimes magnitudes. This suggests that the effect of the negative moment b2 reinforcement may not be affected by the properties of the bridges, such as number of spans, span lengths, widths, skew angles, number of girders and girder types.

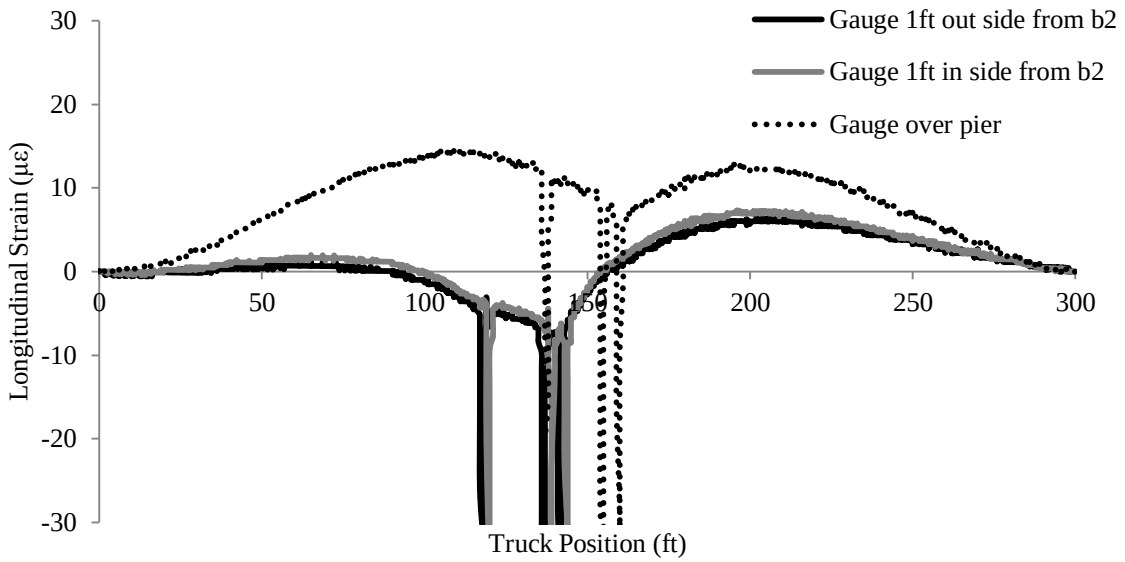

Figure 8. Typical strain variation of deck gauges

3.5 Longitudinal Strain Profiles of Girder Gauges

Strain variation of the girder gauges also showed an expected variation pattern (Figure 9). No significant difference was found among gauges on other bridges (Appendix).

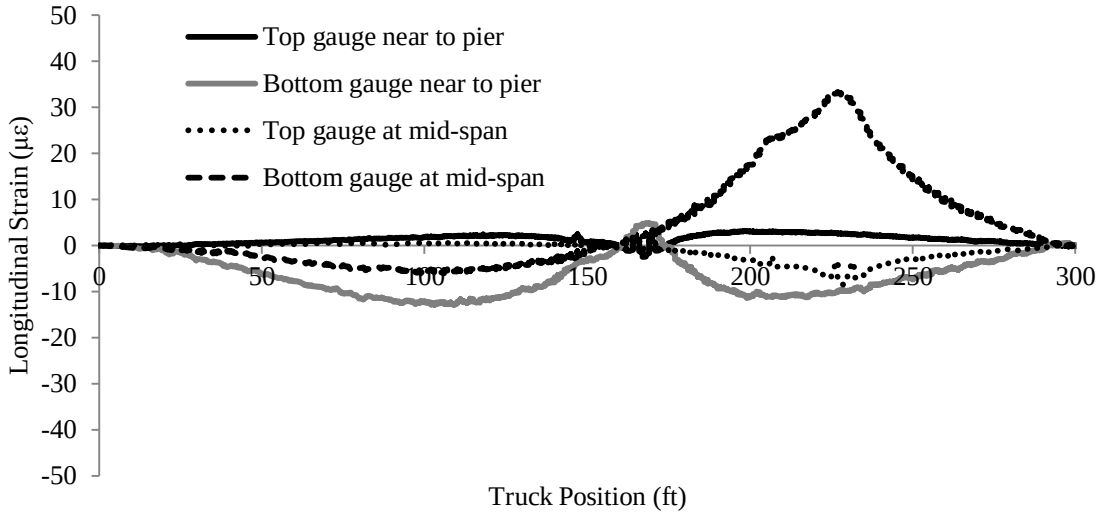

Figure 9. Typical strain variation of girder gauges

3.6 Longitudinal Strain Profiles of Rosettes

In the absence of knowing the principal strain directions before designing an experiment, one needs three independent strain measurements to calculate the principal strains at a particular location. A strain gauge rosette is an arrangement of multiple closely-placed gauges, which can be used to obtain those independent strain measurements. During the field test 45° rectangular strain gauge rosettes were used to determine the principal strains in the bridge deck (Figure 10). The magnitude and the direction of the principal strains of the rosettes location are calculated using [21],

$$\epsilon_{1,2} = \frac{\epsilon_A + \epsilon_B}{2} \pm \frac{1}{\sqrt{2}}\sqrt{(\epsilon_A - \epsilon_B)^2 + (\epsilon_B + \epsilon_C)^2} \quad \ldots\ldots\ldots (1)$$

$$\phi = \frac{1}{2}\tan^{-1}\left(\frac{\epsilon_A - 2\epsilon_B + \epsilon_C}{\epsilon_A - \epsilon_C}\right) \quad \ldots\ldots\ldots (2)$$

$\epsilon_A, \epsilon_B, \epsilon_C$ = Strain gauge data of the rosettes

ϵ_1 = Major principal strain

ϵ_2 = Minor principal strain

ϕ = Angle to the major principal strain

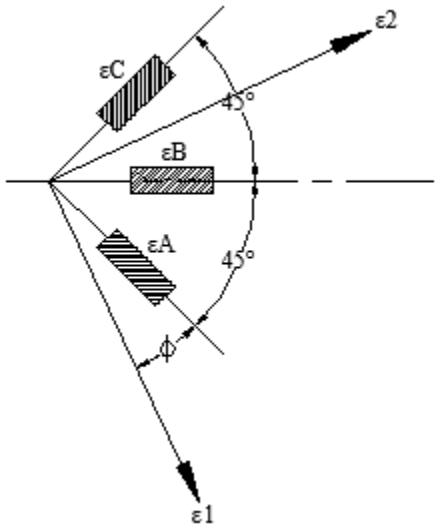

Figure 10. 45° rectangular strain gauge rosettes

Based on the principal strain profiles, no significant difference was observed between the inside and outside rosettes at the end of the b2 reinforcement. However, in two-span bridges, when truck axle was in the vicinity of the rosettes, an expected strain variation was observed (Figure 11). But when the truck axle was away from the rosettes, major and minor principal strains of approximately the same magnitudes with opposite signs were observed (Figure 12). In the three-span bridges, approximately same principal strain magnitudes with opposite with signs was observed (Figure 13 and Figure 14).

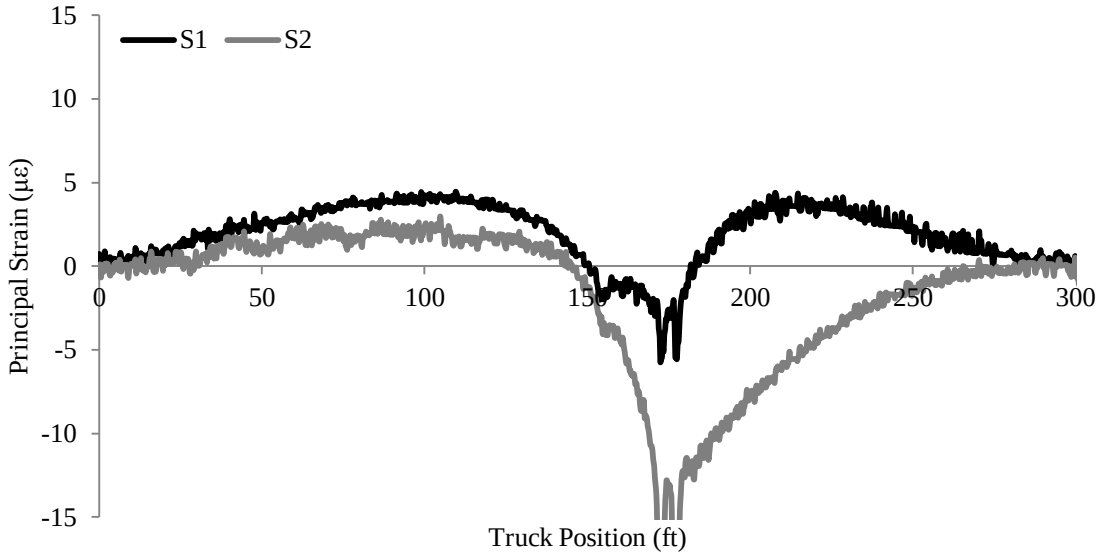

Figure 11. Typical variation of principal strains for two-span bridges with truck axle closer to rosettes

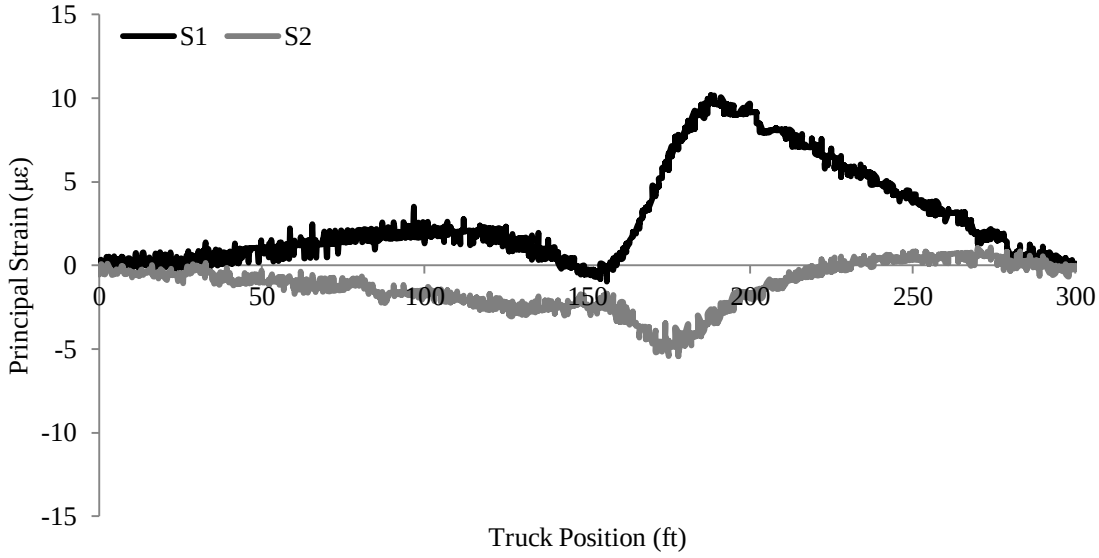

Figure 12. Typical variation of principal strains for two-span bridges with truck axle away from rosettes

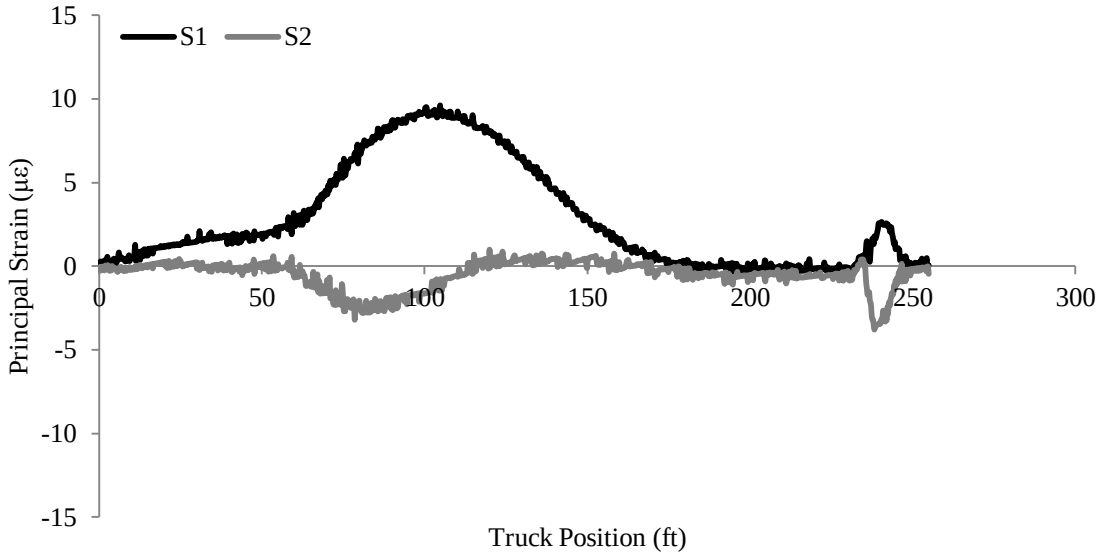

Figure 13. Typical variation of principal strains for three-span bridges with truck axle away from rosettes

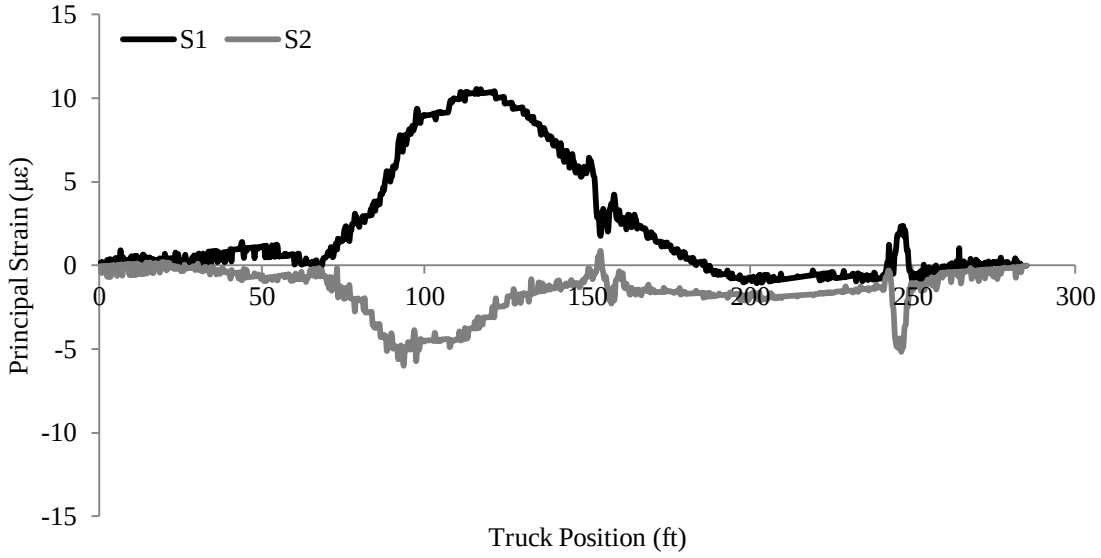

Figure 14. Typical variation of principal strains for three-span bridges with truck axle closer to rosettes

CHAPTER 4. FINITE ELEMENT MODEL OF THE BRIDGES

4.1 Introduction

A significant effort of the research was to investigate the effects of b2 reinforcement on both skewed and non-skewed bridges with Bulb Tee girders. Bridge #3 (Bridge A) and Bridge #2 (Bridge B) have similar characteristics (Table 2), except that Bridge A has a 5 degree skew angle, whereas Bridge B has a 42 degree skew angle. Bridge A and Bridge B were used to investigate the role of skew angle on the negative bending behavior of the PPCB bridges. ANSYS Mechanical APDL 14.5, a general purpose finite element package, was used to develop the three-dimensional finite element models of Bridge A and Bridge B. CHAPTER 4 describes the construction and calibration of the finite element model of Bridge A and Bridge B. The analysis results of Bridge A and Bridge B will be discussed in CHAPTER 5.

4.2 Finite Element Model of Bridge A

4.2.1 Element Type Selection

Bridge A consists of a continuous concrete deck, b2 reinforcement, guard rails, precast pre-stressed girders, pier diaphragm, pier cap, pier columns, footings, piles, abutments and wing walls. Of these components, the pier cap, pier columns, footings, piles and wing walls were not discretely modeled, but were approximated within the boundary condition parameters. The elements used to model all the components of Bridge A are listed in Table 4.

Table 4. Type of elements used in the analysis

Shell 181 element	Beam 188 element
Deck	Girder top flange
Pier diaphragm	Girder bottom flange
Abutment	Intermediate diaphragm
Guard rails	b2 reinforcement
Girder web	

4.2.2 Properties of the Elements

Shell 181 element [22]

The Shell 181 element is a structural element with four nodes in 3D space, with each node having six degrees of freedom. This element is suitable for the analysis of thin to moderately-thick shell structures. It can be used in linear and nonlinear applications, which involve large rotations and large strains. The Shell 181 element has the capacity to model layered applications, such as modeling of composite shells and sandwich constructions.

Beam 188 element [22]

This is a structural element with two nodes in 3D space. Each node has six degrees of freedom and one optional degree of freedom to provide warping freedom. This element can be used to analyze slender to moderately-thick beam structures. Beam 188 element is based on Timoshenko beam theory; hence, this element can deal with shear deformation effects. This element is suitable for linear and non-linear applications which involve large rotations and strains.

4.2.3 Material Properties

According to the structural drawings, Bridge A consists of pre-stressed girders with a specified compressive strength (f'_C) of 9 ksi. The specified compressive strength of the deck concrete is 4 ksi. Reinforcing steel with a 60 ksi yield strength was used for all mild steel reinforcement. An ultimate strength of 270 ksi was used for all high-strength strands specified in the pre-stressed girders.

Reinforcement in each component of the bridge, except the b2 reinforcement, was smeared into the associated finite element. To this end an effective modulus of elasticity of each component of the bridge was determined by,

$$E_{eff} = \frac{A_C E_C + A_S E_S}{A_C + A_S} \qquad \text{..... (1)}$$

Where,

E_{eff} = Effective modulus of elasticity

A_C = Area of concrete

A_S = Area of steel

E_C = Modulus of elasticity of concrete

E_S = Modulus of elasticity of steel

4.2.4 Finite Element Model

Figure 15 shows a plan view of the finite element model of Bridge A. The bridge deck was meshed with 6 in. (Z direction) by 9 in. (X direction) shell elements.

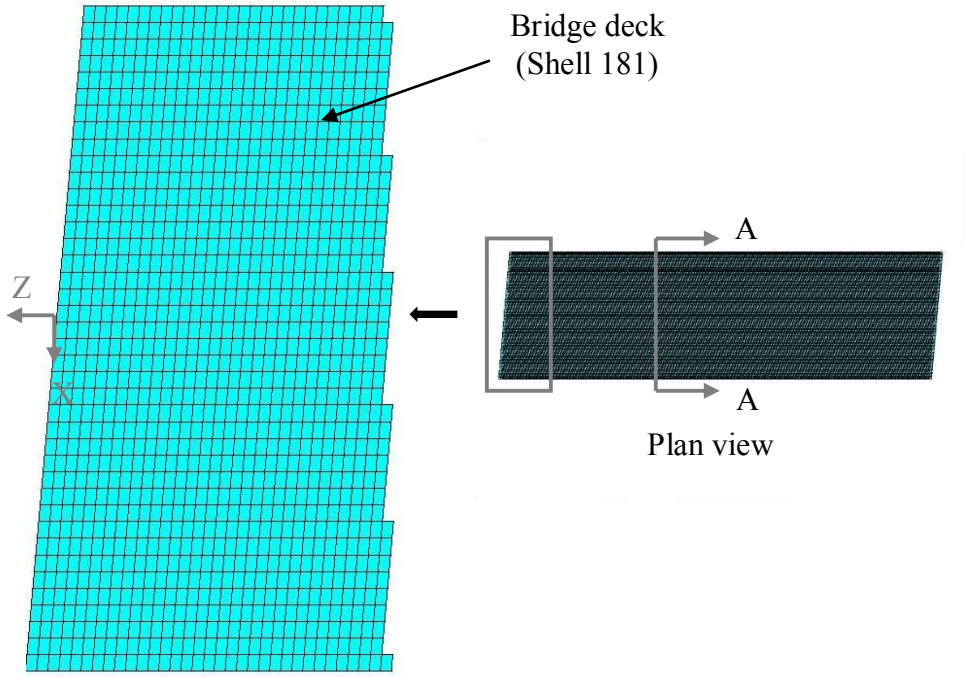

Figure 15. Finite element model of the Bridge A: Plan view

Figure 16 shows the finite element model of all the components of the bridge, except the abutments and the b2 reinforcement.

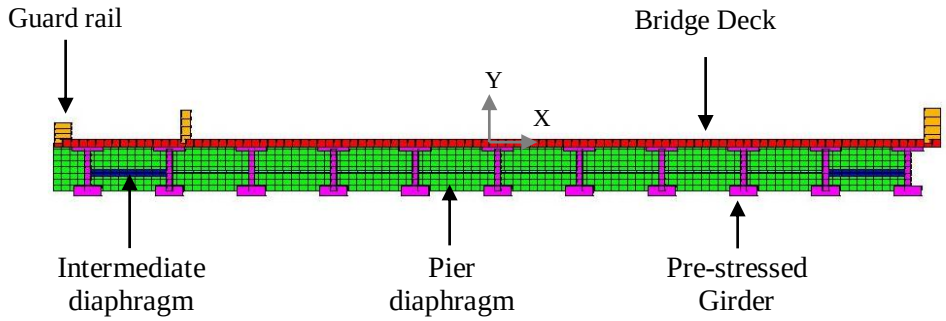

Figure 16. Cross section A-A

A schematic deck girder cross section with the actual reinforcement is shown in Figure 17. The idealized bridge deck and girder model, and b2 reinforcement are shown in Figure 18. Instead of actual b2 reinforcement spacing, equal 9 in. spacing was used in the finite element model however it is important to note that the total amount of reinforcement area remains the same. The connection between the bridge deck and girders was made using rigid elements, which transfer the degrees of freedom of the master nodes (nodes of the deck elements) to the slave nodes (nodes of the top flange elements).

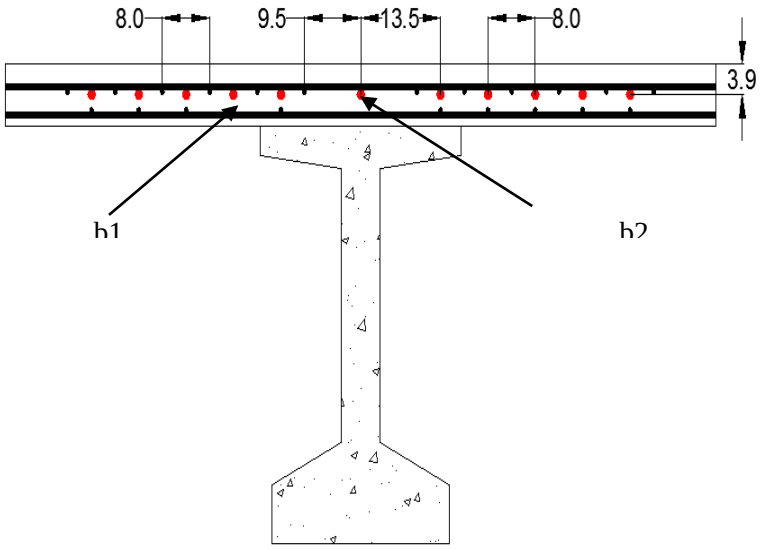

Figure 17. Actual deck, girder and b2 reinforcement

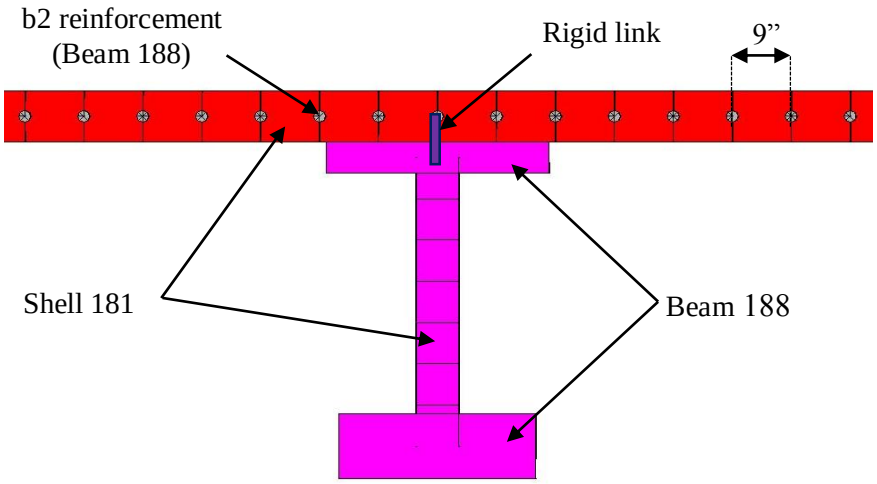

Figure 18. Idealized deck, girder and b2 reinforcement

Figure 16 illustrates the idealization of the pier diaphragm. Elements in the pier diaphragm were meshed with 6.5 in. (Y direction) by 9 in. (X direction) elements. The girder webs were also meshed with shell elements with 6.5 in. (Y direction) and 9 in. (X direction) dimensions. Figure 19 shows the finite element model of the abutment. To make the nodes of the deck and girder web coincide, the abutment was meshed with shell elements, having 6.5 in. (Y direction) and 9 in. (X direction) dimensions.

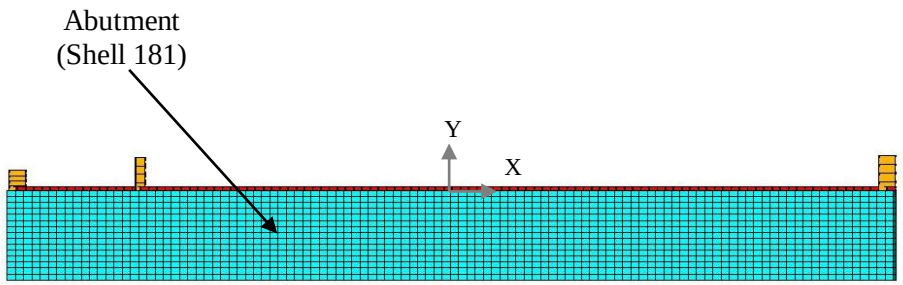

Figure 19. Finite element model of the abutment

4.2.5 Support Conditions of the Finite Element Model

4.2.5.1 Support Condition at the Pier Diaphragm

The girders of Bridge A are connected to the pier cap through a pintle, which restrains the three translational degrees of freedom at the end of the girders. The pier cap is supported on five pier columns, which are connected to the pile foundation. The support conditions for the girders at the pier were approximated by a roller support, which restrained the Y direction translation (Figure 20) from movement.

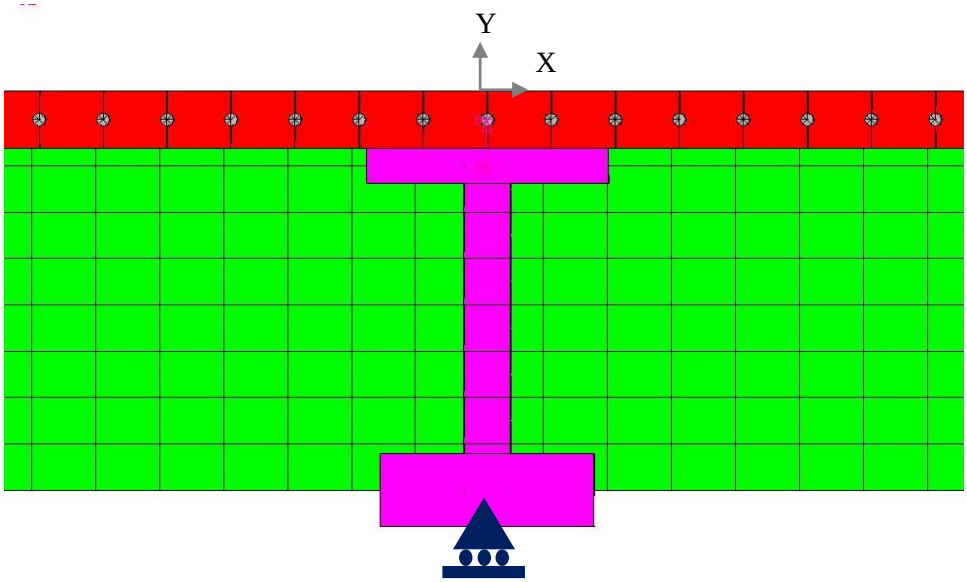

Figure 20. Support condition at the pier diaphragm

4.2.5.2 Support Conditions at the Abutment

Bridge A is an integral abutment bridge. The bottom of the abutment is supported on soil and connected to 21 piles, which are 3.9 ft apart. Also, the ends of the abutments are connected to the wing walls. As an approximation, the soil forces were neglected and the nodes of the abutments at the pile head locations were restrained in the Y direction as shown in Figure 21.

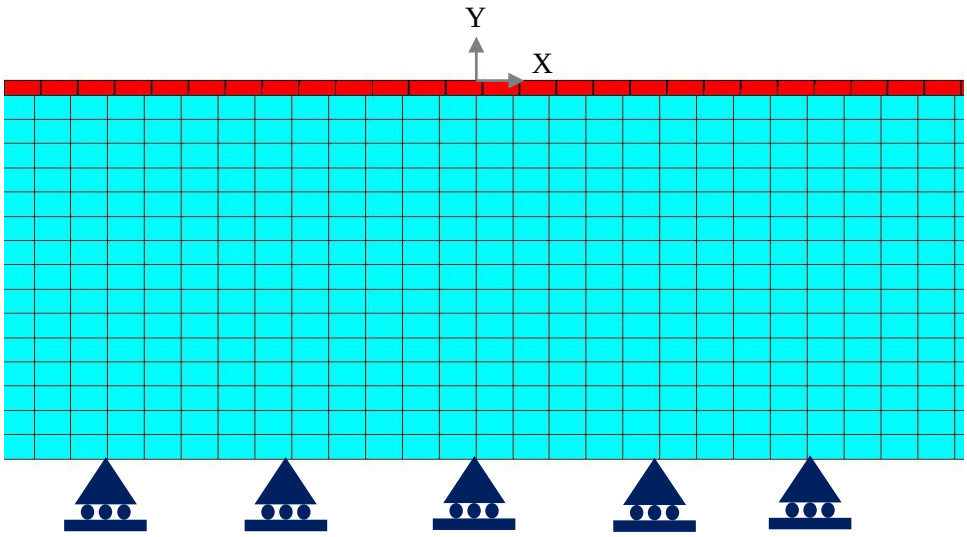

Figure 21. Support conditions at the abutment

4.2.6 Loading Conditions

Four main loading types were applied to the finite element model. The moving truck load was modeled with load steps and with point loads at the truck wheel locations (Figure 7). A uniform surface load was also used for several analyses. Temperature load was applied as a body force. Shrinkage load was applied as an equivalent temperature load.

4.2.7 Calibration of the Model for Field Test

Calibration of the finite element model from the field test results (CHAPTER 3) involved using data from three sets of gauges: deck gauges, girder gauges and rosettes. During the calibration process, strain values from the finite element model at the gauge locations were compared with the strain gauge values for all load cases. As described in CHAPTER 3, gauges close to the truck axle show larger strain magnitudes than gauges away from the truck axle. In addition to making qualitative assessments regarding the accuracy of the model, peak strain values were used to calculate the percentage strain difference between the finite element model and the field test results.

$$\text{Strain difference percentage} = \frac{|\epsilon_{\text{FEM}} - \epsilon_{\text{Field Test}}|}{\epsilon_{\text{Field Test}}} \times 100 \quad \ldots\ldots\ldots (2)$$

4.2.7.1 Calibration for the Deck Gauges

The calibration results of the deck gauges are presented in this section. The comparison of typical finite element results and field test results from the deck gauges, which are in the vicinity of the truck axles is shown in Figure 22 and Figure 23. Figure 24 shows the comparisons of typical strain variation of the deck gauges away from the truck axles. As should be evident by reviewing these results the finite element results of the deck gauges are in agreement with the field test results. As a result, no changes to the model were made.

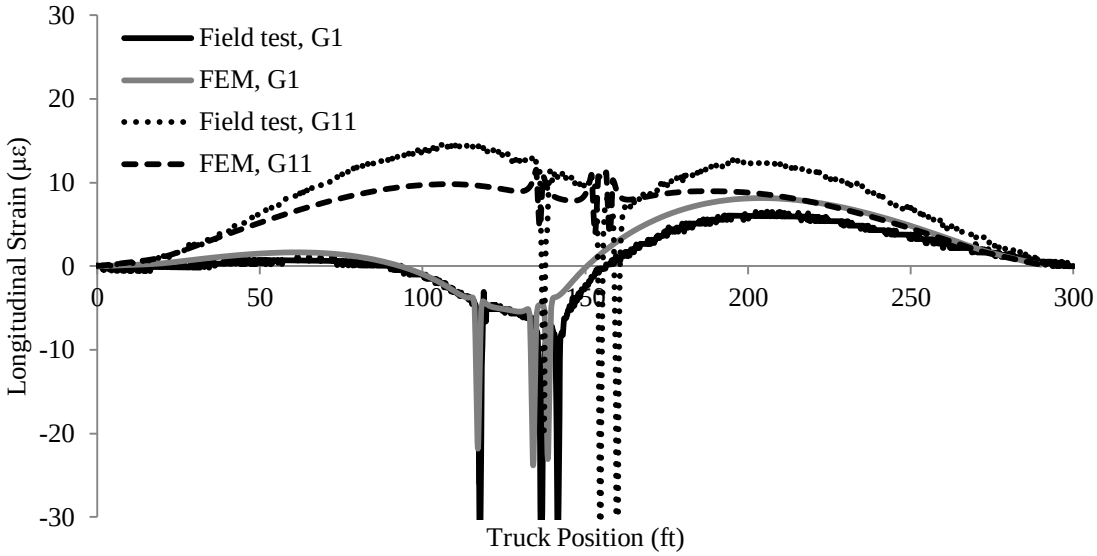

Figure 22. Strain variation of deck gauges (G1 and G11) close to axles, (LC1)

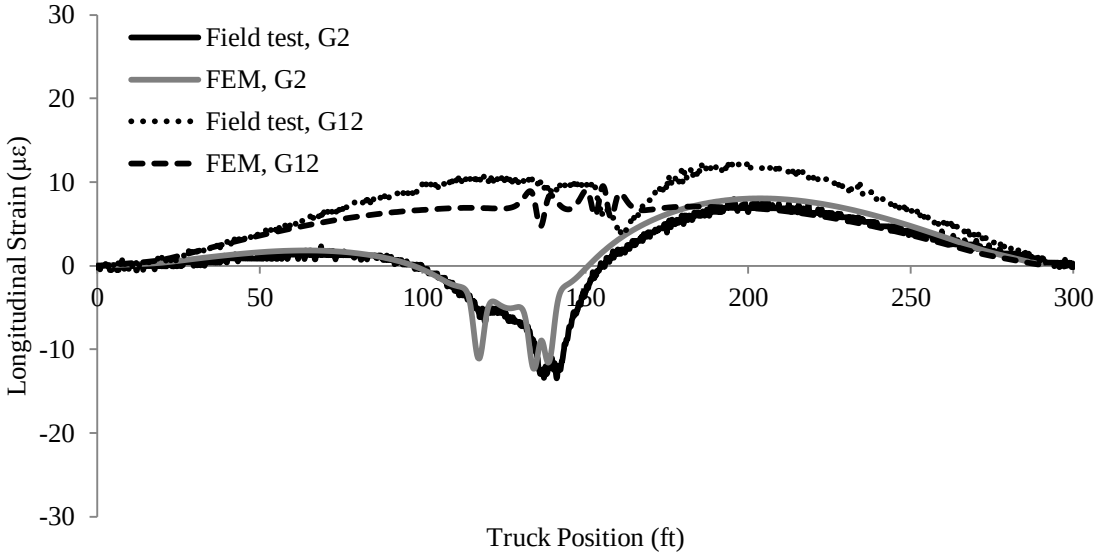

Figure 23. Strain variation of deck gauges (G2 and G12) close to axles, (LC1)

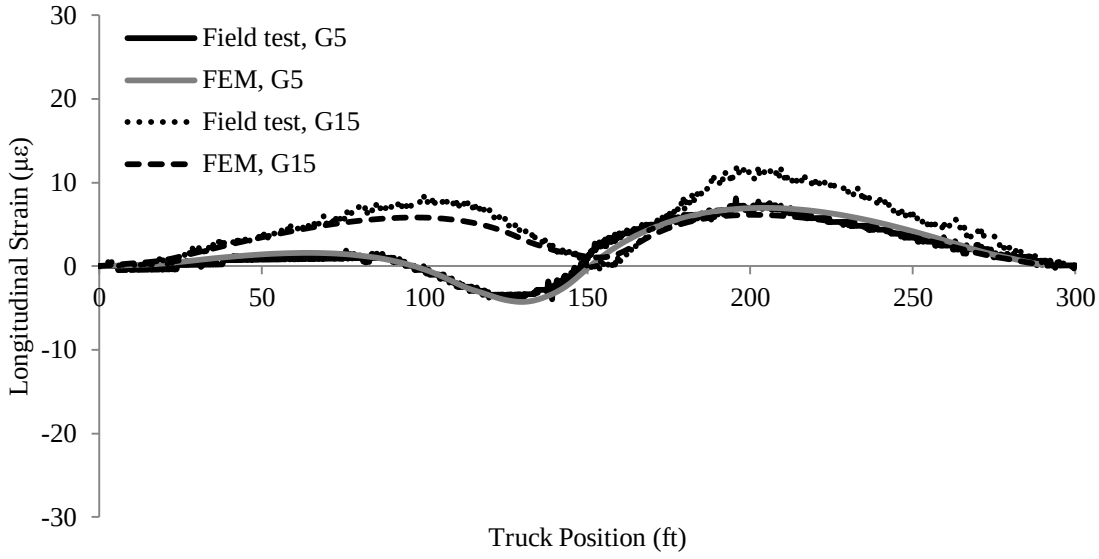

Figure 24. Strain variation of deck gauges (G5 and G15) away from axles, (LC1)

4.2.7.2 Calibration for the Girder Gauges

Calibration results for the girder gauges are presented in this section. According to Figure 25, field test results for the gauges at the top flange at the pier and mid span locations agree with the FEM results. However, strain magnitudes of those gauges are very small.

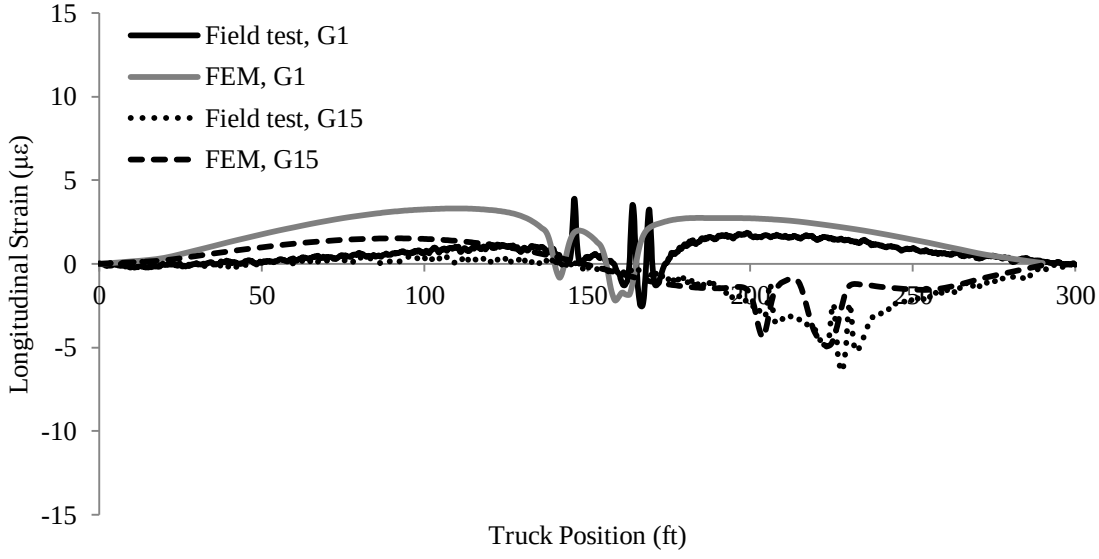

Figure 25. Strain variation of girder gauges (G1 and G15) close to axles, (LC1)

Figure 26 and Figure 27 show the finite element and field test results of girder gauges "close" to the truck axles. The pattern of both the finite element and field test results are similar. But, there is a maximum of 30% average strain difference between FEM results and field test results.

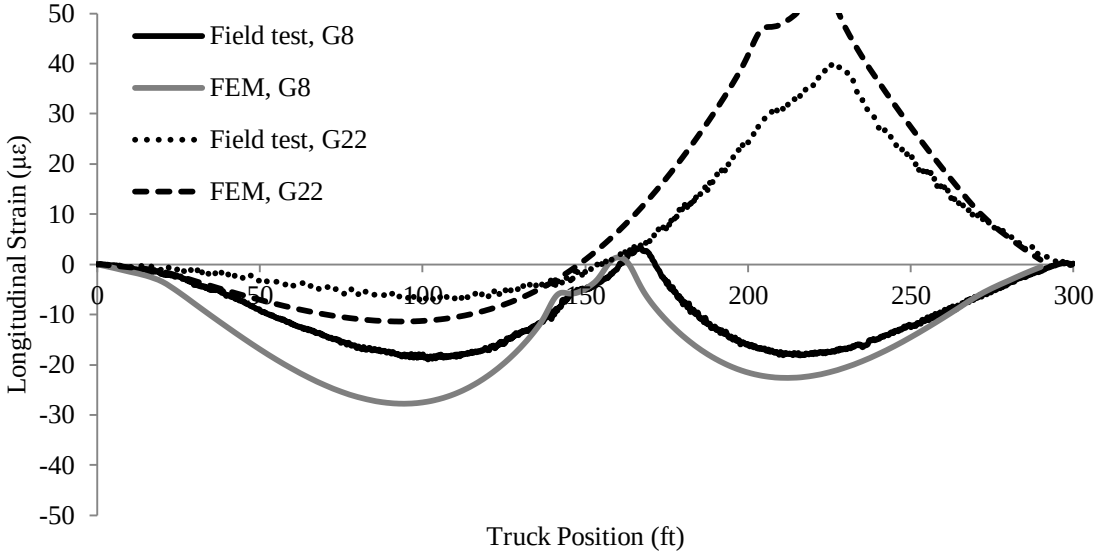

Figure 26. Strain variation of girder gauges (G8 and G22) close to axles, (LC1)

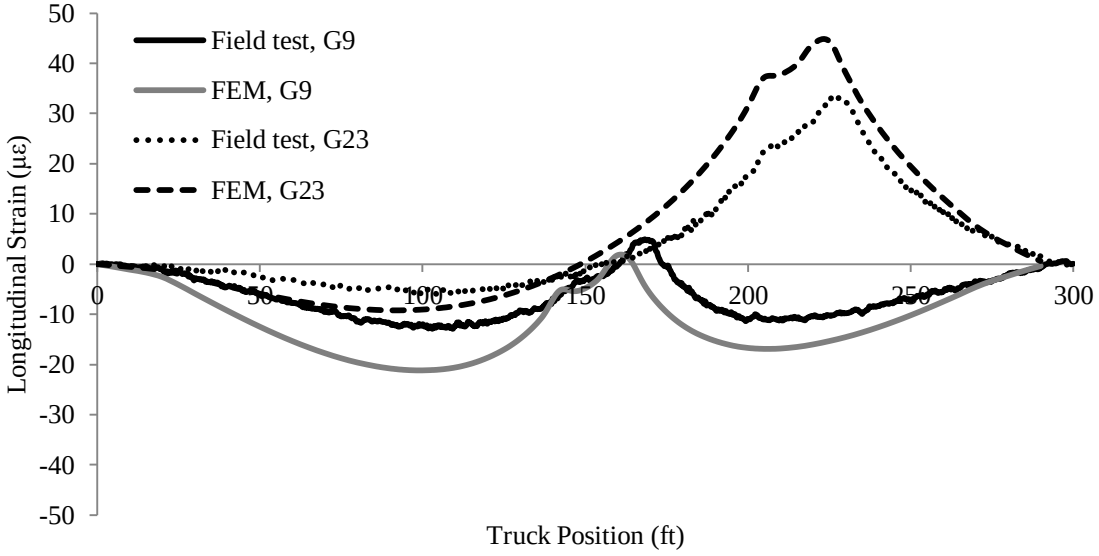

Figure 27. Strain variation of girder gauges (G9 and G23) close to axles, (LC1)

Since the Modulus of Elasticity (E) is equal to $57000\sqrt{f'_c}$, the specified characteristic strength of the concrete, f'_c of the girders (and, thereby, E) was changed to minimize the percentage strain difference. Figure 28 and Figure 29 show the strain variation of the girder gauge near the pier (G8) and the girder gauge at the mid span (G22) respectively, with various girder f'_c values. These results shows that with the increase of f'_c of the girders, the strain values approach the field test results which indicates that the stiffness (E) of the girders is larger than the specified plan values might indicate.

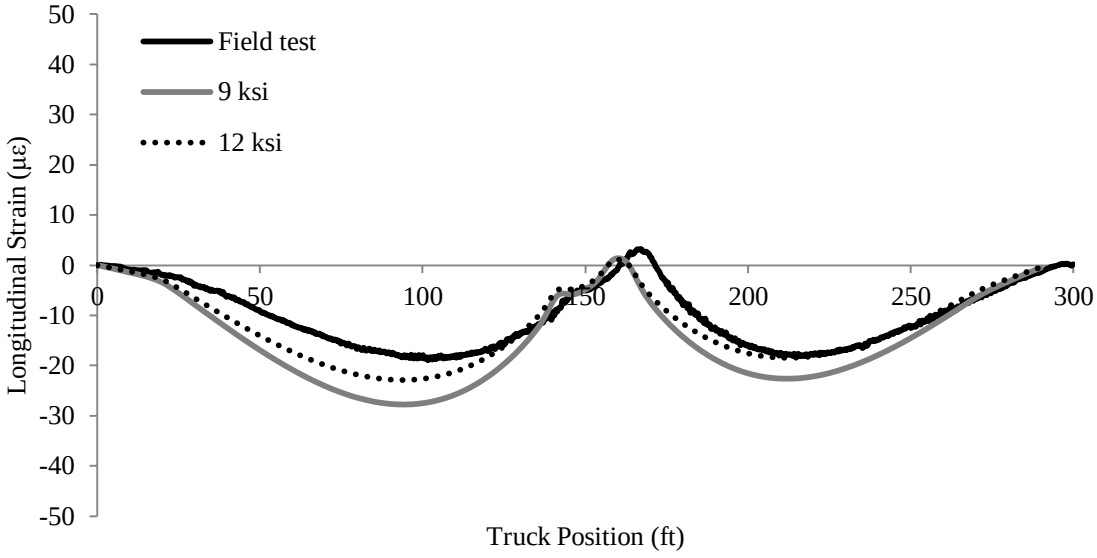

Figure 28. Strain variation of girder gauge G8 with different girder f'_c

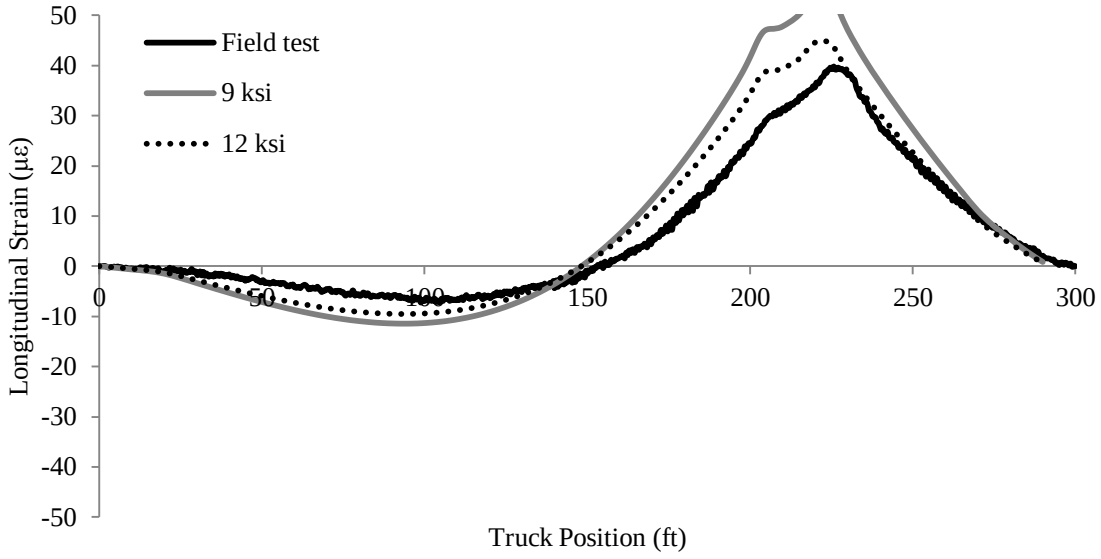

Figure 29. Strain variation of girder gauge G22 with different girder f'_c

Importantly, Figure 30 and Figure 31 show that the change of the strength and Modulus of Elasticity of the girder does not significantly affect the strain in the deck.

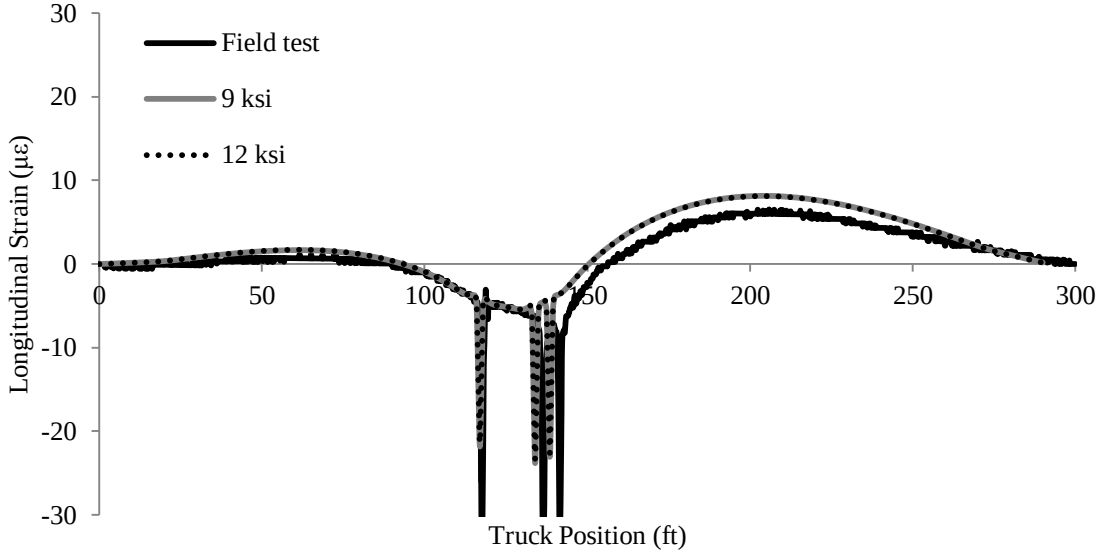

Figure 30. Strain variation of deck gauge G1 with different girder f'_c

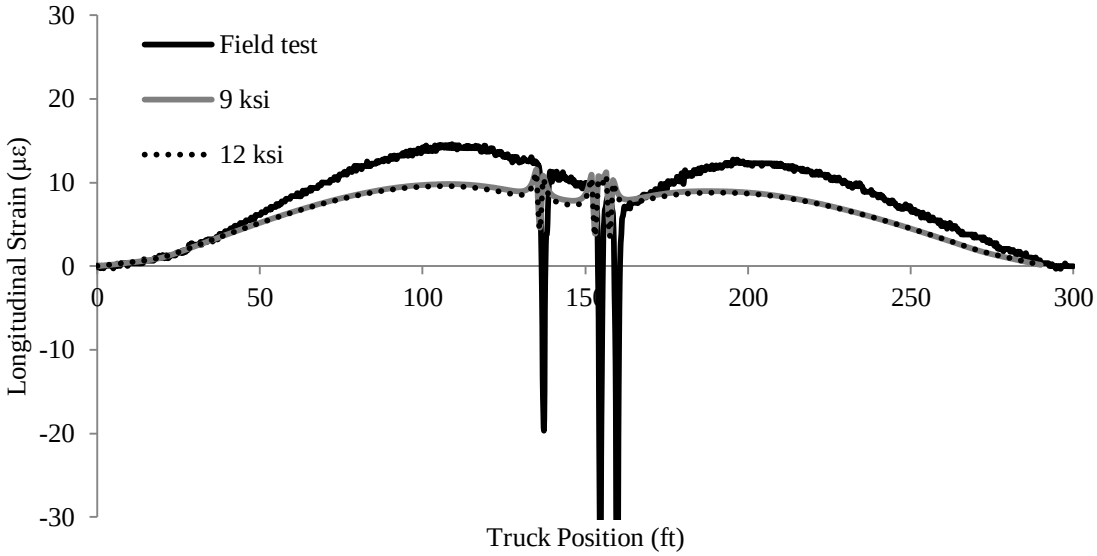

Figure 31. Strain variation of deck gauge G11 with different girder $f_c^{'}$

Figure 32 shows the variation of the average percentage difference of peak strain with the girder strength. Beyond a 15 ksi of girder concrete strength, the average percentage strain difference is less than 15%. Since the strength of the girders beyond 15 ksi is not realistic, it was decided to use 12 ksi for the girder strength, which gives about a 23% average difference in the strain peak.

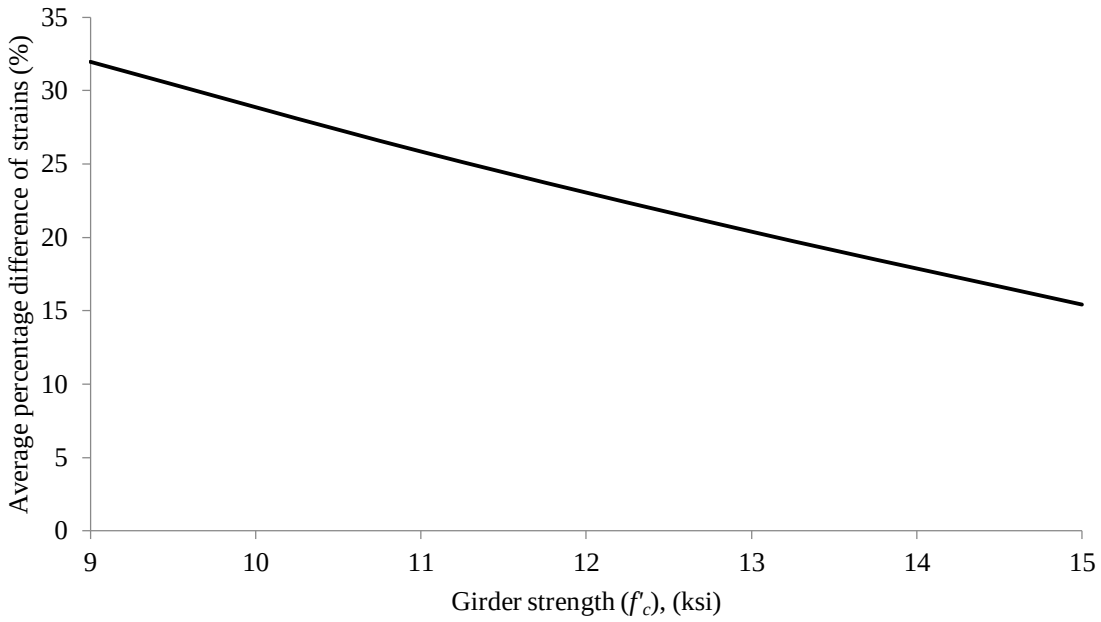

Figure 32. Variation of average % difference with the girder strength

The support conditions at the abutments were changed from rollers (Figure 21) to: (1) pinned and (2) fixed conditions in an attempt to reduce the average percentage. Figure 33 and Figure 34 show the strain variation of the girder gauges at the pier and mid-span sections for these different abutment support conditions. There is no significant difference between the results for the pinned support and the fixed support condition. Both conditions reduce the difference between the FEM results and the field test results.

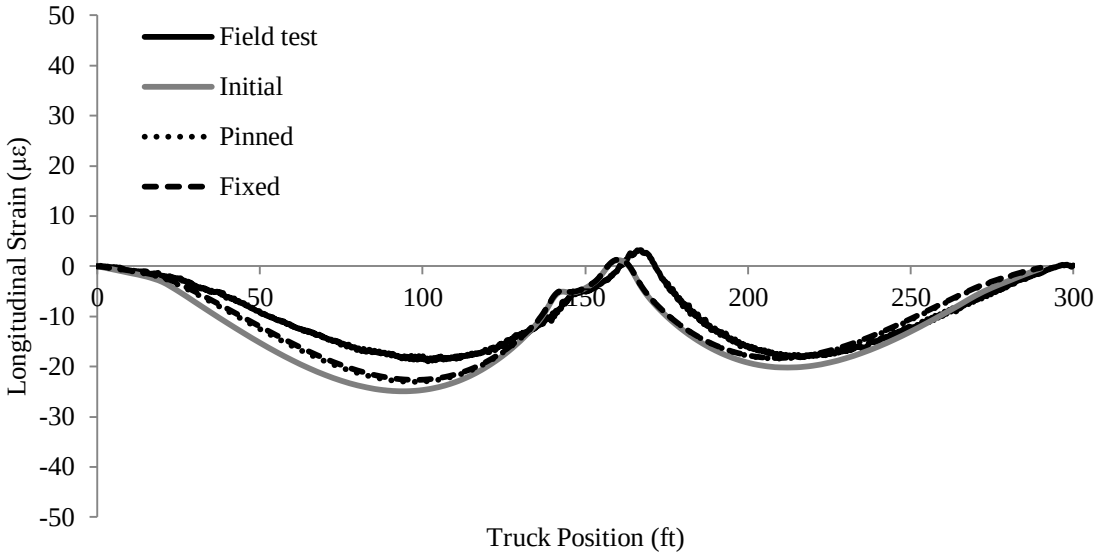

Figure 33. Strain variation of girder gauge G8 with abutment boundary conditions $f'_c = 12ksi$

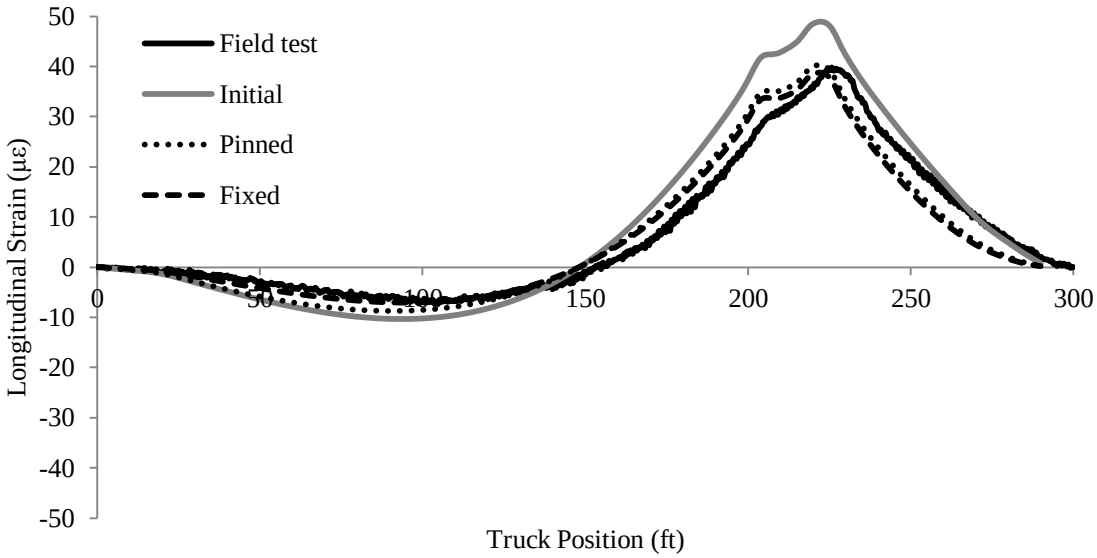

Figure 34. Strain variation of girder gauge G22 with abutment boundary conditions $f'_c = 12ksi$

According to Figure 35, deck strains near the end of the b2 reinforcement do not significantly change with the type of the support conditions at the abutments. Figure 36 shows that a change of support condition at the abutment affects the deck strains around the pier.

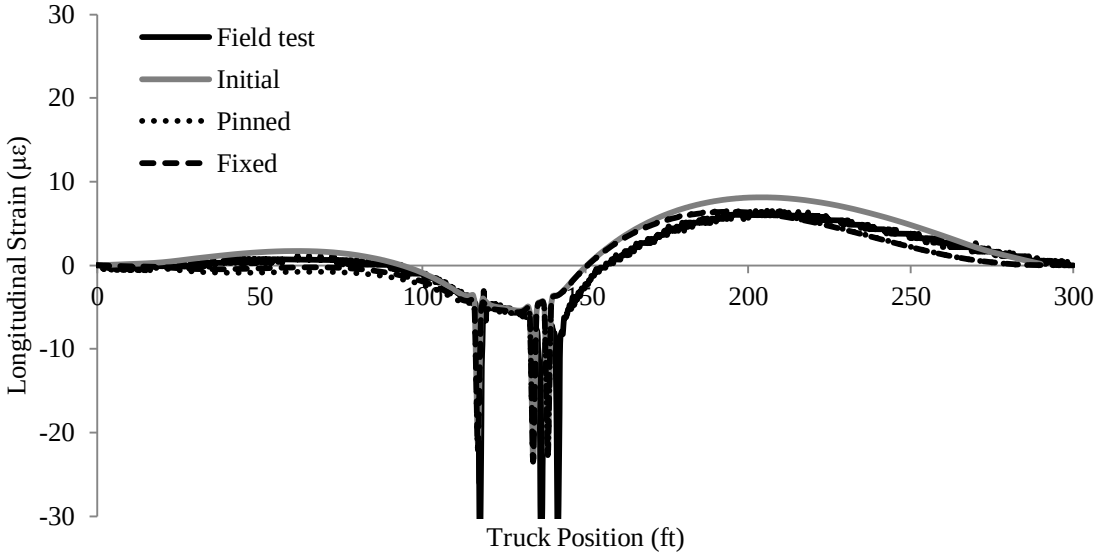

Figure 35. Strain variation of deck gauge G1 with abutment boundary conditions $f'_c = 12ksi$

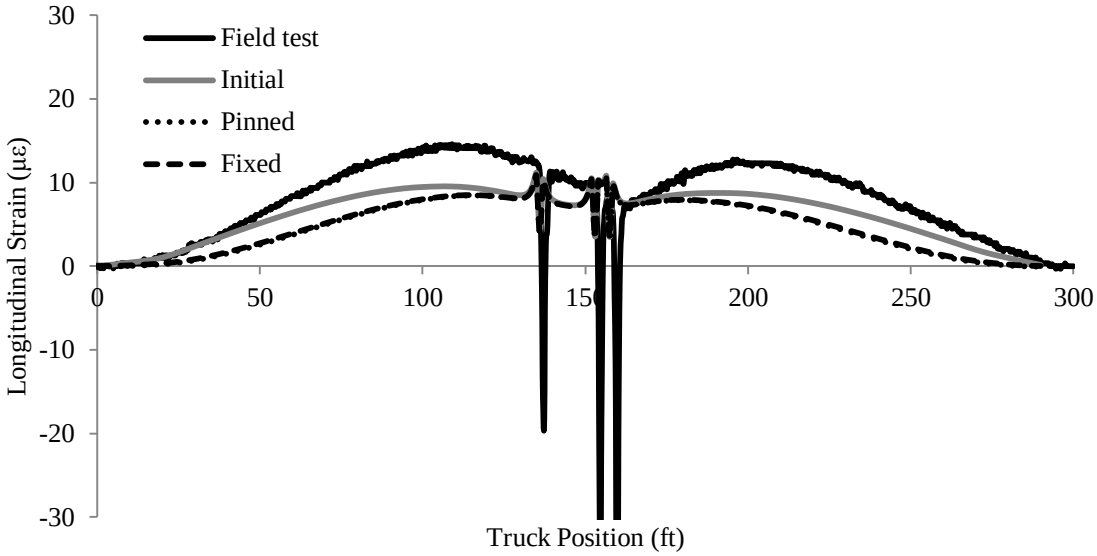

Figure 36. Strain variation of deck gauge G11 with abutment boundary conditions $f'_c = 12ksi$

A summary of the calibration results is shown in Table 5. According to these results, Case 6 shows an average of 10% strain difference between the FEM and field test results for both deck and girder gauges. Therefore, Case 6 was selected to continue with the next steps of the research.

Table 5. Summary of calibration results

	f_c' of the girders (ksi)	Average error percentage (based on girder gauges) (%)	Average error percentage (based on deck gauges) (%)	Boundary conditions	
				Restraint at the abutment (on piles)	Restraint at the pier (under the girders)
1	9	30	-	Roller	Roller
2	11	25	-	Roller	Roller
3	13	20	-	Roller	Roller
4	15	15	-	Roller	Roller
5	12	25	10	Roller	Roller
6	12	10	10	Pinned	Roller
7	12	10	15	Fixed	Roller

4.2.7.3 Calibration of the Rosettes

Comparisons were made between the FEM and field test results of the major principal strains (ε_1) calculated from the individual sensors comprising the rosettes. According to Figure 37 and Figure 38 a significant difference between the FEM and field test results for the principal strains up to the 150 ft truck position can be observed. Elsewhere the finite element results reasonably predict the field test behavior.

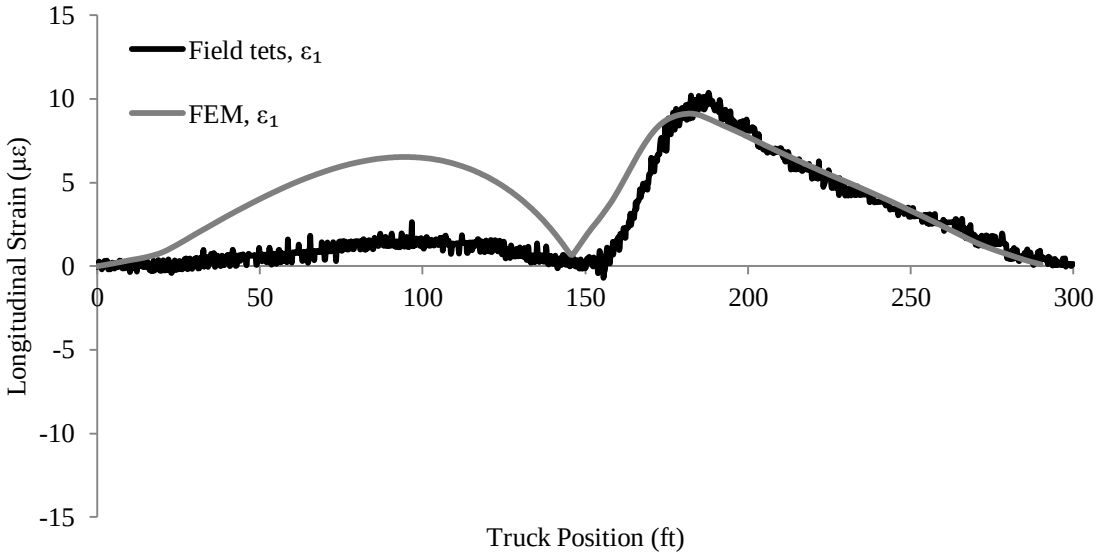

Figure 37. Variation of principal strains of rosette R5 for LC1

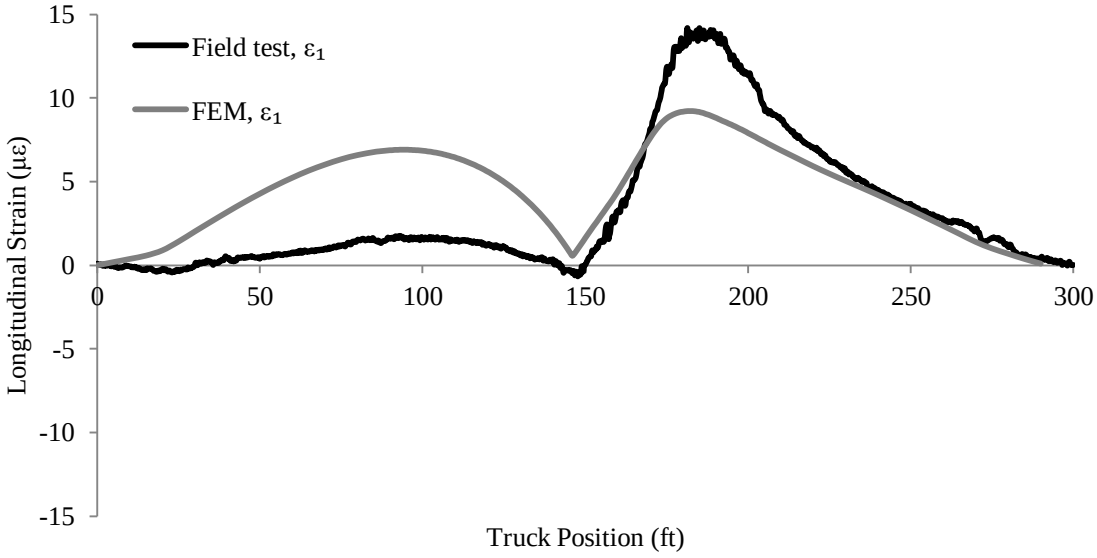

Figure 38. Variation of principal strains of rosette R6 for LC1

4.2.8 Comparison of Cracking Strain with Field Cracks

The finite element analysis results were also compared with the cracking strain to simulate cracks that were found during the field inspection by the Bridge Engineering

Center (BEC) staff and the Bridge Condition Reports of 2010 and 2012, and from Iowa DOT OBS Bridge Maintenance and Inspection Unit.

4.2.8.1 Crack Map

Five significant transverse cracks, namely C1 to C5, were found on the bridge deck through field inspection (Figure 39). The Bridge Condition Report of 2010 indicated only one transverse crack (C3) on the bridge deck. The Bridge Condition Report of 2012 described the same crack with no other cracks having been reported.

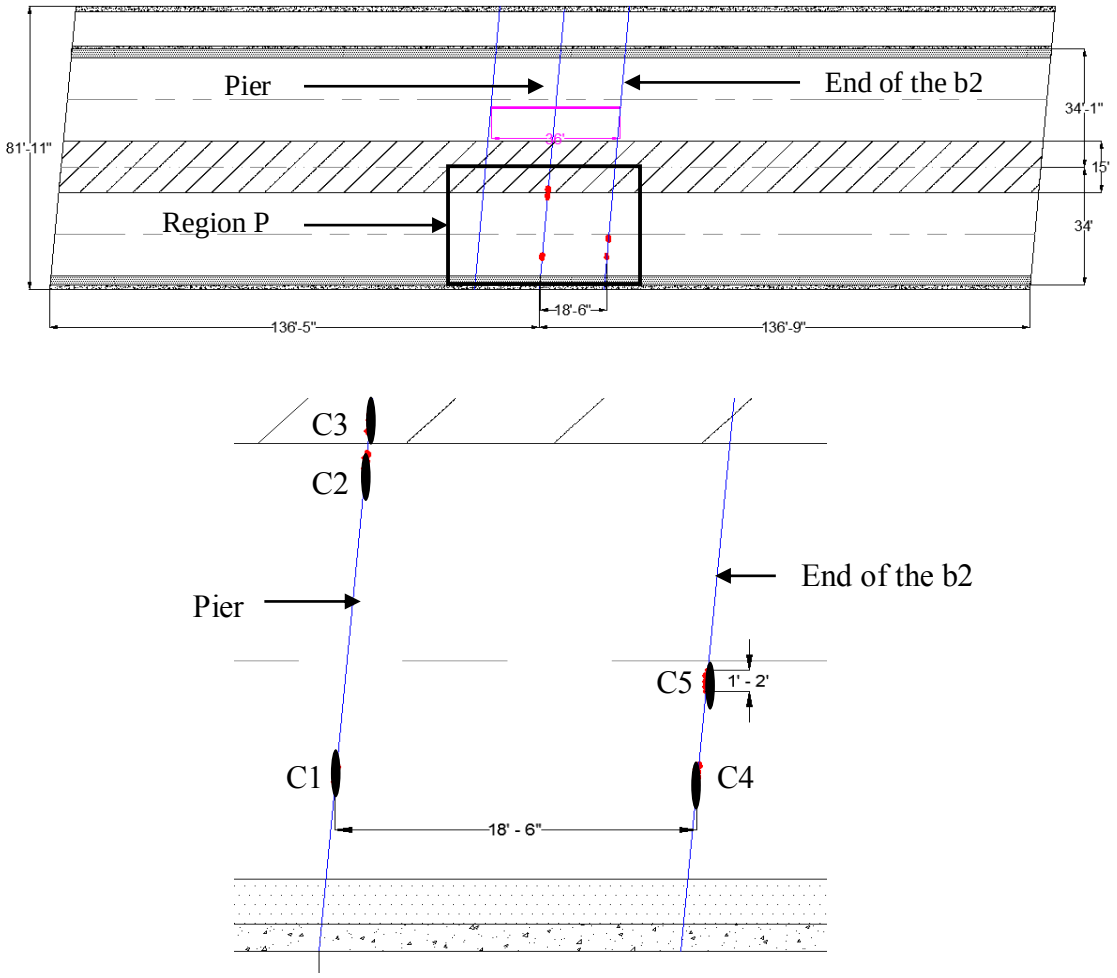

Figure 39. Crack map

4.2.8.2 Comparison with Live Load

Comparison of the cracks began with live load on the bridge. The following relationship can be used to calculate the approximate cracking strain of concrete.

$$\text{Cracking strain of the concrete} = \frac{7.5\sqrt{f'_c}}{57000\sqrt{f'_c}} \approx 130\mu\epsilon \ldots\ldots\ldots\ldots (3)$$

f'_c = specified strength of the concrete

The truck used during the field test (Figure 7) was not large enough to generate strains in the bridge deck that would causing cracking of the deck. Therefore, a large truck load, HS20 (Figure 40) was used to study the relationship with deck strain and for conceptual crack calibration.

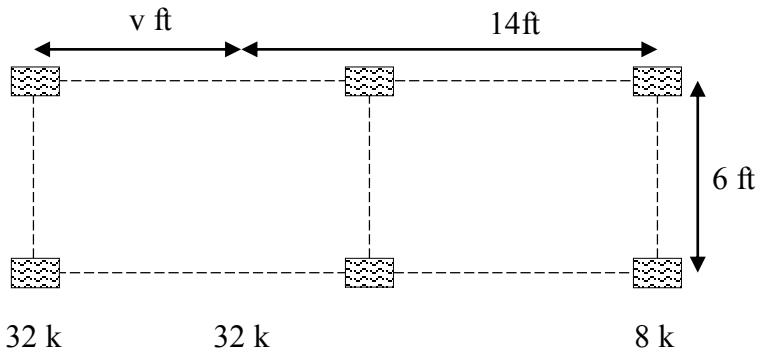

Figure 40. Details of the HS20 truck loading

The HS20 design truck load consists of variable distances (v) between the rear axles, which can vary from 14 ft to 30 ft. The distance v was selected in such a way that produced the largest effect on the structure. To find the distance v, number of HS20 trucks and locations of the HS20 trucks which produced the worst effect on the structure, one HS20 truck with variable distance v equal to 14 ft was run along Lane#1 and Lane#2. Then the major principal strains over the pier and at the end of the b2 reinforcement were recorded. Later, the same procedure was conducted with a 30 ft variable axle distance HS20 truck. Figure 41 and Figure 42 show typical major principal variations for locations at the end of the b2 reinforcement and over pier with one HS20 truck. The HS20 truck with a 14 ft axle spacing induces larger strains than the HS20 truck with a 30 ft axle. Eight trucks were placed at 112 ft and 196 ft positions on Lane #1 to Lane #4 to induce the maximum strain due to the live load.

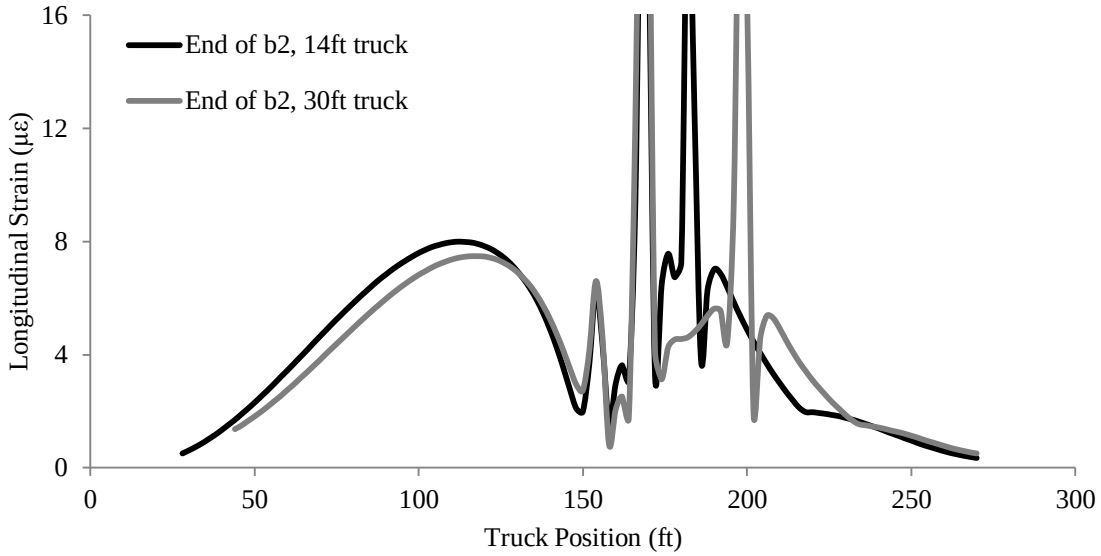

Figure 41. Typical variation of ε_1 strain for truck over Lane1, end of the b2 reinforcement

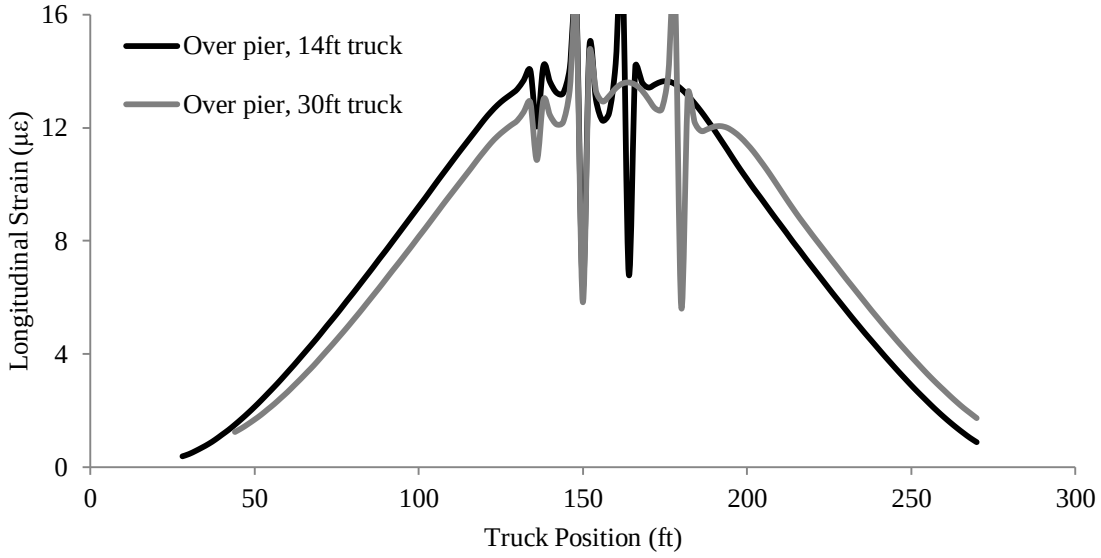

Figure 42. Typical variation of ε_1 strain for truck over Lane1, at the pier

Strain in the bridge deck was large at the locations of these concentrated forces, causing local stress concentrations that were not the focus of this project. Therefore, a Uniformly Distributed Load (UDL) of 0.0004 ksi, equivalent to eight HS20 trucks was

applied to avoid these stress concentrations. The deck strain in the longitudinal direction (Z direction) (ε_Z), over the pier and at the 18 ft location of the b2 reinforcement, from the eight HS20 truck loadings are compared to the results from the equivalent UDL, in Figure 43.

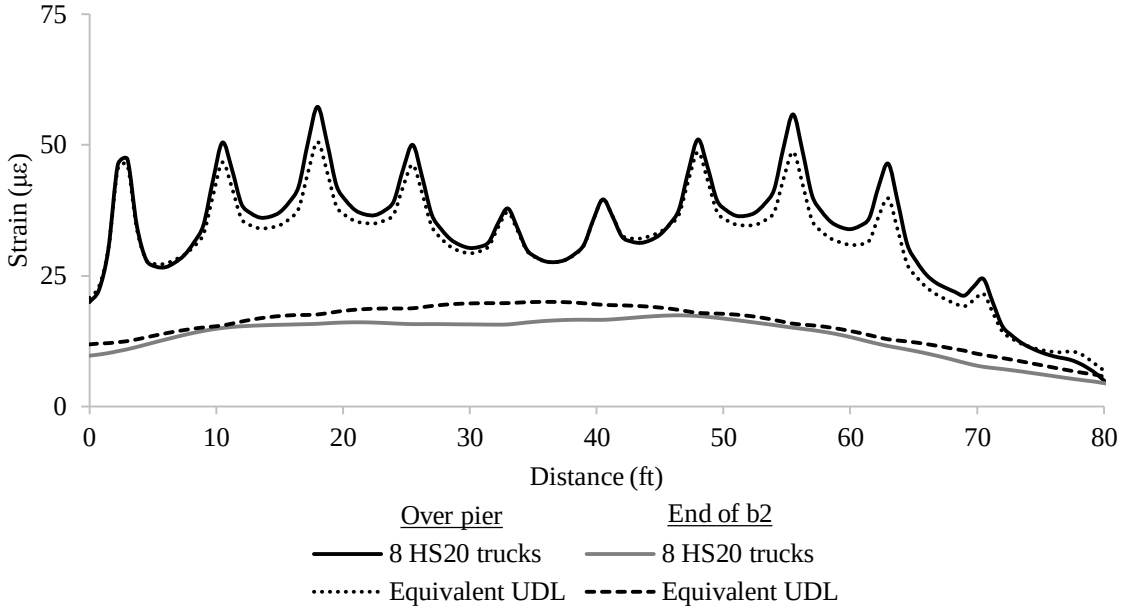

Figure 43. Strain due to equivalent eight HS20 truck loads

Figure 44 illustrates the major principal strain distribution of Region P, which shows the finite element analysis results predicts no cracking strains at the field crack locations with equivalent UDL.

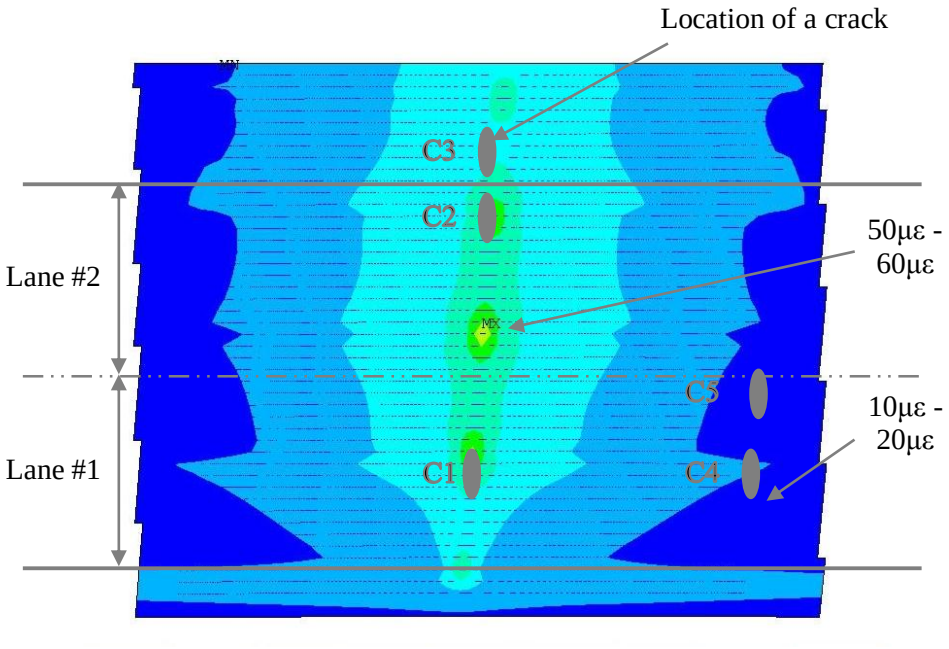

Figure 44. Major principal strain variation around Region P, equivalent UDL

4.2.8.3 Comparison with Temperature Load

As explained at the beginning of CHAPTER 4, rigid links were used to make the connection between the bridge deck and the girders. However, rigid links do not contain any material properties. Hence, rigid links cannot be used in an analysis where temperature effects are involved. During the calibration of temperature, the rigid links were replaced with Beam 188 element with large stiffness.

Cold weather condition is generate tensile stresses over the intermediate support. A −80 °F temperature difference due to 60 °F average construction temperature and -20 °F average cold weather condition was applied to the model to investigate the cracking due to the temperature. The strains induced by the cold temperature were not large enough to simulate the cracking strain on the bridge deck (Figure 45).

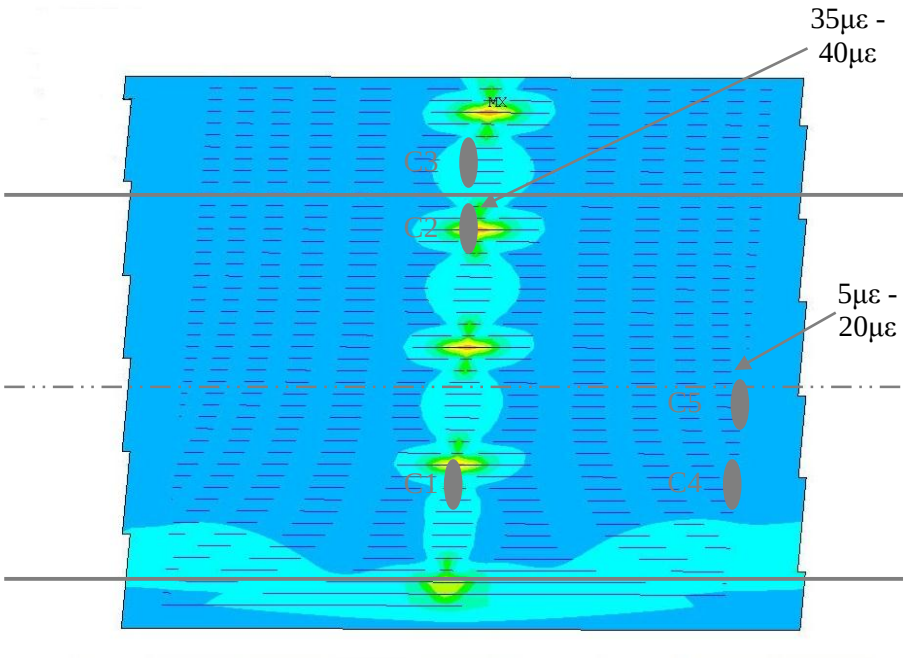

Figure 45. Major principal strain variation around Region P due to cold weather

4.2.8.4 Comparison with Shrinkage Load

According to literature, approximately 50% of the shrinkage of concrete decks takes place during the 56 days following deck placement. The bridge was loaded with a 56-day shrinkage load. To calculate the shrinkage, the following relationship given in the AASHTO LRFD specification was used.

$$(\in_{sh})_t = -k_s k_h \left(\frac{t}{35+t}\right) \times 0.51 \times 10^{-3} = \text{-0.000134} \quad \text{..... (4)}$$

Where:

$(\in_{sh})_t$ = shrinkage strain at time t (56 days)

k_s = Volume/surface ratio factor (0.46)

k_h = Humidity factor (0.93)

Shrinkage load was applied to the model as an equivalent temperature load calculated using Equation 5.

$$T_{equ} = {(\in_{sh})_t}/{\alpha} = \text{-24.5°F} \quad \text{..... (5)}$$

Where:

T_{equ} = equivalent temperature

α = Coefficient of thermal conductivity (0.0000055/°F)

According to Figure 46, the 56 days of shrinkage load can be used to simulate the transverse cracks of the bridge deck, because concrete strains are in the vicinity of the cracking strain.

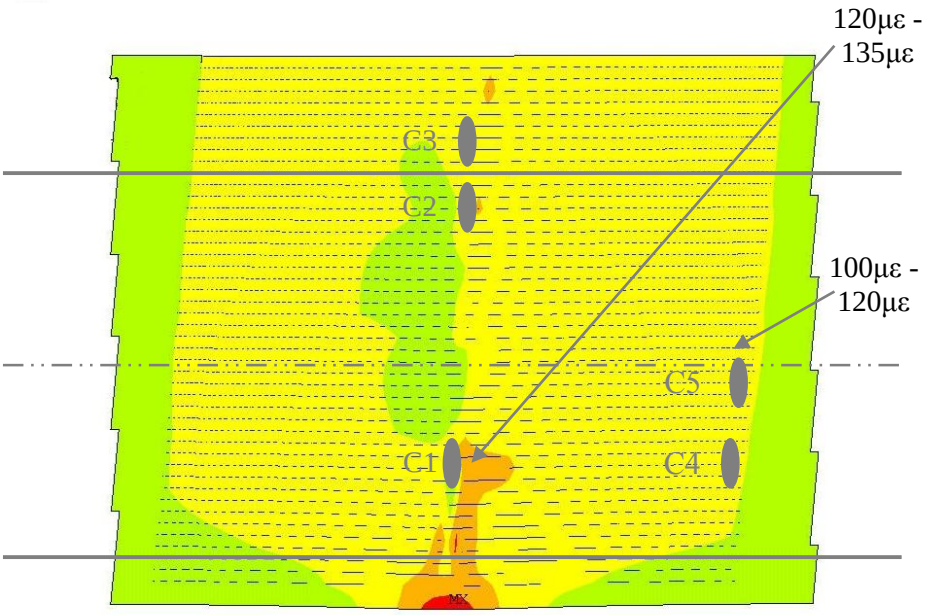

Figure 46. Major principal strain variation around Region P, due to shrinkage after 56 days

4.3 Finite Element Model of Bridge B

The major difference between Bridge A and Bridge B is that Bridge B has a higher skew angle (42 degrees) than Bridge A (5 degrees). Some other minor differences between these two bridges are listed in Table 6. The goal of conducting detailed analysis of Bridge B was to evaluate the influence of skew on the negative moment region behavior in PPCB.

Table 6. Comparisons of the properties of Bridge A and Bridge B

Properties	Bridge A	Bridge B
Span (ft)	136	156
Girder height (in.)	54	63
Average b2 reinforcement spacing (in.)	9	6
Length of the b2 reinforcement (ft)	36	38
Total b2 reinforcement (in^2/in)	0.140	0.187
Total deck reinforcement (in^2/in)	0.205	0.252

The finite element model of Bridge B was developed similarly to how the finite element model of Bridge A was developed. Figure 47 shows a plan view of the finite element model of Bridge B. The deck of Bridge B was modeled with 6 in. (Z direction) by 6 in. (X direction) shell elements.

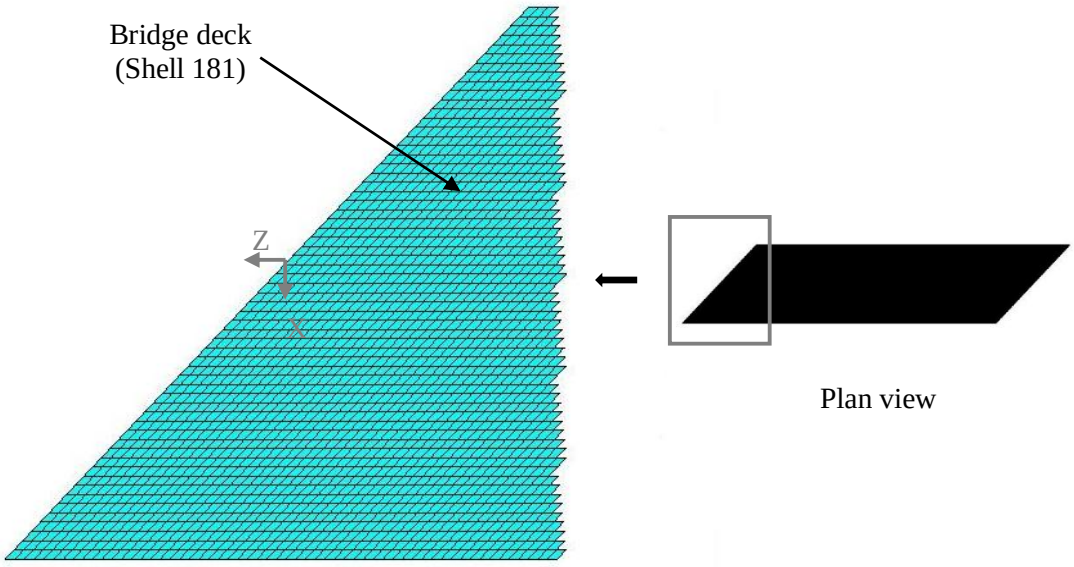

Figure 47. Finite element model of the Bridge B: Plan view

Recall that Bridge A has one b2 reinforcement layer (Figure 17). Bridge B has two b2 reinforcement layers, one layer above and one below the middle of the deck thickness. However, both b2 reinforcement layers are very close to the center of the deck. As a result,

both b2 reinforcement layers were modeled as one b2 reinforcement layer located near the centroid of the concrete deck.

The live load calibration results of Bridge A were used to establish the initial conditions for Bridge B. As mentioned in Case 6 (Table 5), pinned supports at the abutments and roller supports at the pier were also used as the support conditions of Bridge B. The strength of the girders was as assumed to be 12 ksi, as it was for Bridge A.

4.3.1 Calibration of Bridge B

4.3.1.1 Calibration for the Deck Gauges

Typical calibration results of the deck gauges are presented in this section for deck gauges G1, G 15, G5, and G19 for LC1. Figure 48 shows typical strain comparisons for strain sensors located near the truck load (i.e., G1 and G15). Figure 49 shows similar comparisons for strain sensors located away from the truck load. In general there were very small differences between the fields collected data and the analytical predictions.

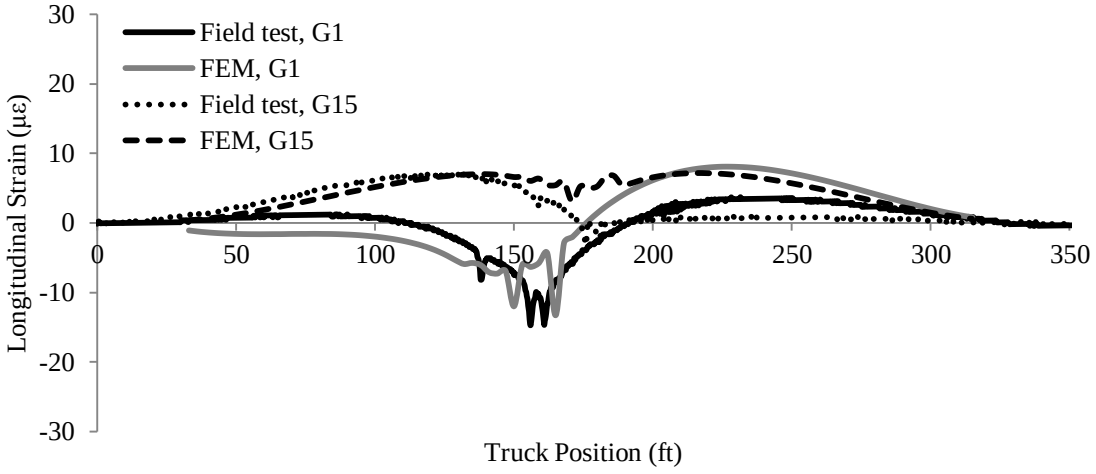

Figure 48. Strain variation of deck gauges (G1 and G15) closer to axles, (LC1)

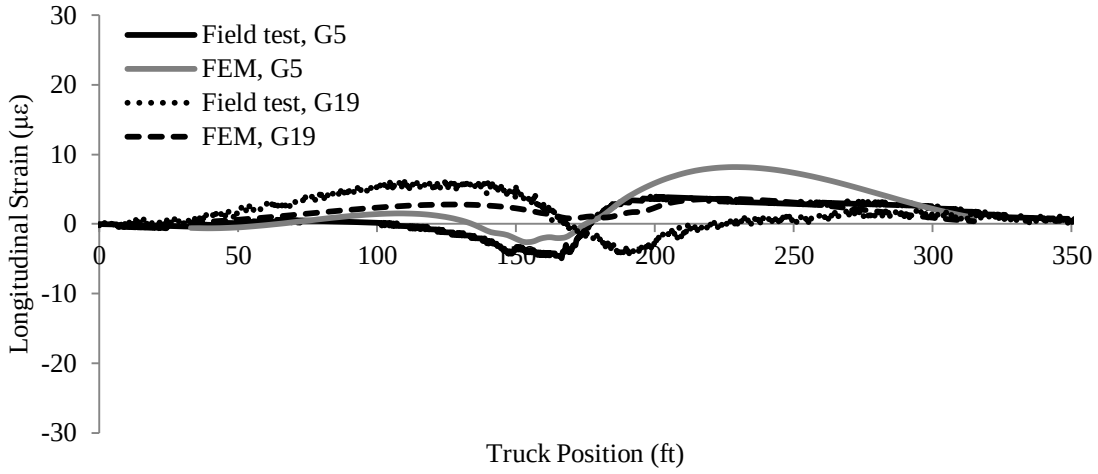

Figure 49. Strain variation of deck gauges (G5 and G19) away from axles, (LC1)

4.3.1.2 Calibration for the Girder Gauges

Analytical and field test results for several of the Bridge B girder gauges are presented in Figure 50 and Figure 51. These show the strain comparisons of girder gauges close to the truck axles and away from the truck axles, respectively. As can be seen, the finite element results are generally in good agreement with the field test results.

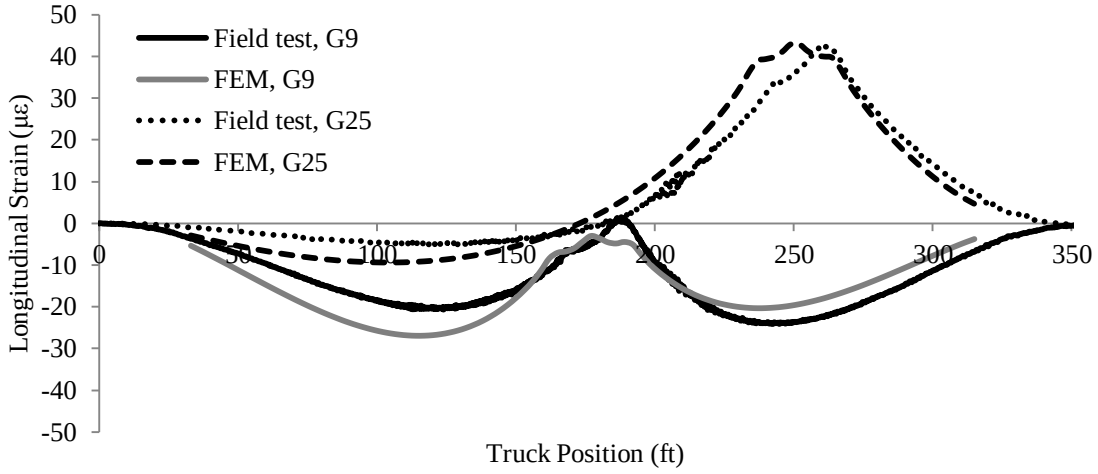

Figure 50. Strain variation of girder gauges (G9 and G25) closer to axles, (LC1)

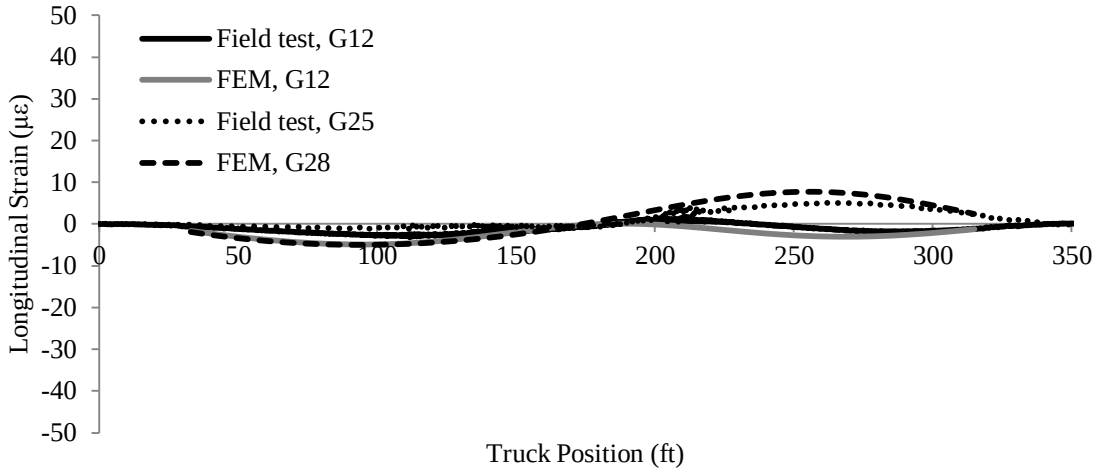

Figure 51. Strain variation of girder gauges (G12 and G28) away from axles, (LC1)

4.3.1.3 Calibration for the rosettes

Comparisons were made between the FEM and the major principal strains (ε_1) determined from field test results. According to Figure 52, there is a significant difference between the FEM and field test results of the principal strains around the pier. Other than that, the finite element model predicts the field test results of the rosettes.

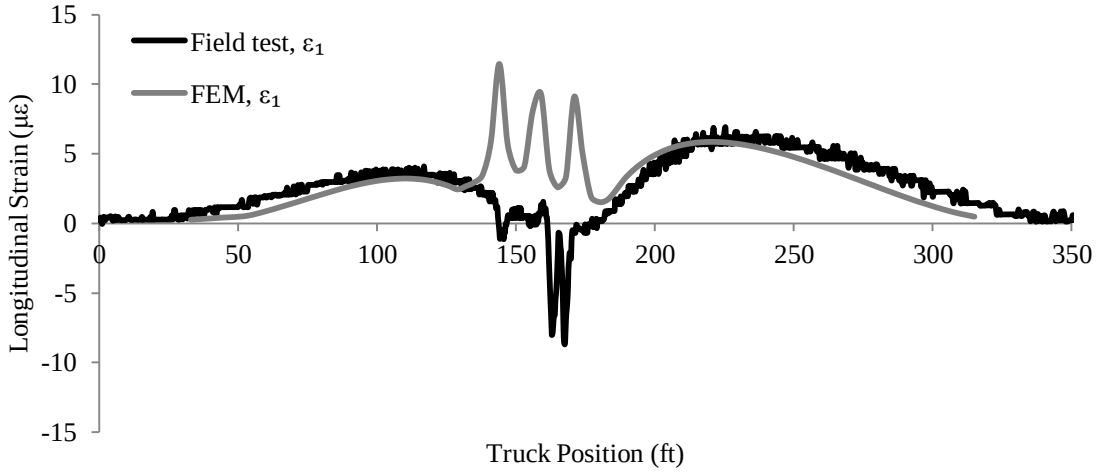

Figure 52. Variation of principal strains of rosette R2 for LC1

Collectively the above mentioned results for Bridge B show that the deck gauges had small differences and the girder gauges were in agreement with the field test results. However, in an attempt to minimize the differences further three conditions (Table 7) were in an attempt to the strain prediction within the deck.

Table 7. Calibration types of Bridge B

Type	f_c' of the deck (psi)	Boundary conditions	
		Restraint at the abutment (on piles)	Restraint at the pier (under the girders)
1	4000	U_X, U_Y, U_Z	U_Y
2	5000	U_X, U_Y, U_Z	U_Y
3	4000	U_X, U_Y, U_Z θ_X, θ_Y, θ_Z	U_Y

Figure 53 shows the comparison of the finite element results of gauge G1 for the different calibration types. No significant strain difference can be observed. Therefore, Type 1 was selected for use in the parametric study of Bridge B.

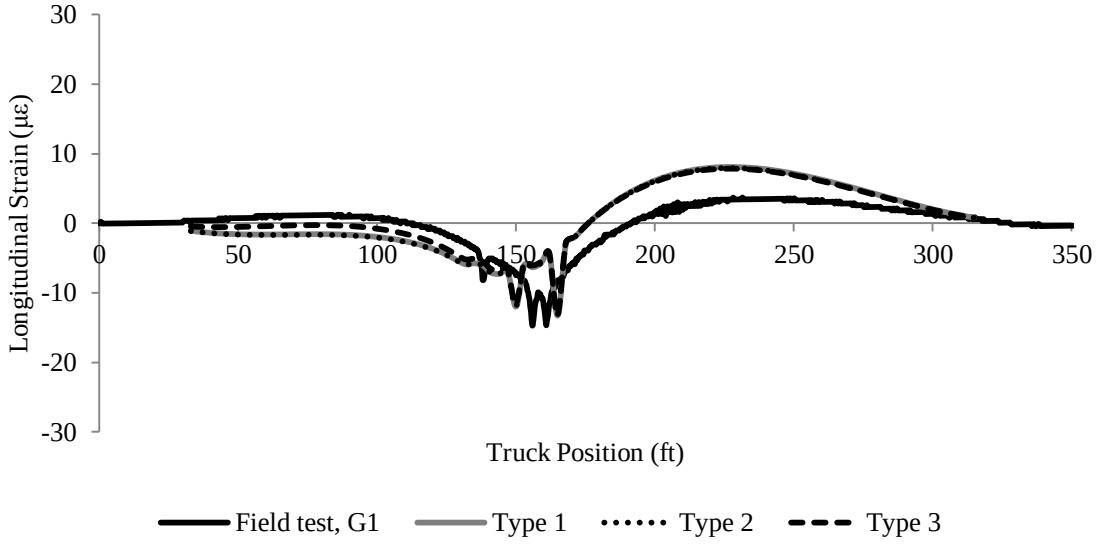

Figure 53. Strain variation of girder gauge G1 with different calibration types

CHAPTER 5. PARAMETRIC STUDY

5.1 Model Configuration

The main objective of this research project was to investigate various aspects of the so-called b2 reinforcement used in the negative moment region of PPCB bridges. To accomplish, this a parametric study was conducted using the basic model described previously. To fully understand the behavior of the bridge in multiple "states", three different model configurations were utilized: (1) Model 1 - an uncracked deck model, (2) Model 2 - cracked deck model and (3) Model 3 - cracked deck with cracked pier diaphragm model. In many ways these three models were interpretations of how several states of behavior would be translated into a theoretical model.

5.1.1 Model 1 - Uncracked deck model

The parametric study was first conducted on the calibrated bridge models which consist of fully uncracked section properties. In many ways the Model 1 configuration is based upon the field observed behavior (e.g., minimal deck cracking, etc.) and based upon previously observed behavior in similar bridges. In the following sections a detailed summary of the results associated with Model 1 will be given. However, in brief, based on the parametric study results of Bridge A with an uncracked deck model, one can conclude that negative moment b2 reinforcement does not significantly affect the behavior of the bridge deck before cracking. This is probably because the negative moment b2 reinforcement represents a very small increase in the stiffness of the uncracked concrete deck. As a result, the parametric study was continued by assuming a fully cracked deck (Model 2) in the negative moment region. The goal with Model 2 was to accentuate the contribution of the b2 bars by reducing the stiffness of the surrounding deck concrete to zero (i.e., a fully cracked state). The length, area and distribution pattern of the b2 reinforcement were the main parameters of the study.

5.1.2 Model 2 - Cracked deck model

The parametric study with a cracked deck over the pier (Figure 54) was conducted following the set of steps shown in Figure 55. The parametric study was carried out for both live load and a 56 day shrinkage load.

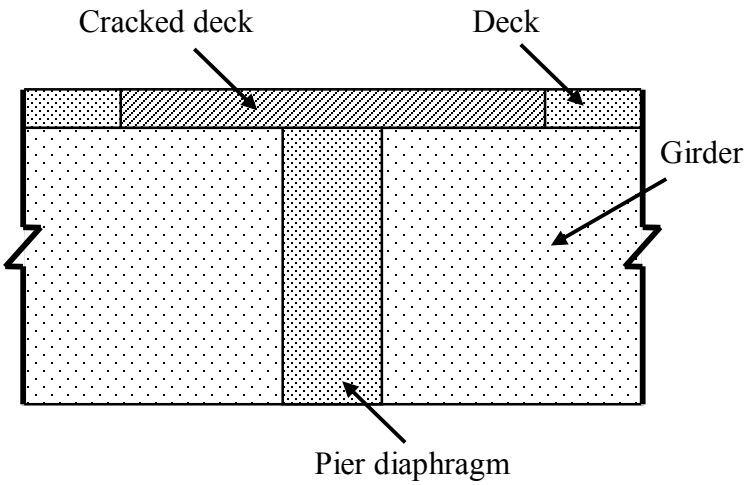

Figure 54. Cracked deck condition

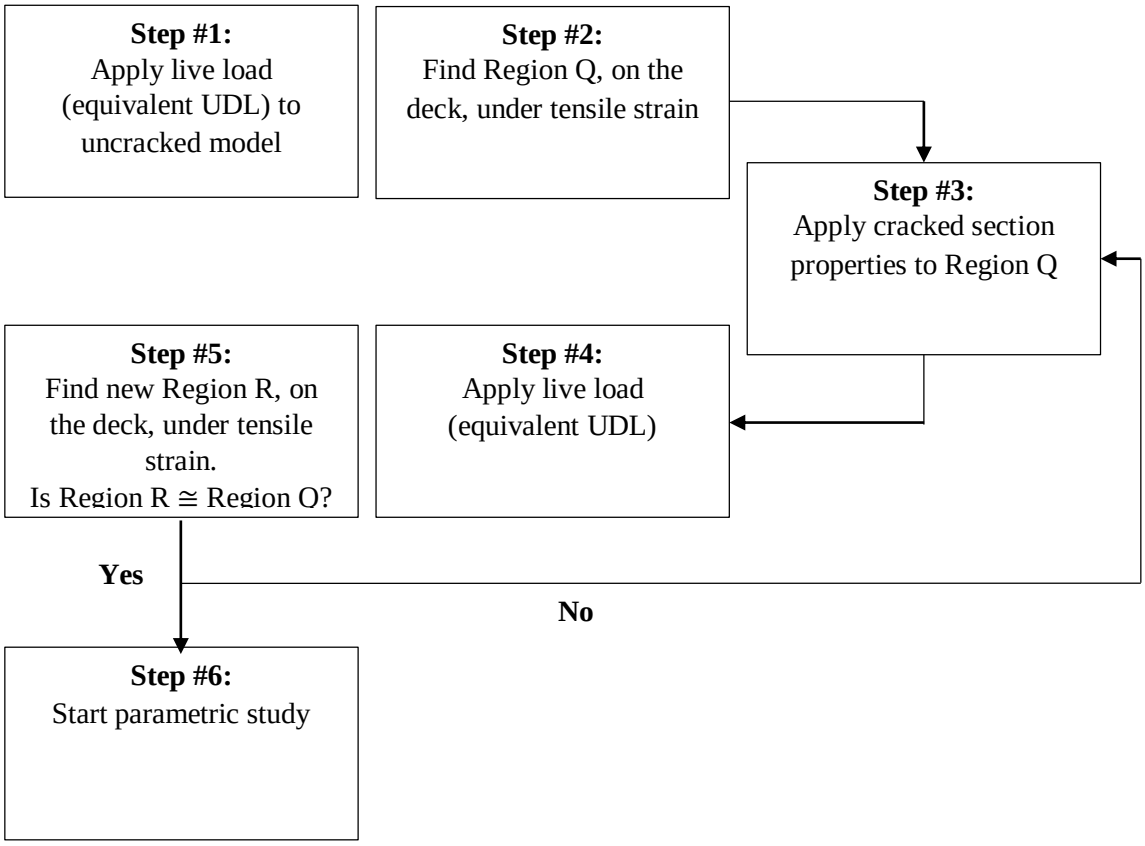

Figure 55. Method to determine cracked section

Step 1:

The equivalent UDL of 0.0004 ksi over the four lanes was used to determine the region of the deck that might experience tensile strains.

Step 2:

The longitudinal strain (ε_Z) of the bridge deck along five longitudinal lines is shown in Figure 56, which indicated that Region Q, on the deck, under tensile strain was approximately 30 ft on each side of the pier.

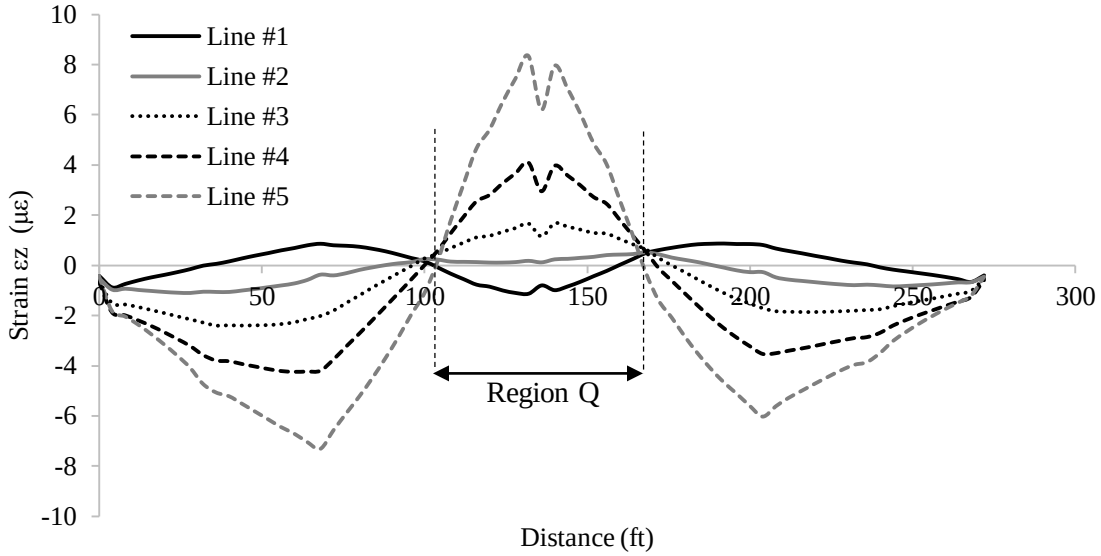

Figure 56. Negative moment region over pier

Step 3:

The effective moment of inertia of the uncracked bridge deck ($I_{Uncracked}$) and cracked deck ($I_{Cracked}$) was then calculated. The Modulus of Elasticity (E) of the uncracked bridge deck finite elements was proportioned by the $I_{Cracked}/I_{Uncracked}$ ratio (0.006) to calculate the cracked section properties for Region Q.

Step 4;

The equivalent UDL of 0.0004 ksi was again placed on the model with the updated cracked section properties in Region Q.

Step 5:

The negative bending moment region with cracked section properties (Region R) was found to be approximately equal to the negative bending moment region with

uncracked section properties (Region Q); i.e., about 30 ft to each side of the pier. Thus, it was determined that the Region Q approximation was good.

Step 6;

A parametric study of Bridge A with the cracked deck in Region Q was then conducted. The length, area and distribution pattern of the b2 reinforcement were the main parameters of the study.

5.1.3 Model 3 - Cracked deck with cracked pier diaphragm model

Following extensive discussions with the Iowa DOT, it was determined that the Iowa DOT designs the continuity connection at the pier diaphragm by assuming a fully cracked deck and diaphragm (i.e., the girders resist no tension). Therefore, a cracked deck with a cracked pier diaphragm at the pier was studied to simulate the conditions assumed during design (Figure 57). In this work it was assumed that the diaphragm had cracked to over ½ of the total girder depth.

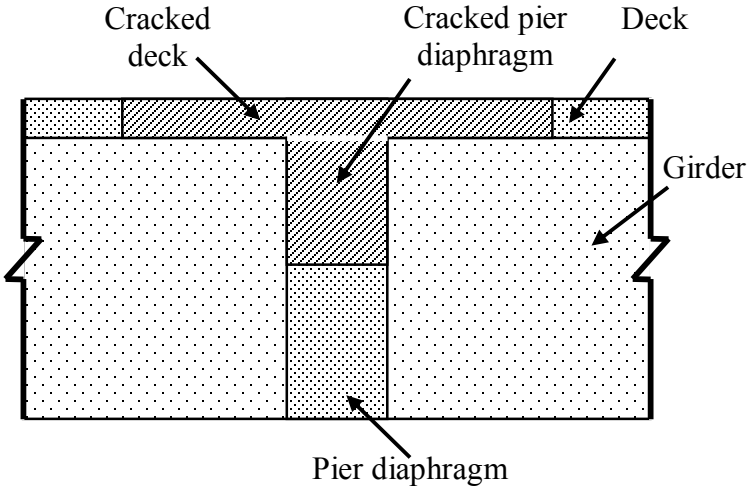

Figure 57. Uncracked deck condition

5.2 Parametric Study of Bridge A

The parametric study was conducted with live load (Equivalent UDL, CHAPTER 4) and 56 days shrinkage load (CHAPTER 4) to specifically investigate the effects of the length (L), area (A) and distribution pattern of the b2 reinforcement on the negative bending behavior of PPCB bridges. By changing the parameters, the average longitudinal

strain (ε_z) over the pier, at the 1/8 span location and at the 1/4 span location (Figure 58) were compared to formulate conclusions.

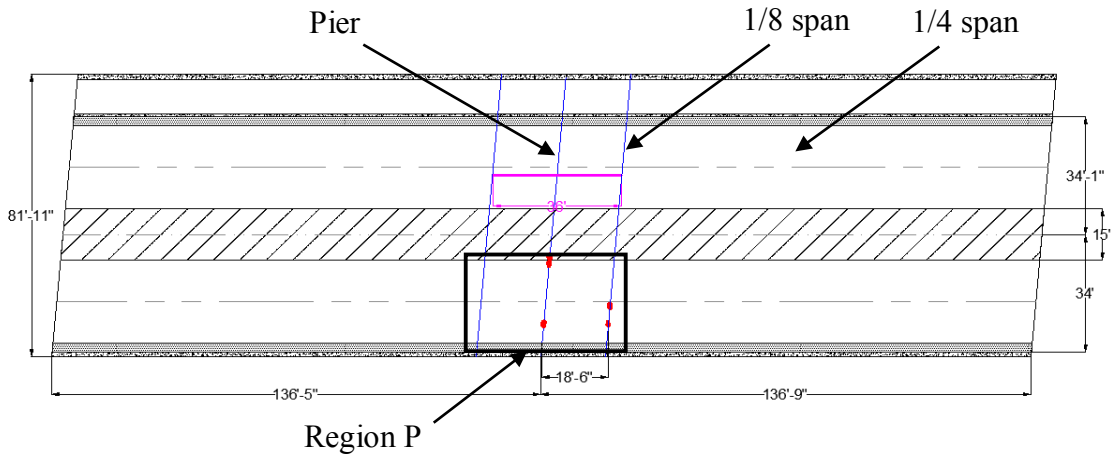

Figure 58. Parametric study region

5.2.1 Live Load

Figure 59(a) shows the major principal strain (ε_1) distribution of Bridge A with an uncracked deck (Model 1) due to the equivalent UDL. Strains are smaller than the cracking strain (Equation 3) over the pier and at the 1/8 span location of the deck. Figure 59(b) shows the ε_1 strain distribution of Bridge A with twice the length of the b2 reinforcement. The strain distribution pattern and magnitude are similar to the strain distribution for the as-built b2 reinforcement length (Figure 59(a)). The strain distribution of Bridge A with twice the b2 reinforcement area is shown in Figure 59(c). When compared with the strain distribution of the as-built b2 reinforcement area (Figure 59(a)), no significant difference can be observed. Figure 59(d) shows the ε_1 strain distribution of Bridge A with 36 ft and 72 ft staggered b2 reinforcement. When compared with the strain distribution of the as-built b2 reinforcement distribution pattern (Figure 59(a)), no significant difference can be observed.

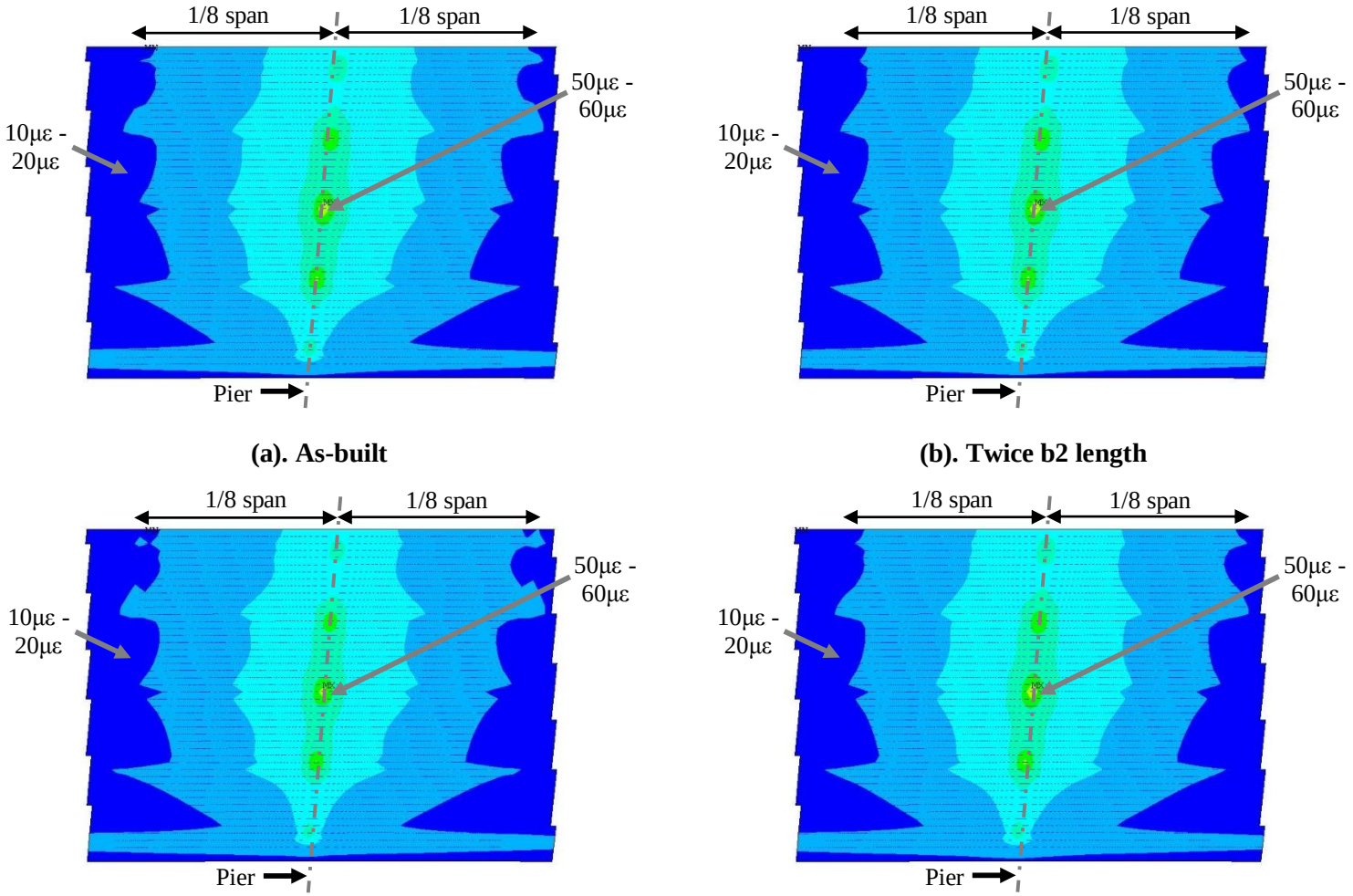

Figure 59. Variation of ε_1 of Bridge A of Model 1, Load = Equivalent UDL

Table 8 illustrates the average longitudinal strains (ε_z) at three different locations on Bridge A with the as-built properties, twice the length, twice the area, and a staggered distribution pattern of the b2 reinforcement using the three different, previously described models under live load (Equivalent UDL, CHAPTER 4). Compared to Model 1, much higher strains were observed on the top surface of the bridge deck of Model 2 and Model 3. As can be seen sometimes the strains are much larger than the cracking strain (130 με) indicating that it may be possible to develop cracks. Further, these analysis result would seem to indicate that once cracking starts (i.e., you move from Model 1 condition to Model 2 condition to Model 3 condition) that cracks could be expected to continue to develop and grown. This may be true even without an increase in external loads. In general the higher strains over the pier and girders (regardless of the model type) would seem to indicate a higher density of cracks and/or wider cracks occurs in these areas. As one would expect the parametric study results under live load indicate higher tensile strains over the pier for all model configurations. Further, at the 1/8 span location, the results indicate an approximately 20% to 30% lower tensile strains than those at the pier. Even further, at the 1/4 span the deck appears to be in compression under the simulated live load.

The length of the b2 reinforcement was changed into twice the as-built b2 reinforcement length to investigate the effect of the b2 reinforcement length. Recall that the as-built b2 reinforcement was terminated at the 1/8 span location. Therefore termination point of the b2 reinforcement with twice the initial length would be at 1/4 span location from the pier. Compared to the results from the as-built condition, Model 1 does not show a significant different difference due to a lengthening of the b2 reinforcement. Model 2 and Model 3 show a significant reduction in average longitudinal strain only at the 1/8 span location.

The effect of the b2 reinforcement area was studied by doubling the as-built b2 reinforcement area. Due to the change of b2 reinforcement area no significant strain difference is observed over in Model 1. Compared to the as-built condition, Model 2 and Model 3 show a small reduction of longitudinal strain over the pier.

The b2 reinforcement was terminated at 1/8 span and 1/4 span locations to develop the staggered reinforcement distribution pattern. Recall that the as-built b2 reinforcement

distribution pattern was consist of uniform b2 reinforcement which are terminated at 1/8 span location. Compared to the as-built condition no noticeable strain difference were found in Model 1. Average longitudinal strains only at 1/8 span location were increased in Model 2 and Model 3.

Table 8. Average longitudinal strain (με) of Bridge A due to the live load

parameter	Model 1			Model 2			Model 3		
	Pier	1/8 span	1/4 span	Pier	1/8 span	1/4 span	Pier	1/8 span	1/4 span
As-built	26.0	6.5	-9.0	196.8	39.3	-12.4	304.2	94.2	-12.1
Twice length	26.0	6.2	-8.7	198.3	8.5	-11.8	258.6	6.0	-14.1
Twice area	24.9	6.6	-8.8	152.1	48.9	-12.2	196.7	56.5	-14.0
Staggered b2 at 1/8	26.0	6.4	-8.9	197.8	22.1	-12.1	258.5	20.7	-14.5

5.2.2 Shrinkage Load

To investigate the effect of the b2 reinforcement, a shrinkage load at 56 days (CHAPTER 4) was applied to the bridge deck. As shown in Figure 60(a), strains over the pier and at the 1/8 span location of the b2 reinforcement are in the vicinity of the cracking strain of the concrete (Equation 3). Figure 60(b) presents the strain distribution with twice the length of b2 reinforcement. Compared to Figure 60(a), no significant strain difference is observed over the pier. Little difference can be found at the 1/8 span location of the b2 reinforcement. The strain distribution of Bridge A with twice the b2 reinforcement area is shown in Figure 60(c). Compared with Figure 60(a), there is no noticeable difference between the strain distributions. The major principal strain distribution of Bridge A with staggered b2 reinforcement area is shown in Figure 60(d). Compared to Figure 60(a), no

significant strain difference can be found over the pier. Small differences can be found at the 1/8 span location of the b2 reinforcement.

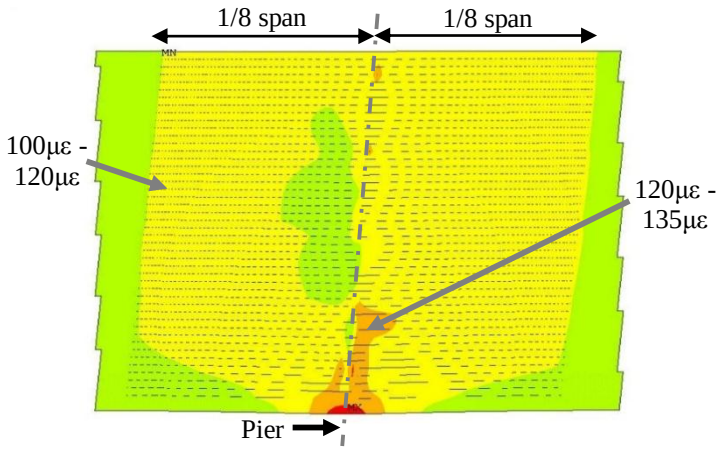

(a). As-built

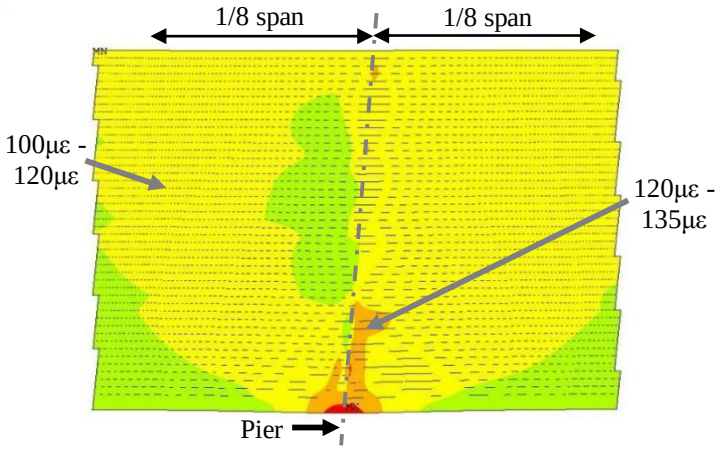

(b). Twice b2 length

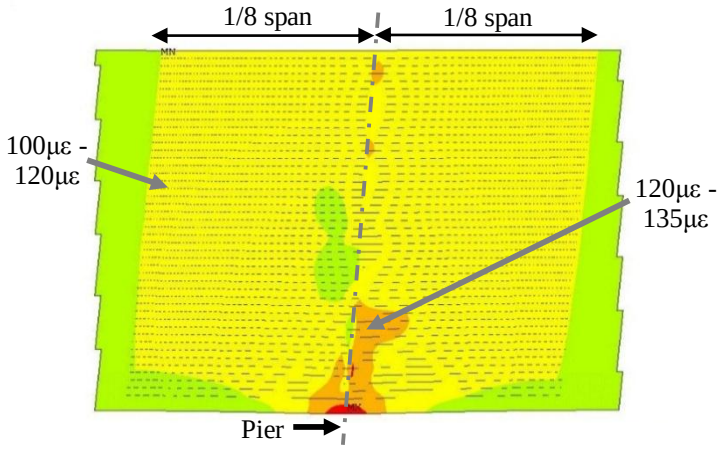

(c). Twice b2 area

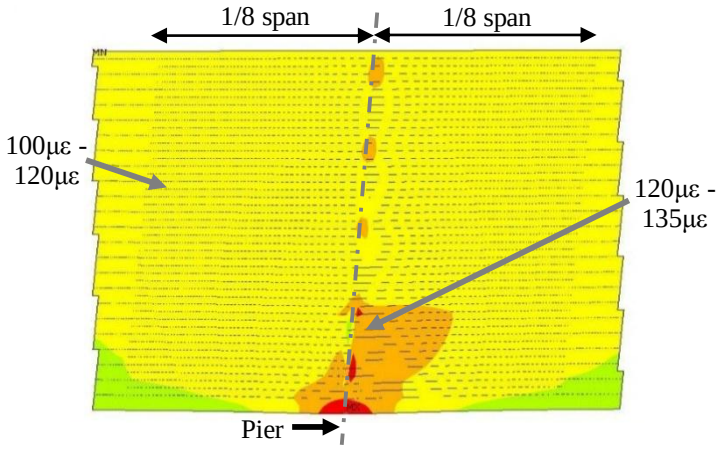

(d). Staggered b2 pattern

Figure 60. Variation of ε_1 of Bridge A of Model 1, Load = Shrinkage (56 days)

Table 9 presents the average longitudinal strains (ε_z) at three different locations on Bridge A with the as-built properties, twice the length, twice the area, and staggered distribution pattern of the b2 reinforcement using the three different, previously described models for 56 days shrinkage load (CHAPTER 4). Similar to the live load study results, the parametric study results of Model 1 due to the 56 days shrinkage load does not significantly affect the behavior of the bridge. Results shows the tensile strains with the highest strain occurring at the 1/8 span location. Compared to the results from the as-built condition, a change in b2 reinforcement length with either Model 2 or Model 3 shows a significant reduction in average longitudinal strain only at 1/8 span location. Whereas no significant difference can be observed due to the change in b2 reinforcement area or pattern of Model 2 and Model 3.

Table 9. Average longitudinal strain (με) of Bridge A due to 56 days shrinkage load

parameter	Model 1			Model 2			Model 3		
	Pier	1/8 span	1/4 span	Pier	1/8 span	1/4 span	Pier	1/8 span	1/4 span
As-built	86.2	103.0	96.0	112.2	218.2	52.3	174.6	254.8	52.4
Twice length	85.7	106.9	97.1	127.1	187.1	57.8	161.0	185.9	56.3
Twice area	87.4	106.6	95.6	107.7	227.9	52.5	130.3	233.9	51.3
Staggered b2 at 1/8	85.9	106.4	96.4	121.5	225.3	55.0	155.2	225.2	53.4

5.2.3 Summary

A parametric study of Bridge A was conducted by changing the length, area and distribution pattern of the b2 reinforcement. Three different types of conditions, namely: (1) Model 1 -Uncracked deck, (2) Model 2 - Cracked deck and (3) Model 3 - Cracked deck with cracked diaphragm, were used in the study of the strain distribution and magnitude in the negative bending moment region. The bridge with the uncracked deck showed no significant difference in the strain distribution due to the live load and

the 56 days shrinkage load. Both the cracked deck and the cracked deck with cracked pier diaphragm models show similar strain distributions, except that the cracked deck with cracked pier diaphragm condition shows slightly larger strains over the girders. The results show that an increase of b2 reinforcement area reduces the strain magnitudes over the pier, whereas an increase of length of the b2 reinforcement decreases the strain level at the 1/8 span location of the b2 reinforcement. The staggered b2 reinforcement distribution pattern also reduces the strains at the 1/8 span location of the b2 reinforcement.

5.3 Parametric Study of Bridge B

The parametric study of Bridge B was conducted similar to the parametric study of Bridge A by changing the length (L), area (A) and distribution pattern of the b2 reinforcement and considering the differences in behavior under live load (Equivalent UDL, CHAPTER 4) and 56 days shrinkage load (CHAPTER 4).

5.3.1 Live Load

Figure 61 shows the major principal strain distribution around Region P (Figure 58) of the uncracked Bridge B due to live load. Comparing Figure 59 with Figure 61, one can observe a significant reduction of strain over the pier. Also of importance is to note that the strains are lower than the cracking strain (Equation 3) over the pier and at the 1/8 span location of the deck. Figure 61 (b), (c), (d) show the ε_1 strain distribution of Bridge B with twice the length, twice the area and staggered b2 reinforcement at 1/4 span and 1/8 span locations respectively. When compared with the strain distribution of the as-built b2 reinforcement condition (Figure 61(a)), no significant difference can be observed.

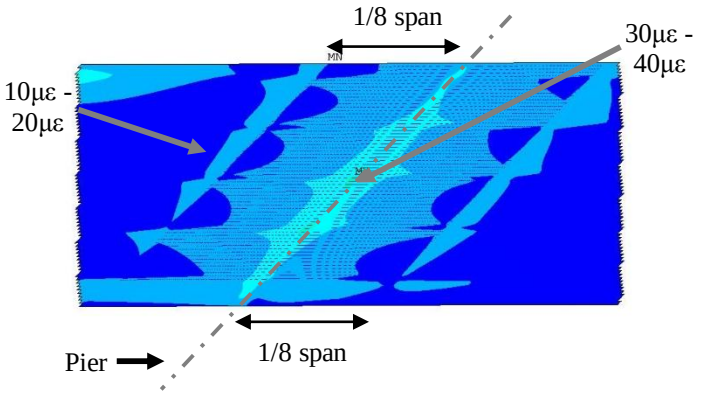

(a). As-built

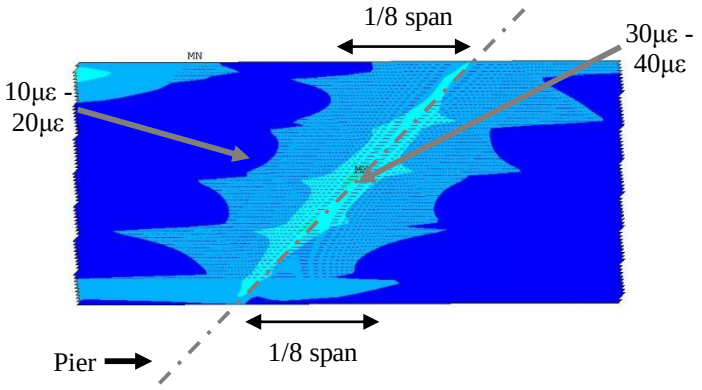

(b). Twice b2 length

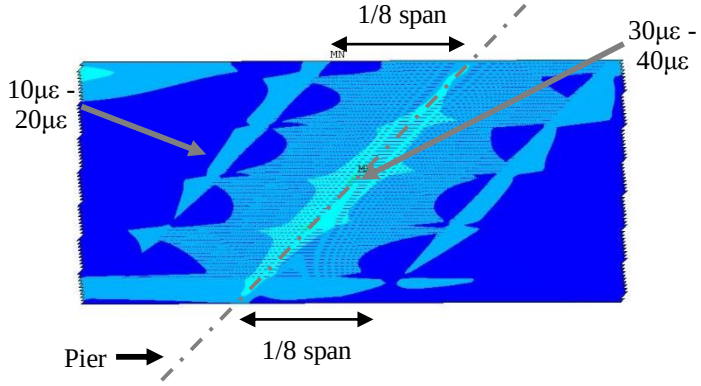

(c). Twice b2 area

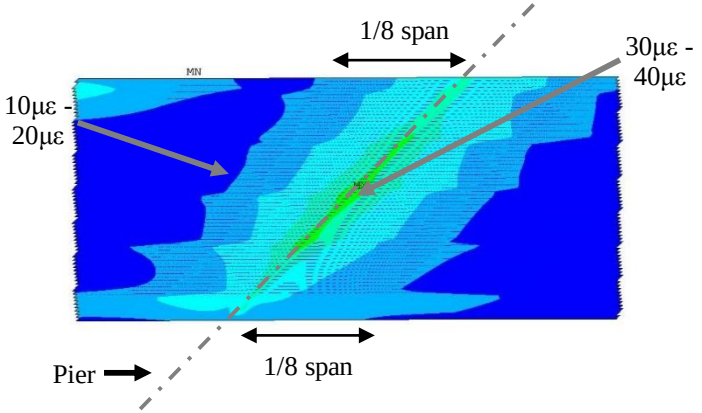

(d). Staggered b2 pattern

Figure 61. Variation of ε1 of Bridge B of Model 1, Load = Equivalent UDL

Table 10 present the average longitudinal strains (ε_z) at three different locations on Bridge B with the as-built properties, twice the length, twice the area, and a staggered distribution pattern of the b2 reinforcement for the previously described three different models under live load (Equivalent UDL, CHAPTER 4). Similar to Bridge A results, compared to Model 1, much higher strains were observed on the top surface of the bridge deck of Model 2 and Model 3, indicating possible crack development (depending upon whether one initially assume cracking or not). The parametric study results under live load indicate higher tensile strains over the pier for all model configurations. At the 1/8 span location, the results indicate an approximately lower tensile strains than those at the pier. Whereas at the 1/4 span the deck appears to be in compression under the simulated live load. Similar to Bridge A parametric study results, changing the b2 reinforcement parameters does not show a significant difference when Model 1 is used. Twice the b2 reinforcement length show a significant reduction in average longitudinal strain only at the 1/8 span location for Model 2 and Model 3. Compared to the as-built condition, Model 2 and Model 3 show a small reduction of longitudinal strain over the pier due to doubling the as-built b2 reinforcement area. Compared to the as-built condition, the staggered b2 reinforcement pattern shows lower longitudinal strains only at 1/8 span location in Model 2 and Model 3.

Table 10. Average longitudinal strain (με) of Bridge B due to the live load

parameter	Model 1			Model 2			Model 3		
	Pier	1/8 span	1/4 span	Pier	1/8 span	1/4 span	Pier	1/8 span	1/4 span
As-built	15.4	9.8	-4.8	31.6	76.2	-33.2	37.8	82.1	-35.4
Twice length	15.4	6.6	-3.2	33.2	2.0	4.2	39.1	1.8	7.2
Twice area	15.4	9.8	-4.8	31.6	76.2	-33.2	37.8	82.1	-35.4
Staggered b2 at 1/8	24.3	10.3	-6.1	160.9	31.1	-34.8	219.4	32.9	-49.3

5.3.2 Shrinkage Load

A simulated shrinkage load at 56 days was also applied to Bridge B as part of the parametric study. Figure 62 presents the strain distribution around the negative moment region (Region P). Compared to Figure 60, a small increase in strain magnitude over the pier can be observed. The parametric study was carried out by changing the length (L) Figure 62(b), area (A) Figure 62(c) and distribution pattern of the b2 reinforcement Figure 62(d). No significant differences were observed.

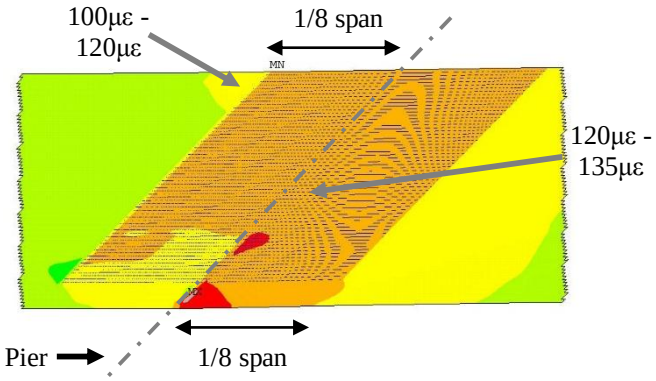

(a). As-built

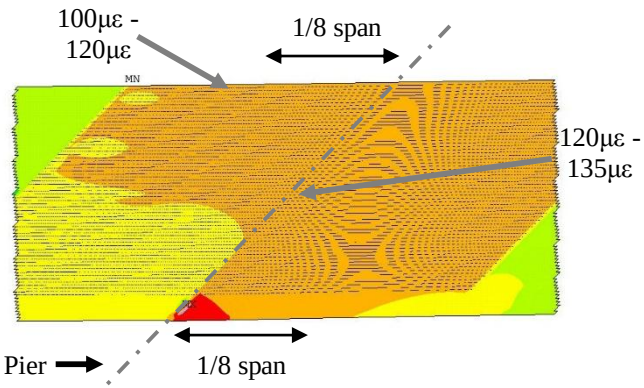

(b). Twice b2 length

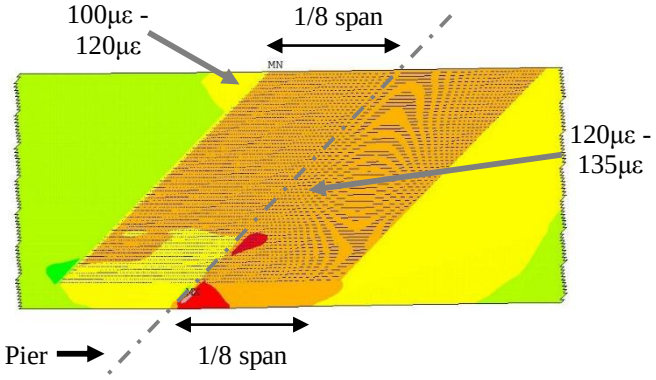

(c). Twice b2 area

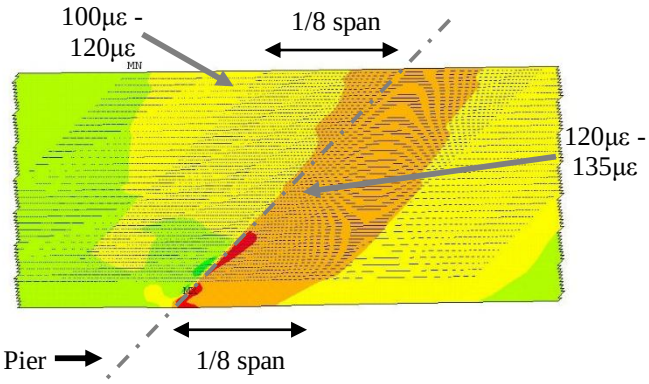

(d). Staggered b2 pattern

Figure 62. Variation of ε1 of Bridge B of Model 1, Load = Shrinkage (56 days)

Table 11 shows the average longitudinal strains (ε_z) at three different locations on Bridge B for the previously described models due to the 56 days shrinkage load (CHAPTER 4). The parametric study results of Model 1 due to the 56 days shrinkage load does not significantly affect the behavior of the bridge. Due to the shrinkage load higher tensile strains were observed at the 1/8 span location. Compared with the as-built condition, twice b2 reinforcement length of either Model 2 or Model 3 shows a significant reduction in average longitudinal strain only at 1/8 span location. Whereas no significant difference can be observed due to the change in b2 reinforcement area or pattern of Model 2 and Model 3.

Table 11. Average longitudinal strain (με) of Bridge B due to 56 days shrinkage load

parameter	Model 1			Model 2			Model 3		
	Pier	1/8 span	1/4 span	Pier	1/8 span	1/4 span	Pier	1/8 span	1/4 span
As-built	78.8	118.4	100.3	95.1	239.4	235.7	97.4	242.4	234.6
Twice length	76.9	124.5	107.9	97.6	146.7	479.2	99.8	146.6	480.7
Twice area	78.8	118.4	100.3	95.1	239.4	235.7	97.4	242.4	234.6
Staggered b2 at 1/8	73.6	114.7	102.6	112.0	196.5	351.4	138.1	197.5	343.9

5.3.3 Summary

Bridge B was used to study the effect of skew angle on the negative moment of the PPCB bridge decks. The parametric study of Bridge B was conducted similar to the parametric study of Bridge A. The results are similar, except that Bridge B shows smaller strains over the pier due to the live load. However, compared to Bridge A, a slight increase in strains over the pier, due to 56 days shrinkage load of Bridge B, can be observed.

CHAPTER 6. EVALUATION OF SECONDARY MOMENTS OF BRIDGE A

6.1 Calculation of Secondary Moments Based on PCA Method

Multi-span PPCB bridges made continuous for live load have been shown to be effective in reducing construction and maintenance costs, while also typically improving ride quality. As discussed in CHAPTER 1, construction of this type of bridges involve two primary stages. During the first stage, the PPCB girders are placed on supports (Figure 63(a)) and they behave like a simply supported structure. After the concrete deck is placed and fully cured, the bridge moves to the second stage and it behaves like a fully continuous structure over the intermediate support (Figure 63(c)).

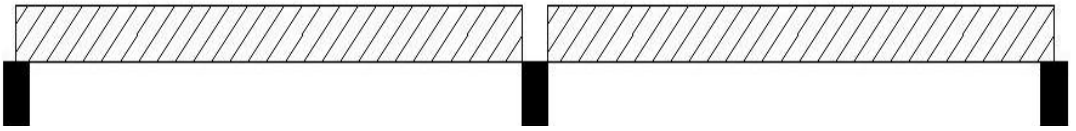

(a) Pre-stressed girders on sub-structure

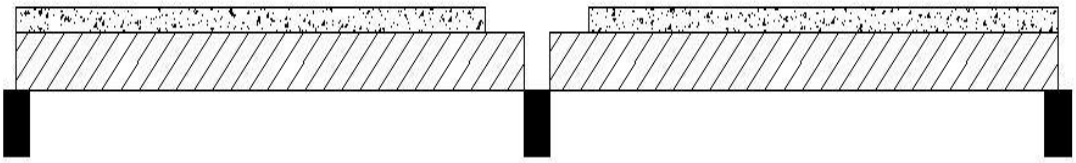

(b) Negative moment reinforcement over pier

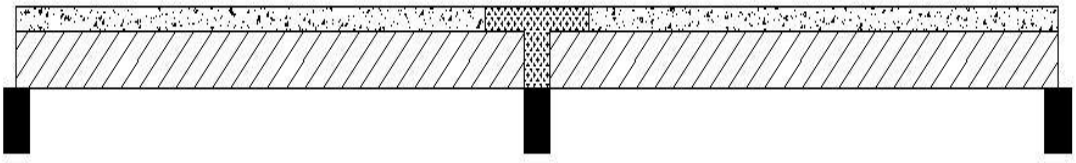

(c) After the cast-in-place deck placement

Figure 63. Construction sequence of PPCB bridge decks [17]

During the first stage the pre-stressed girders experience upward deformation, mainly due to creep of the pre-stressing force (Figure 64(a) and Figure 64(b)), which is partially counteract by the dead load creep. After the continuity connection is made, upward creep deformation will continue and ultimately induce a positive moment at the continuity connection over the pier (Figure 64(c) and Figure 65).

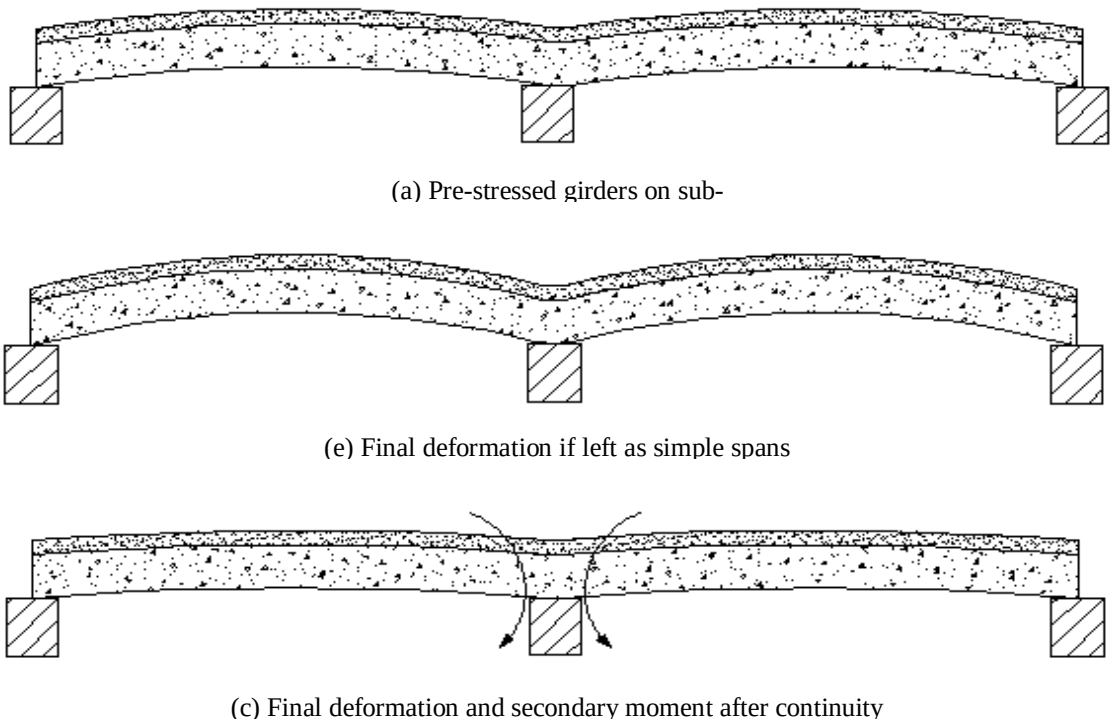

Figure 64. Development of deformations and restraint moments in a two-span continuous beam [17]

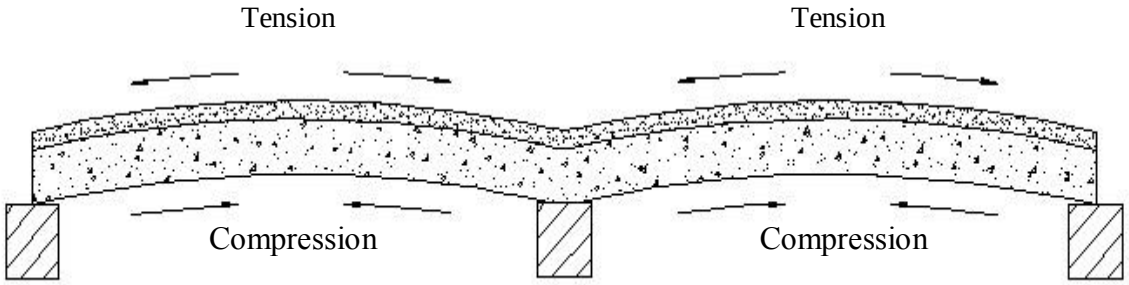

Figure 65. Secondary positive moment due to creep [23]

After the concrete deck placement, differential shrinkage occurs between the concrete deck and girders due to the age difference of the concrete. This situation creates a negative secondary moment at the continuity connection (Figure 66).

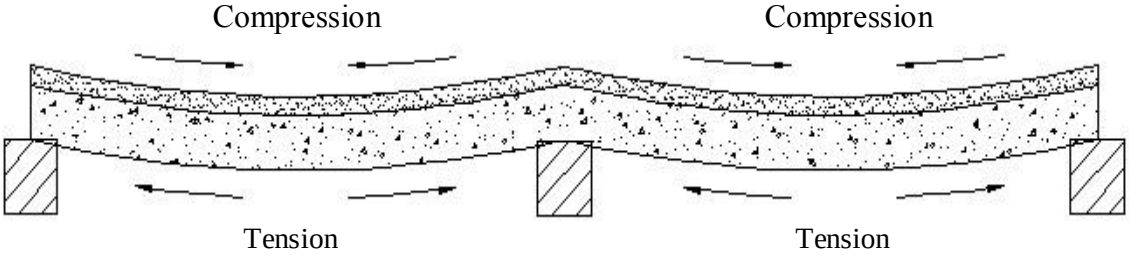

Figure 66. Secondary negative moment due to differential shrinkage [23]

According to the Michael D McDonagh et al. [13] in a PCA report [14], when combined and summed these secondary moments from creep and differential shrinkage may reduce the total moment at the continuity connection – even to the point where the regions over the pier never experience a total negative moment. It is further suspected that the reduction of total negative moment due to the secondary positive moment effects might move the point of inflection and reduce the amount and extent of deck cracking in the regions over and near the piers. To illustrate the general impact of considering secondary moments during bridge design, the calculation of the secondary moments at the intermediate support of an interior girder of Bridge A (on Meredith Drive, over I35/80) is presented in the following sections. The reader is advised to consider the impact these secondary moments might have on the design of negative moment b2 reinforcement.

6.1.1 Design Data

The calculations shown in the following subsections follow the method summarized by the PCA report mentioned above. As with any such calculation, there are several important pieces of design information needed. The information below, which was taken from the Bridge A plans and other sources, provides the information needed.

Material properties

Material properties	Value / (psi)
Deck concrete strength at 28 days	4,000
Diaphragm concrete strength at 28 days	4,000
Pre-stressed concrete girder strength at release	8,000
Pre-stressed concrete girder strength at 28 days	9,000

Section properties

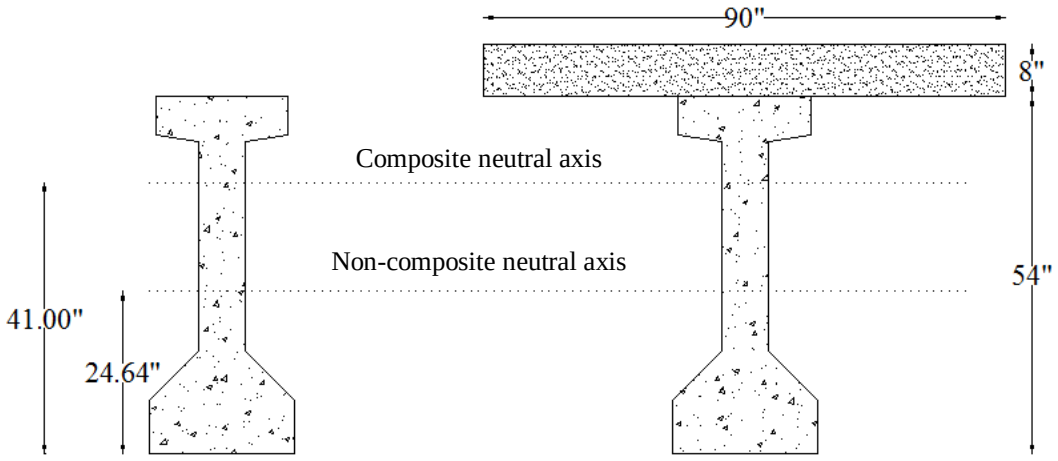

(a) Non-composite section (b) Composite section

Figure 67. Section properties

Section properties	Non-composite	Composite
Area, A (in^2)	748.8	1468.8
Neutral axis from bottom, Y_b (in)	24.64	41.00
Moment of inertia, I (in^4)	285860	

Pre-stressing properties (Provided by the Iowa DOT)

Pre-stressing steel area (in^2/strand)	0.28
Initial per-stress (ksi/strand)	196
Final per-stress after losses (ksi/strand)	165
Final pre-stressing force after losses (kip/strand)	46.7
No. of strands, Draped	14
No. of strands, Straight	42
P_1 (kip)	653.8
P_2 (kip)	1961.40
P_3 (kip)	70.51

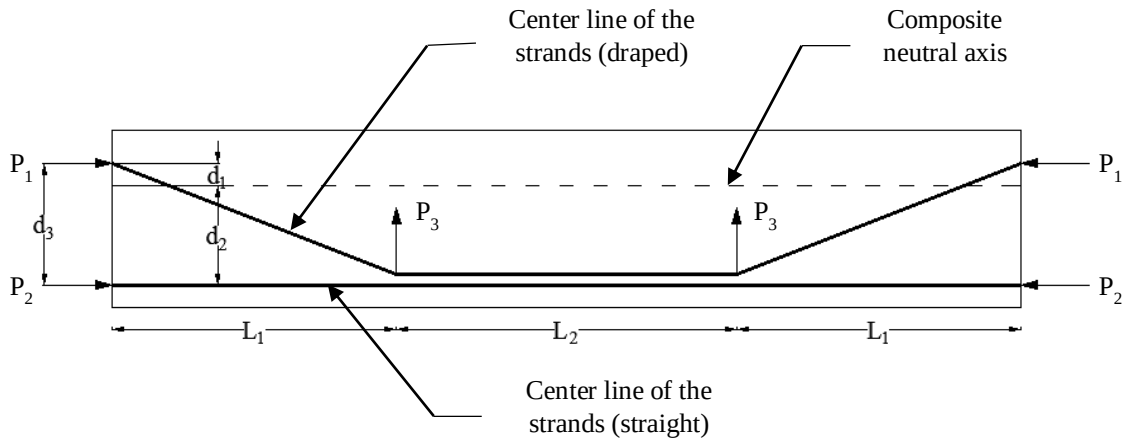

Figure 68. Tendon profile

L_1 = 54.5 ft	L_2 = 27.0 ft	L = 136.0 ft
d_1 = 8.0 in.	d_2 = 41.0 in.	d_3 = 46.0 in.

6.1.2 Design Assumptions

For the calculations summarized below it has been assumed that the pre-stressing force was released 2 days after concrete placement. Further, it was assumed that the continuity connection was constructed 28 days after the pre-stress was applied. As should be clear, these represent important "dates" and deviation from them can have a notable impact on the results.

6.1.3 Calculation of Positive Secondary Moment at Intermediate Support

As discussed earlier, the secondary positive moments for Bridge A occur due to creep of the pre-stressed girders (M_C). Further, the creep due to the pre-stressed force (M_{C1}) is in the opposite direction to the creep due to dead load (M_{C2}). Calculation of each of these components using elastic structural analysis considering monolithic behavior of the deck and girders are given below.

6.1.3.1 Due to the Pre-Stressed Force Creep

Slope due to the pre-stressing force (Figure 69(a)) at the intermediate support for a simple span beam is determined using the M/EI diagram. A similar method can be used to calculate the slope at the intermediate support due to the restraining moment (Figure 69(b)).

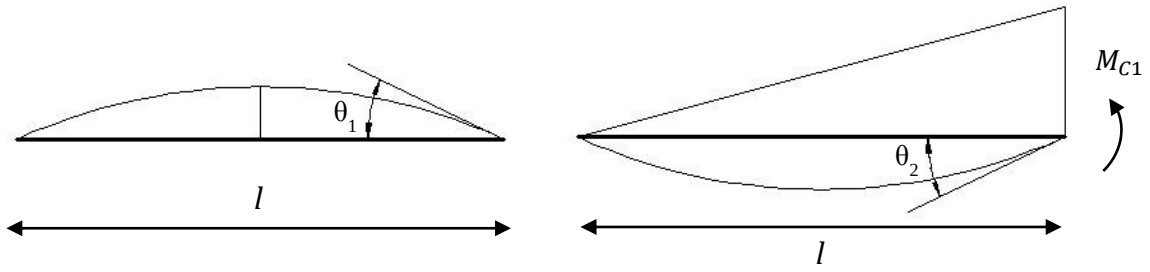

(a) Slope due to pre-stressing force (b) Slope due to secondary moment, M_{C1}

Figure 69. Variation of slope due pre-stressing creep [14]

$$\theta_1 = \frac{1}{2EI}(P_1 d_1 L - P_2 d_2 L - P_3 L_1^2 - P_3 L_1 L_2) \qquad \theta_2 = -\frac{M_{C1} L}{3EI}$$

These slopes should be equal and opposite to ensure that equilibrium and compatibility are maintained. Therefore, the secondary moment due to pre-stressing creep is,

$$M_{C1} = -\frac{3EI}{L}(\theta_1)$$

$$\theta_1 = \frac{1}{2EI}(P_1 d_1 L - P_2 d_2 L - P_3 L_1^2 - P_3 L_1 L_2)$$

$$= \frac{-148870260}{2EI}$$

Positive secondary moment at intermediate support due to pre-stressed creep, M_{C1}

$$= -\frac{3EI}{L}(\theta_1)$$

= 11928.7 kip-ft

6.1.3.2 Due to the Dead Load Creep

Slope due to dead load creep (Figure 70(a)) and due to the secondary moment (M_{C2}) (Figure 70(b)) at the intermediate support for a simple span beam can similarly be determined from the M/EI diagram.

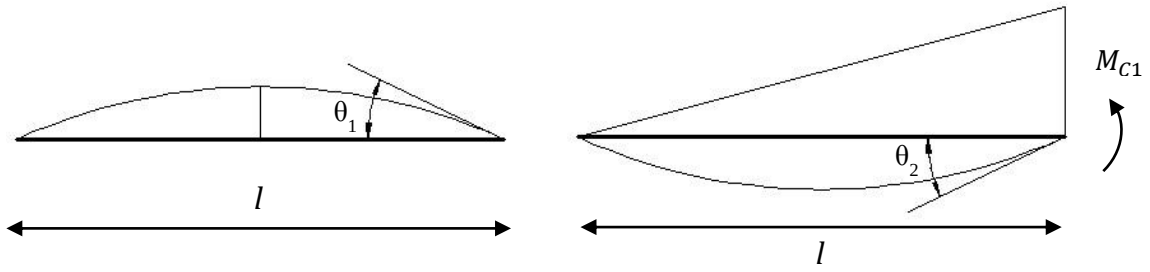

(a) Slope due to pre-stressing force (b) Slope due to secondary moment, M_{C1}

Figure 70. Variation of slope due dead load creep [14]

$$\theta_3 = \frac{M_D L}{3EI} \qquad \theta_4 = -\frac{M_{C2} L}{3EI}$$

Once again, after the continuity connection made, these slopes should be equal and opposite to ensure equilibrium and compatibility are maintained. Therefore, the secondary moment due to dead load creep is,

Dead load moment at mid-span, M_D	M_{C2}	$= -M_D$
	Girder	$= \frac{748.8}{144} \times 0.150 \times \frac{136^2}{8}$
		= 1803.36 kip-ft
	Deck	$= \frac{90 \times 8}{144} \times 0.150 \times \frac{136^2}{8}$
		= 1734.00 kip-ft
	Total	= 1803.36 + 1734.00
		= 3537.36 kip-ft
Positive secondary moment at intermediate support due to dead load creep, M_{C2}		= -1.0 × 3537.36
		= -3537.36 kip-ft

6.1.4 Calculation of Negative Secondary Moment at Intermediate Support

As discussed earlier, a negative secondary moment due to differential shrinkage between the cast-in-place deck and the concrete girders is also created in PPCB. According to the PCI report the negative secondary moment can be calculate by the following.

$$M_S = \epsilon_g \times E_b \times A_b \times \left(e_2' + \frac{t}{2}\right)$$

Where,

ϵ_g = Differential shrinkage strain

E_b = Elastic modulus of the concrete deck

A_b = Cross-sectional area of the concrete deck

$\left(e_2' + \frac{t}{2}\right)$ = Distance between the mid-depth of the slab and centroid of the composite section

t = Thickness of the concrete deck

According to the PCA report, in the lack of test data the ultimate shrinkage at 50% relative humidity can be taken as 0.0006 in. / in., in post construction analyses it should ideally be corrected with the shrinkage humidity correction factor (Figure 10, [23]) that accounts for the actual conditions present and final creep/shrinkage adjustment factor (Figure 8, [23]), which allows to accommodate the amount of deck shrinkage has already take place since the deck placement at the time the post-construction analysis is completed.

Final creep/shrinkage adjustment factor (Figure 8, [23])	= 0.4
Shrinkage humidity correction factor (Figure 10, [23])	= 1.0
ϵ_g	$= 1.0 \times 0.4 \times 0.0006$
	= 0.00024 in. / in.
Negative secondary moment at intermediate support due to pre-stressed creep, M_S	$= \frac{0.00024 \times 3605000 \times 720 \times 17}{1000 \times 12}$
	= 882.50 kip-ft

6.1.5 Calculation of Creep Factors

The factor ϕ is defined as the ratio of creep strain to elastic strain. The factor ϕ describes the amount of creep strain still to occur compared with the original elastic strain.

$$\phi = \frac{\in_{Creep}}{\in_{Elastic}} = \in_{Creep} \times E$$

Where,

$\in_{Creep}$ = Creep strain

E = Elastic modulus at the continuity connection established

In most design work, the elastic modulus is used to predict the creep value for the concrete mix at 28 days (Figure 5, [23]). Further, the 20 year creep value is typically taken as the ultimate creep of the concrete.

Elastic modulus at strand release	= 5407494.80 psi
Specific creep at 20 years (Figure 5, [23])	$= 0.16 \times 10^{-6}$ in. / in. / psi

As mentioned before, if a post-construction analysis is ever completed the specific creep value should be adjusted with pre-stressed release adjustment factor (Figure 6, [23]) to account for the time when the girders were pre-stressed. In this sample calculation it was assumed that the pre-stressing force was released at 2 days after casting of the girders. In this sample calculation it was assumed that the continuity connection was constructed 28 days after the pre-stress was applied. The pertinent adjustment factors are then:

Pre-stressed release adjustment factor (Figure 6, [23])	= 1.66
Volume / surface adjustment factor (Figure 7, [23])	= 1.20
Final creep/shrinkage adjustment factor (Figure 8, [23])	= 0.6

Therefore, final creep strain and the factor ϕ can be calculated as follows.

$$\in_{Creep} = 0.6 \times 1.20 \times 1.66 \times 0.16 \times 10^{-6}$$

$$= 0.191 \times 10^{-6} \text{ in. / in. / psi}$$

$$\phi = 0.191 \times 10^{-6} \times 57000 \times \sqrt{9000}$$

$$= 1.03$$

Having the factor ϕ evaluated, the Creep factor, $\left(1 - e^{-\phi}\right)$ and the Shrinkage factor, $\left(\frac{1-e^{-\phi}}{\phi}\right)$ can be calculated as follows.

$$\text{Creep factor, } \left(1 - e^{-\phi}\right) = (1 - e^{-1.03})$$

$$= 0.64$$

$$\text{Shrinkage factor, } \left(\frac{1-e^{-\phi}}{\phi}\right) = \left(\frac{1-e^{-1.03}}{1.03}\right)$$

$$= 0.62$$

6.1.6 Final Secondary Moment

According to the PCA report the resultant secondary moments can be calculated as follows.

$$M_{\text{Final, Secondary}} = (M_{C1} - M_{C2}) \times \left(1 - e^{\phi}\right) - M_S \times \left(\frac{1-e^{\phi}}{\phi}\right)$$

$$M_{\text{Final, Secondary}} = (11928.7 - 3537.36) \times 0.64 - 882.50 \times 0.62 + 0$$

$$= 4823.3 \text{ kip-ft}$$

6.1.7 Live Load Moment

The negative moment at the intermediate support of Bridge A due to the live load was calculated using BEC Analysis program (A live load structural analysis program for bridge structures). In this case Bridge A was treated as a two span continuous beam (Figure 71) having a composite deck girder cross-section as shown in Figure 67. As shown in Figure 71, HS 20 truck load was used for the analysis. The live load negative moment over the intermediate support of Bridge A was calculated as -922.71 kip-ft.

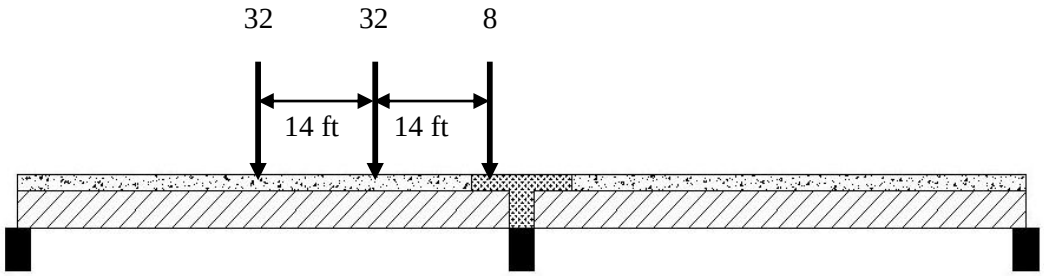

Figure 71. Simplified model of Bridge A used to calculate live load negative moment

According to the calculated secondary moments based PCA method, five times larger positive moments due to secondary effects than the live load negative moment was observed to exist at the intermediate pier. This imply that the secondary moments play an important role of the structural behavior of PPCB bridges. Usually, the negative moment deck reinforcement design based on the live load negative moments at the intermediate support only. Therefore, if one can take advantage of the fact that these secondary moments are present, lesser amount of negative moment reinforcement will be expected. It may even be possible that the deck over the piers may never actually experience tensile stresses. However this secondary moments are highly time-

dependent and many uncertainties are associated with it. Therefore further field/laboratory tests may be required to confidently consider the secondary moments in the negative moment reinforcement design process.

CHAPTER 7. EFFECTS OF THE CONTINUITY DIAPHRAGM

7.1 Introduction

A Cast in Place (CIP) continuity diaphragm at the intermediate support are present in most PPCB continuous bridges built in the United States. Generally, the diaphragm is integrated with the deck through continuous reinforcement and tied to the girders with anchor bars. Depending upon the bridge type, some diaphragms are post-tensioned and some of them have non-pre-stressed reinforcement. Continuity diaphragms are supposed to improve the load distribution and load carrying capacity due to both lateral loads (wind load) and vertical load (traffic) on the bridge, while minimizing the installation of expansion joints and maintenance cost. Improved riding quality and enhanced structural redundancy are some other advantages of the continuity diaphragm [25].

Several problems are associated with the continuity diaphragm. First, AASHTO specification does not specify the effect of diaphragms on the load distribution factor calculations and capacity evaluations [26] [27]. AASHTO LRFD specification does not specify the strength of the concrete in the continuity diaphragm. Wassef et al. [20] also stated that the diaphragm concrete has higher strength compared to the unconfined concrete strength measured during typical concrete cylinder test, due to the confinements in the diaphragm. However design of the girders and design of deck continuity reinforcement does not account for the diaphragms effects. Continuity diaphragms have construction and detailing problems, especially with the increase of the skew angle girder spacing get reduce, construction process get more difficult and diaphragms become less effective in carrying and distributing the loads [28]. Therefore effect of the continuity diaphragm on the behavior of the PPCB bridges is questionable.

7.2 Objective

Investigate the effect of the continuity diaphragm on the behavior of continuous PPCB bridges.

7.3 Research Plan

Task 1 – Literature review

A literature review was conducted to collect the information on the effects of the continuity diaphragm on the negative moment behavior of the continuous PPCB bridges.

Task 2 – Analytical study

Finite element models of two bridges (Bridge A and Bridge B, CHAPTER 4), were analyzed with and without continuity diaphragm to investigate the effects of the continuity diaphragm on the negative moment behavior of the continuous PPCB bridges.

7.4 Literature Review

Cai et al. [26] conducted research to determine the effect of the intermediate diaphragms and skew angle on the behavior of the pre-stressed concrete bridges. Six bridges with different girder types, span length, number of lanes, skew angles and diaphragm layouts were considered. Finite element models of these bridges developed with shell elements (deck) and beam elements (girders, diaphragm and parapets). The composite action was modeled by the rigid links. Four types of diaphragm conditions considered in the finite element model are listed in Table 12.

Table 12. Diaphragm conditions

Type	Condition
Case A	Only end diaphragm
Case B	Case A + Intermediate diaphragm non-composite with the slab
Case C	Case D with 1/3 intermediate diaphragm stiffness
Case D	Case A + Intermediate diaphragm composite with the slab

Maximum strains at the bottom of the girders and load distribution factors obtained from finite element analysis for each case compared with the field test results. Researchers observed that changing the diaphragm condition from Case A to Case D significantly reduced the maximum strains and load distribution factors. Further, they observed that Case B predicted reasonable results for all bridges. Parametric studies showed that the intermediate diaphragm type can noticeably change the maximum

strain and strain distribution pattern. Parametric study of the bridge performance also studied by changing the skew angle and number of intermediate diaphragms. Researchers observed that with the absence of intermediate diaphragms, increased skew angles decreased the maximum strain and load distribution factors. When the intermediate diaphragm present it may have opposite effect. Therefore effects of the diaphragms are more significant in the non-skew bridges than the skewed bridges.

Barr et al. [27] evaluated the effects of intermediate diaphragms, end diaphragms, continuity diaphragm, skew angle and load type on the live load distribution factors of pre-stressed concrete bridges. A three span pre-stressed concrete bridge was used in the study. A finite element model of the bridge was developed with shell elements (deck, intermediate diaphragms, and pier diaphragms) and beam elements (girders, pier cap, columns). Rigid links were used to model the composite action. The finite element model was validated with field tests on the bridge. The parametric study involved 24 variations of the bridge model. Researchers observed that the continuity diaphragm increased the live load distribution factors at the exterior girders and decreased the live load distribution factors at the interior girders. In all cases, an increase of skew angle decreased the live load distribution factors of the bridge, implying that the continuity diaphragm is less effective in bridges with large skew angles.

Saber et al. [28] conducted research on pre-stressed continuous concrete bridges to investigate the load transfer mechanism through the full depth of the continuity diaphragm and the effect of the skew angle. A three-dimensional finite element model was developed with plate elements (deck), solid elements (girders) and beam elements (continuity diaphragm). The parametric study involved 16 combinations of bridge models with different skew angles, girder spacing, span length and diaphragm conditions. According to Saber et al. [29], in bridges without a continuity diaphragm have a gap between the girders. A finite element model with a gap between ends of the girders allows the girders to rotate more, where the actual connection slightly restrains the rotation of the girder ends. Therefore, pre-stressed girders over the intermediate supports were modeled as continuous girders even there is no continuity diaphragm. For each case the bridge deck was continuous over the intermediate support. Effects of the continuity diaphragm on the pre-stressed bridges were evaluated based on the maximum stress and maximum deflections of the girders. Researchers observed a 1%

to 3% increase of maximum tensile stress and a 0.2% decrease of maximum compressive stress due to the continuity diaphragm. Maximum deflection of the girders increased by 0.1% with no continuity diaphragm condition. Researchers concluded that the continuity diaphragm has negligible effect on the maximum stress and defection of the girders and the continuity diaphragm with skew angle greater than 20 degree will be ineffective in pre-stressed bridges.

Later Saber et al. [25] conducted the field verification of the effect of the continuity diaphragm on pre-stressed concrete bridges. A pre-stressed concrete bridge with 48 degree skew angle with a continuity diaphragm selected for the study. A three dimensional finite element model similar to their previous study was developed and verified with the field test results. During the parametric study, stresses of the girders, stresses of the deck and deflection of the girders were compared with and without the continuity diaphragm conditions. Compared to the continuity diaphragm condition, the maximum stress of the girders without continuity diaphragm condition did not exceed 8%. Whereas, maximum stresses of the deck did not exceed 5% and maximum deflection of the girders were below 6%. Therefore researchers concluded that the effects of continuity diaphragm on the bridge performance is negligible, particularly in bridges with large skew angles. Researchers suggested that the continuity diaphragm can be eliminated unless it is necessary for construction, erection lateral stability or earthquake loads. Further, a link slab was proposed to improve the riding quality and reduce the maintenance cost without a continuity diaphragms.

F. M. Russo [23] discussed three different continuity connection types in pre-stressed concrete bridges, namely: (1) Full section continuity, (2) Deck only continuity, (3) No cast in place (CIP) deck continuity. Full section continuity is achieved with a continuity diaphragm at the intermediate support (Figure 72(a)). The deck only continuity concept (Figure 72 (b)), also known as the link slab concept, is constructed with continuous bridge deck and girder ends are not connected. Continuity and the required strength is achieved through the deck reinforcement. No CIP deck continuity (Figure 72(c) is achieved with the continuity diaphragm, which is not integral with the bridge deck. Extended pre-stressed strands are used to support the positive moment, whereas top flange reinforcement is used to support the negative moments at the intermediate support. Oesterle et al. [30] proposed several connection types for negative moment connection.

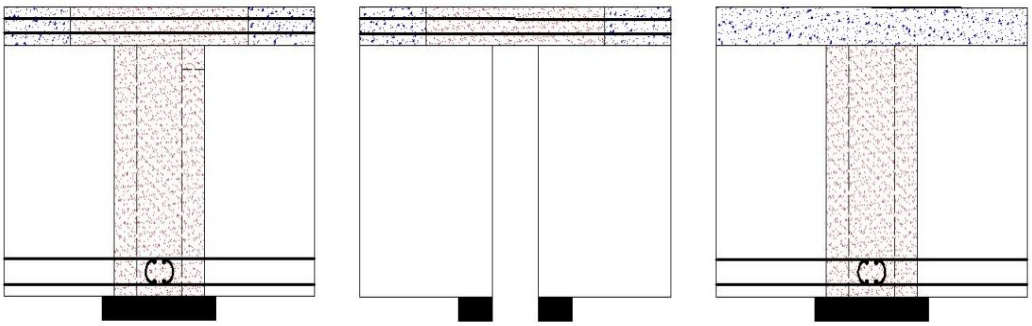

(a) Full section continuity **(b) Deck only continuity** **(c) No CIP deck continuity**

Figure 72. Types of continuity connections [23]

7.5 Analytical Study

According to the parametric study results in CHAPTER 5, the negative moment b2 reinforcement does not significantly affect the negative bending behavior of the pre-stressed continuous bridges. However the complex behavior of the continuity diaphragm may affect the behavior of the negative moment region in the continuous PPCB bridges. In this section, the effect of the continuity diaphragm on pre-stressed concrete bridges were investigated by analyzing Bridge A and Bridge B with and without continuity diaphragm conditions.

7.5.1 Finite Element Models

Finite element models of Bridge A and Bridge B with continuity diaphragms (Figure 73(a)) were discussed in CHAPTER 4. Similar procedure was used to model the finite element models of Bridge A and Bridge B without the continuity diaphragm (Figure 73(b)). Pinned support conditions were used at the abutments, whereas roller support conditions were applied to the ends of the girders at the intermediate supports.

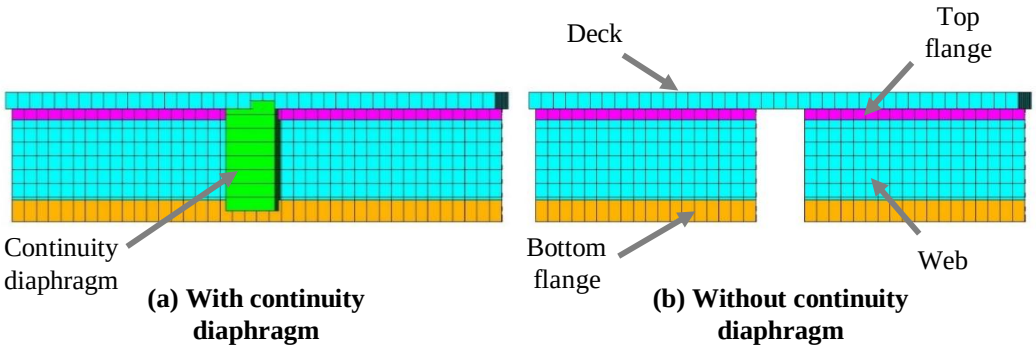

Figure 73. Finite element model at the intermediate support

7.6 Finite Element Analysis Results

The effect of the continuity diaphragm were evaluated based on three strains, namely: (1) longitudinal strain of the deck over the pier, (2) longitudinal strain of the deck at the 1/8 of the span location (3) longitudinal strain of the girders at the mid-span location.

Figure 74 shows variation of the longitudinal strain in the deck over the pier for four different bridge configurations. Without the continuity diaphragm both Bridge A and Bridge B show significant increase of the longitudinal strain of the deck. Compared to the Bridge A without the diaphragm, Bridge B without diaphragm shows approximately same peak strains, probably because of the skew angle effect of Bridge B.

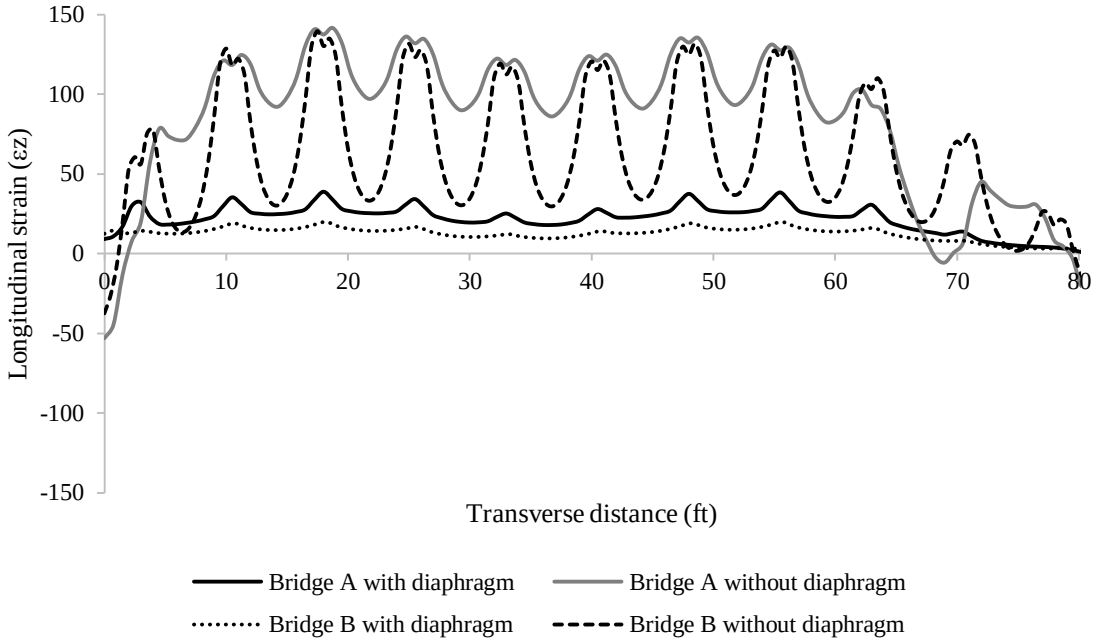

Figure 74. Longitudinal strain variation over the pier

The variation of longitudinal strains of the deck at the 1/8 span location of bridges are shown in Figure 75. Both Bridge A and Bridge B with continuity diaphragm experience similar tensile strains variations. Whereas without the continuity diaphragm, Bridge A and Bridge B experience compressive strains. Compared to the Bridge B without diaphragm, significant strain observed in Bridge A from transverse distance 50 ft to 80 ft. This might be due to the intermediate guard rail on the deck of the Bridge A.

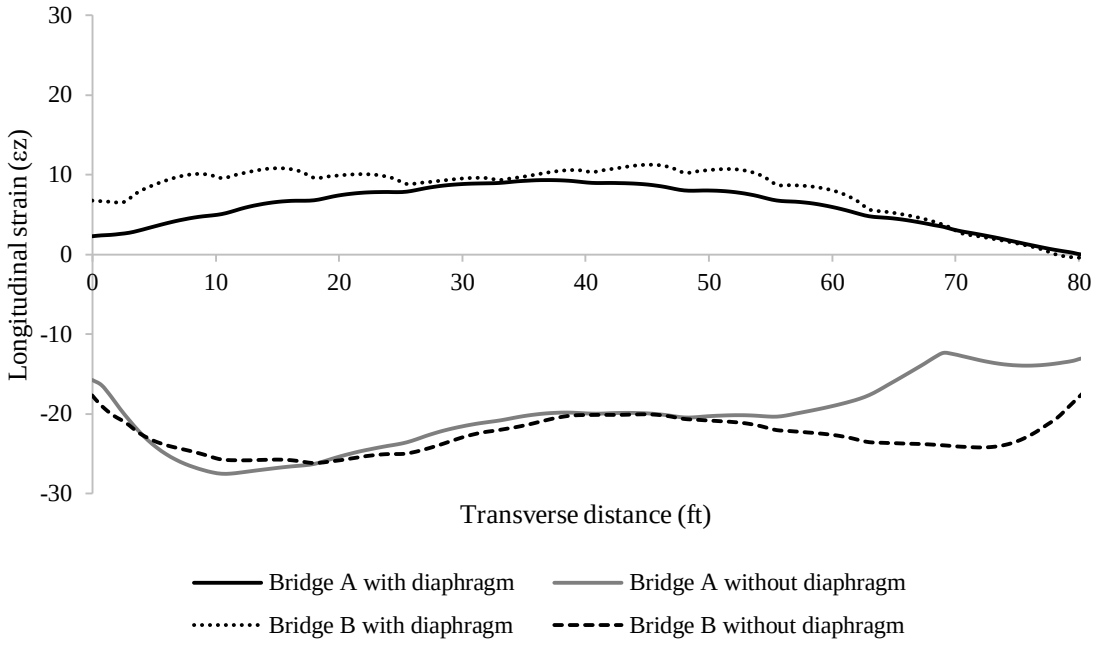

Figure 75. Longitudinal strain variation at the 1/8 span location

Longitudinal strain variations at mid-span of the bottom fiber of each girder are shown in Figure 76. Bridges without continuity diaphragm show higher strains than bridges with continuity diaphragm, probably because of bridge without continuity diaphragm behave as a simply supported structure. Further, the bridge with higher skew angle (Bridge B) shows higher strains than the bridge with smaller skew angle (Bridge A).

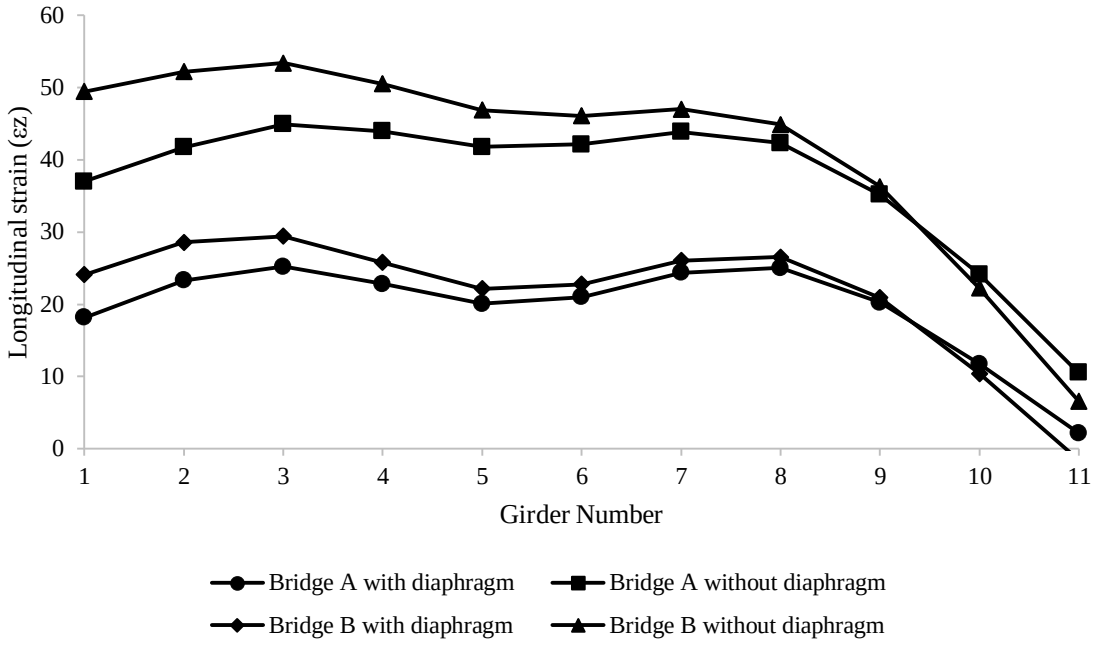

Figure 76. Strain of the girder mid-span

7.7 Summary

Bridge A and Bridge B with the continuity diaphragm and without the continuity diaphragm were analyzed to investigate the effects of the behavior of PPCB bridges. Longitudinal strains of the deck over the pier, at 1/8 span location and bottom of the girders at the mid-span were used to obtain the conclusions. Compared to the bridges with continuity diaphragm, bridges without the continuity diaphragm experienced higher strains. Skew bridges had smaller strains over the piers than non-skew bridges. However, slightly larger strain in the girders at the mid span was observed.

7.8 Conclusions

According to the analytical study, the continuity diaphragm of the multi-span pre-stressed concrete bridge made continuous is effective in reducing the strain of the bridge on the bridge deck and girders.

CHAPTER 8. CONCLUSIONS AND RECOMMENDATIONS

Multi-span Pre-tensioned Pre-stressed Concrete Beam (PPCB) bridges made continuous for live load usually experience a negative live load moment region over the intermediate supports. Sufficient reinforcement (longitudinal continuous deck reinforcement (b1) plus additional longitudinal reinforcement over the intermediate supports (b2)) must be provided to satisfy the strength and serviceability requirements within this negative moment region. The AASHTO LRFD bridge design manual recommends that the negative moment reinforcement be extended beyond the inflection point. Based upon satisfactory previous performance and judgment, the Iowa Department of Transportation (DOT) Office of Bridges and Structures (OBS) terminates the b2 reinforcement at 1/8 of the span length (which does not meet current AASHTO recommendations). Although the Iowa DOT policy results in approximately 50% shorter b2 reinforcement than the AASHTO LRFD specifications, the Iowa DOT has not experienced any significant deck cracking over the intermediate supports. The objectives of the project are as follows.

- Investigate the Iowa DOT OBS policy regarding the required amount of b2 reinforcement to provide negative moment continuity.
- Investigate OBS policy regarding the termination length of b2 reinforcement.
- Investigate the impact of the termination pattern of the b2 reinforcement.
- Investigate the effect of secondary moments on the performance of the PPCB bridges.

8.1 Summary

8.1.1 Literature Review

In PPCB bridges, the predominant mode of deck cracking is transverse cracking, which usually occurs over the transverse reinforcement. The effects of numerous contributing factors and mitigation procedures are not yet fully understood. Most research work has focused on the construction materials, mix designs, construction practices, and environmental conditions during construction to determine why transverse cracks occur on bridge decks. Very little research has been carried out on the effects of structural design factors such as girder type, shear stud configuration, deck thickness, reinforcement size and type, and the effect of vibrations on deck cracking.

Secondary moments due to creep of the girders as well as differential shrinkage between the deck and the girders are known to play an important role in the design of the reinforcement at the bottom of the continuity connection. Several research projects developed and improved methods to calculate the secondary moments and some of them developed more efficient positive moment connections to mitigate the cracks at the bottom of the continuity connection due to these secondary moments. Researchers have also concluded that the positive reinforcing steel at the support has no significant effect on the resulting negative moment.

8.1.2 Field Test

Five bridges with different characteristics (numbers of spans, span lengths, widths, skew angles, number of girders and girder types) were used during a field test program to investigate the effects of various bridge characteristics on the negative bending behavior near the piers. To investigate the effects of the b2 reinforcement, a suite of strain gauges, including rosettes, were placed on the deck top surface 1 ft inside and 1 ft outside the end of the b2 reinforcement. Another set of strain gauges were located over on the top surface of the deck over the pier. Girder strain gauges were also attached to both top and bottom flanges at a mid-span location and at one depth of the girder away from the pier. A standard snooper truck provided by the Iowa DOT crossed the bridge along multiple transverse paths at a crawl speed to generate pseudo-static strain responses in the test bridges.

Even though the field tests involved five bridges with different properties, the strain profiles of the deck gauges and girder gauges look similar in terms of pattern and magnitudes. For example, the strain gauges outside of the b2 reinforcement showed slightly higher strains than the strains inside of the b2 reinforcement. When the truck axles were in the vicinity of the rosettes, an expected compression and tension behavior of the bridge was observed in the two-span bridges. Major and minor principal strains of approximately the same magnitudes with opposite signs were observed when the truck axles were away from the rosettes. In the three-span bridges, principal strains of the same magnitudes with opposite signs were always observed.

8.1.3 Calibration

A significant focus of the research was to investigate the effects of b2 reinforcement on both skewed and non-skewed bridges with Bulb Tee girders. Out of

the five field tested bridge, two bridges - Bridge A (on Meredith Drive, over I35/80) with a smaller skew angle and Bridge B (on I80, over US65) with a larger skew angle - were selected for further study with the finite element models.

8.1.3.1 Bridge A

A finite element model of Bridge A was calibrated with the field test results in the vicinity of negative moment region. The field test results from the deck gauges agreed with the finite element results. Initially, strain differences were found in the girder gauges. Therefore, the Modulus of Elasticity of the girders were increased and the support conditions were modified to minimize the difference between the finite element model and the field test.

The finite element model was then compared with the cracking strain of the concrete (130με) to simulate the transverse field cracks. It was found that a Uniformly Distributed Load (UDL) approximately equivalent to eight HS20 trucks was not sufficient to produce cracking strains. Further an 80 degree temperature drop was also found to not be sufficient to develop cracks. Since 50% of the shrinkage of concrete decks takes place during 56 days following deck placement, a deck shrinkage load of 56 days applied to the model and it was found that this amount of deck shrinkage had the potential to induce strain that exceeded cracking levels.

8.1.3.2 Bridge B

The live load calibration results of Bridge A were used as the initial conditions for calibrating Bridge B, followed by a refined calibration with Bridge B field test results. It was found that the finite element results of Bridge B are agreed with the field test results.

8.1.4 Parametric Study

8.1.4.1 Bridge A

Three different conditions for Bridge A were used in the parametric study: (1) Model 1 - Uncracked deck, (2) Model 2 - Cracked deck and (3) Model 3 - Cracked deck with cracked diaphragm. The length, area and distribution pattern of the b2 reinforcement were the primary parameters of the study. Linear static analysis was used to conduct the parametric study with live load (equivalent UDL) and 56-days shrinkage load. The parametric study results showed that Model 1 had no significant difference in the strain distribution due to both live load and 56 days shrinkage load.

Both Model 1 and Model 2 show similar strain distributions. An increase of b2 reinforcement area slightly reduces the strain magnitudes over the pier. Increased length of b2 reinforcement slightly reduce the strains of the deck at 1/8 of the span location. Staggered b2 reinforcement pattern also slightly reduces the strains of the deck at 1/8 of the span location.

8.1.4.2 Bridge B

The parametric study of Bridge B was conducted similar to that for Bridge A, more importantly to investigate the effect of skew angle on the negative moment behavior. Results of the parametric study of Bridge B are similar to Bridge A, except Bridge B shows smaller strains over the pier due to the live load and slightly larger strains over the pier due to the shrinkage load.

8.1.5 Secondary Moment

Compared to the AASHTO guidelines, the Iowa DOT approximately uses b2 reinforcement that is approximately one half specified. However, no significant effect of the b2 reinforcement was observed in the parametric study nor had any anecdotal evidence been identified to suggest that the b2 reinforcement was not behaving well. It was suspected that secondary moments may be positively impacting the negative moment performance of these bridges. Among the many calculation methods, The PCA method was used to illustrate the effects of the secondary moments on the design of b2 reinforcement. Final secondary moment at the intermediate support of Bridge A was calculated as 4823.3 kip-ft and live load negative moment was calculated as -922.71 kip-ft. Based upon these results it appears that the sol-called secondary moments may actually be large enough to counteract any negative moments resulting from live load. The consequence of this is that it may be possible for bridge decks over piers to never actually experience tensile stresses. However, due to uncertainties associated with these secondary moments, further laboratory/field test may be required to improve gain confidence in the consideration of secondary moments during design.

8.1.6 Effect of the Continuity Diaphragm

Throughout the parametric study, no significant effect of the b2 reinforcement was observed for both skewed and non-skewed bridges. This may be due to the complex behavior of the continuity diaphragms of the PPCB bridges. An evaluation of the effects of the continuity diaphragm on PPCB Bridges was conducted with a

literature search and analytical study. Analytical model involve both Bridge A and Bridge B with and without the continuity diaphragm. Longitudinal strain over the pier, at the 1/8 span location and longitudinal strain bottom fiber of girders at mid-span was used to formulate the conclusions.

According to the literature, several people concluded that the continuity diaphragm has a small effect on behavior of the PPCB bridges and increased skew angle will decreased the stresses of the bridge deck. One group of researchers concluded that the continuity diaphragm has no effect on the behavior of the PPCB Bridges, particularly in bridges with skew angles greater than 20 degrees. Therefore bridge designer may design the bridges as link-slab bridges.

Based on the analytical study it was found that the continuity diaphragm has a noticeable effect on the PPCB bridges. Further, compared to the non-skewed bridge (Bridge A) the skewed bridge (Bridge B) smaller strain over the pier, but larger strains at the bottom fiber of girders at mid-span. No significant effect at the 1/8 span location was observed.

8.2 Conclusions

- The parametric study results show an increased area of the b2 reinforcement slightly reduces the strain over the pier. Whereas, increased length and staggered reinforcement pattern slightly reduce the strains of the deck at 1/8 of the span length.
- Secondary moments affect the behavior in the negative moment region. The impact may be significant enough such that no tensile stresses in the deck may be experienced.
- Finite element results suggested that the transverse field cracks over the pier and at 1/8 of the span length, are mainly due to deck shrinkage.
- Bridges with higher skew angles have lower strains over the intermediate supports.

8.3 Recommendations

Based on the finite element results, termination of b2 reinforcement at 1/8 of the span length is acceptable. Based on the confidence level in predicting the secondary moments, the amount and length of the b2 reinforcement may be reduced. Further field tests and laboratory tests are recommended.

APPENDIX: DETAILED FIELD TEST RESULTS

A summary of the field test results is presented in Chapter 3. This Appendix is summarized the field test results of each bridge. A plan view of the bridge, locations of the deck gauges, locations of the girder gauges, locations of the rosettes and load case details are also included. Results of deck gauges and girder gauges are given only for the Load Case 1 (LC1). Results of the LC4 are approximately symmetric with LC1 results.

Bridge 1; On C50, Over US218

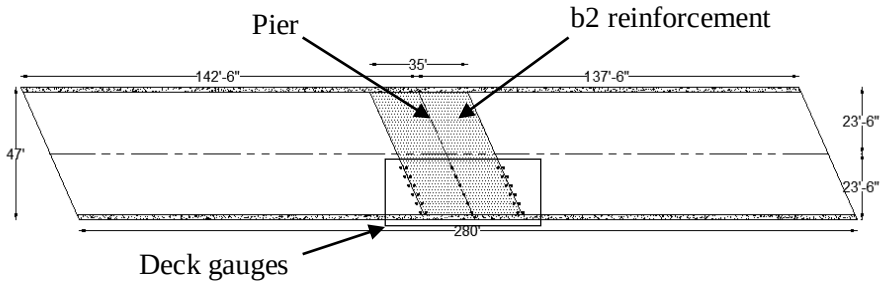

Plan view of the Bridge 1

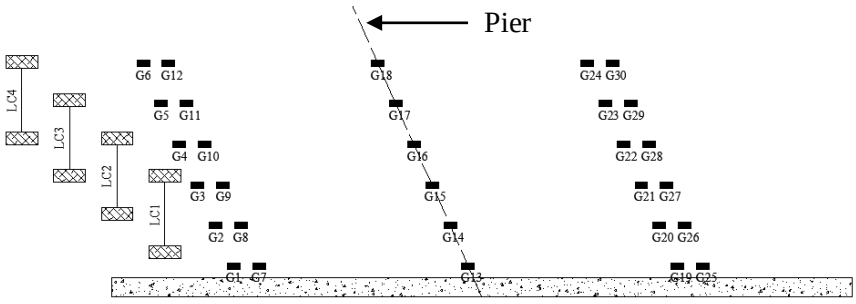

Bridge 1; Instrumentation plan of deck gauges

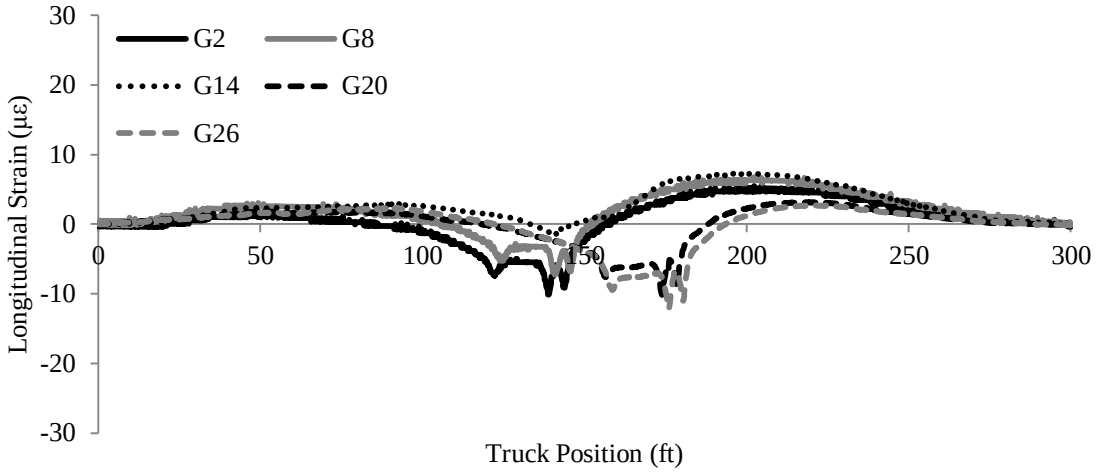

Typical longitudinal strains variation of deck gauges closer to the truck axle (LC1)

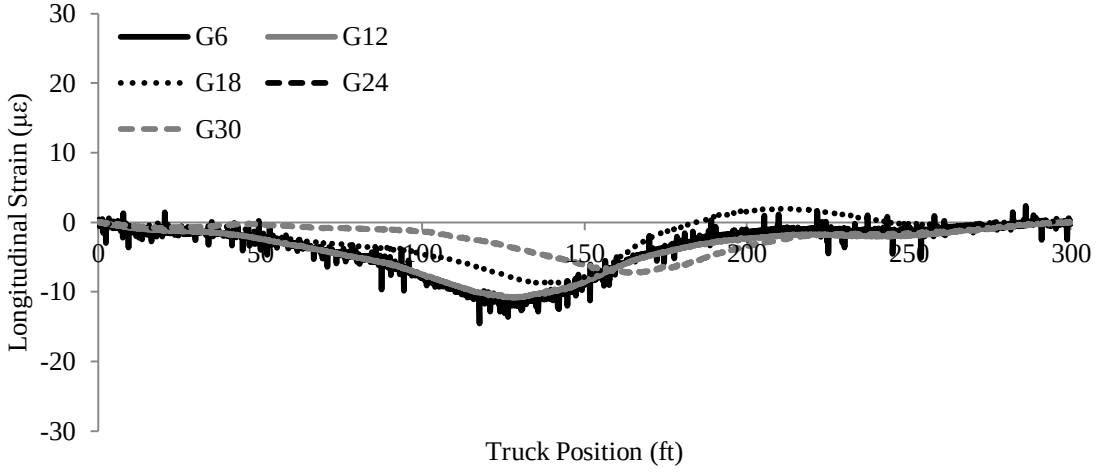

Typical longitudinal strains variation of deck gauges away from the truck axle (LC1)

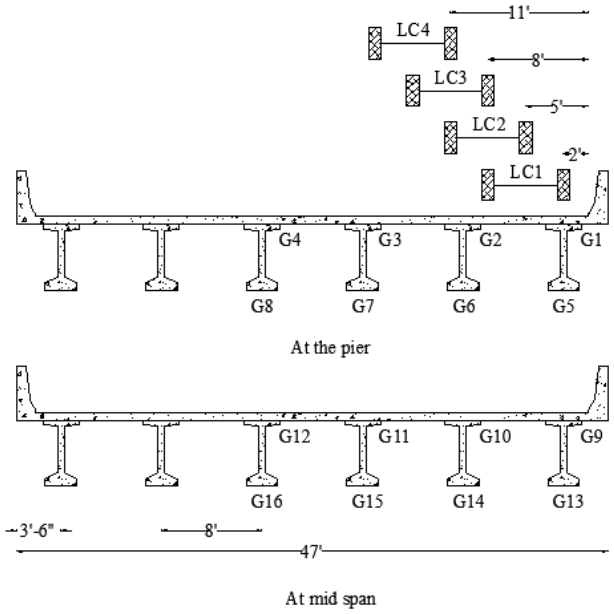

Bridge 1; Instrument plan of girder gauges

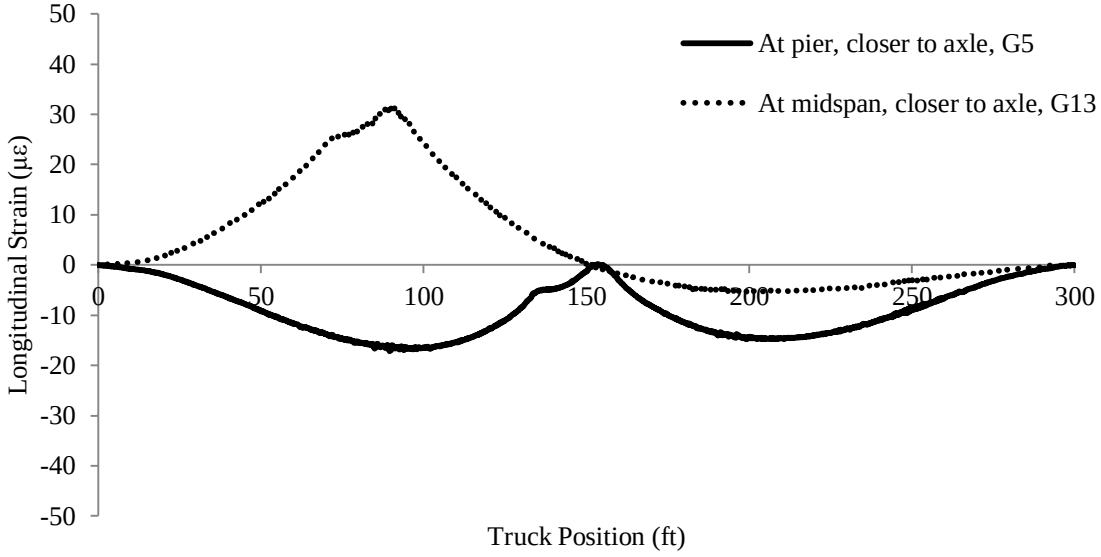

Typical strain variation of girder gauges of Bridge 1 (LC1)

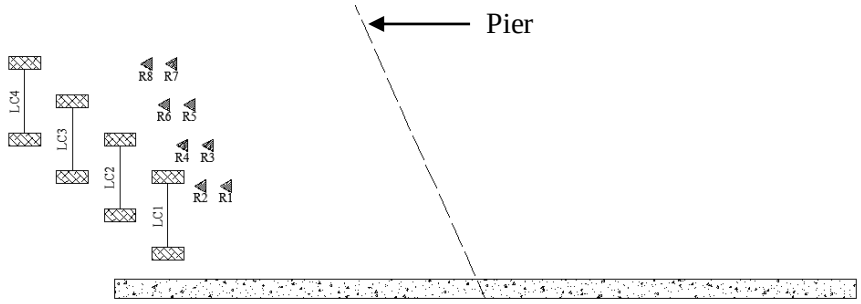

Bridge 1; Instrumentation plan of the rosettes

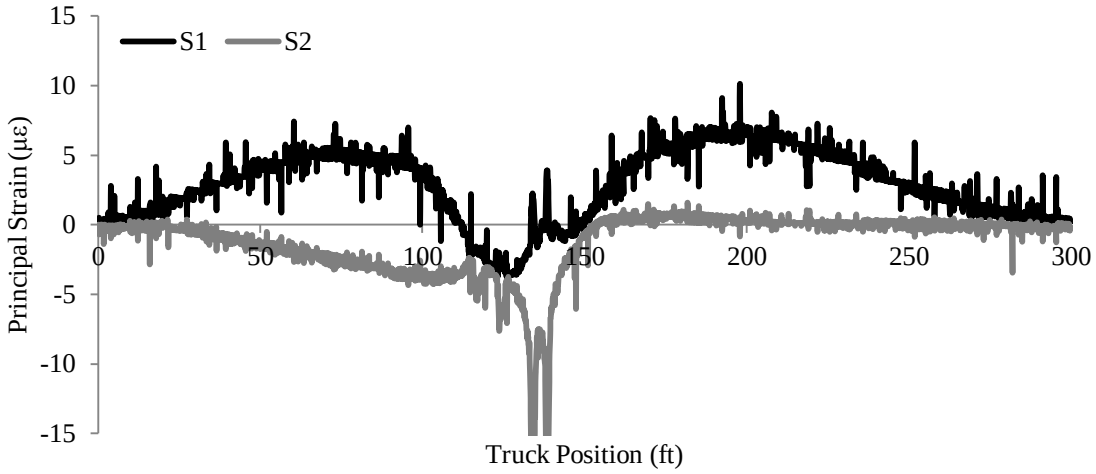

Typical variation of principal strains of rosettes (R7); closer to truck axle (LC4)

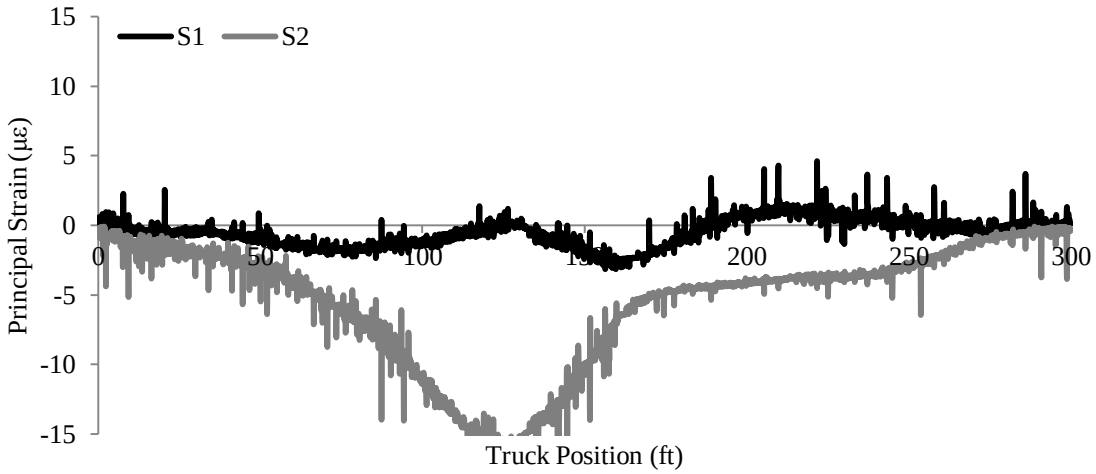

Typical variation of principal strains of rosettes (R7); away from truck axle (LC1)

Bridge 2; On I80, Over US65

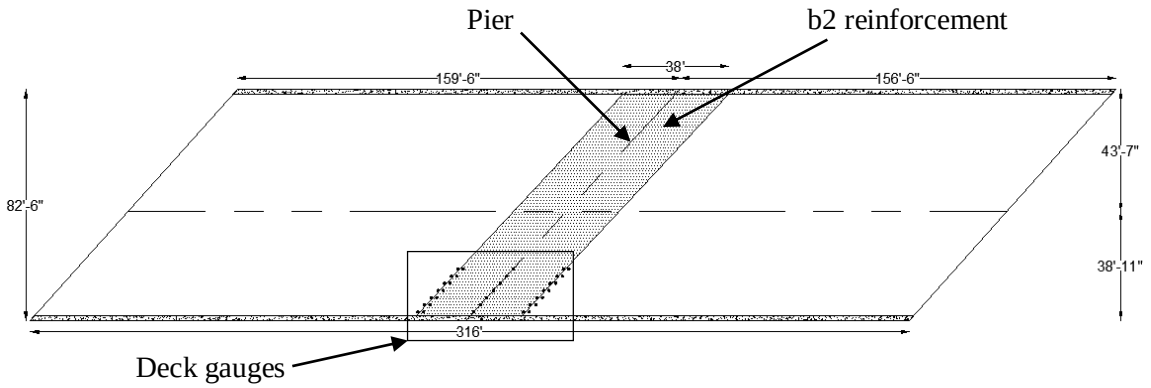

Plan view of the Bridge 2

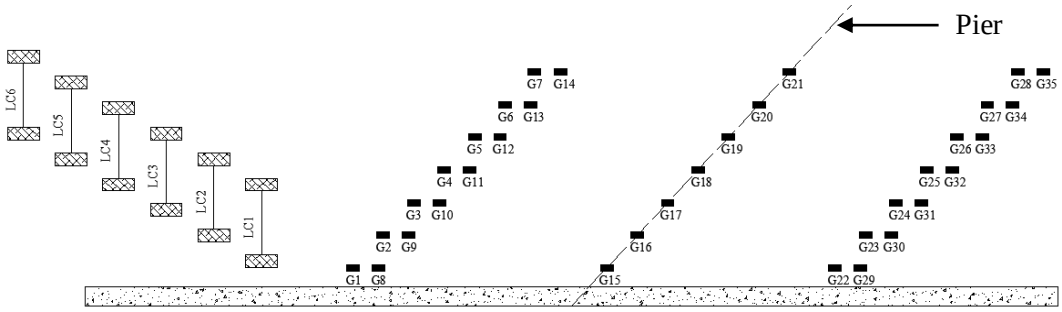

Bridge 2; Instrumentation plan of deck gauges

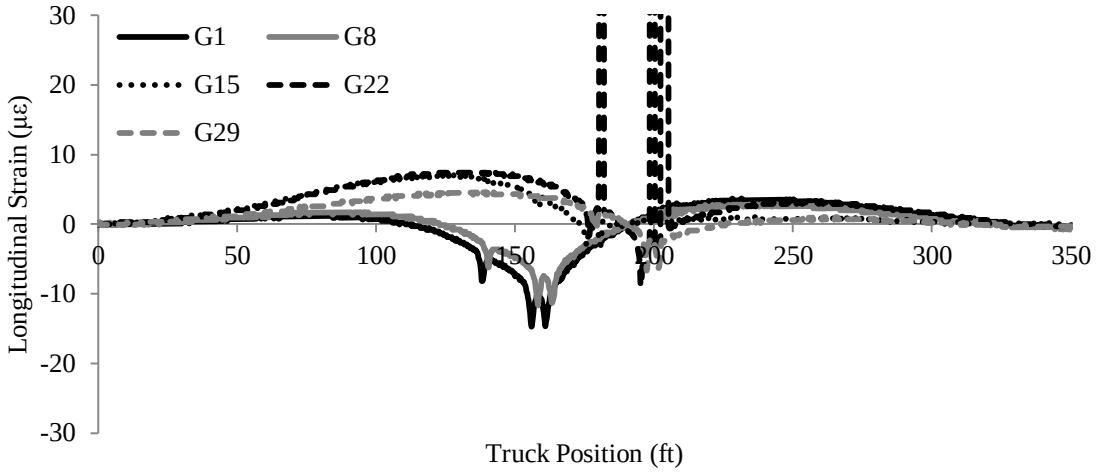

Typical longitudinal strains variation of deck gauges closer to the truck axle (LC1)

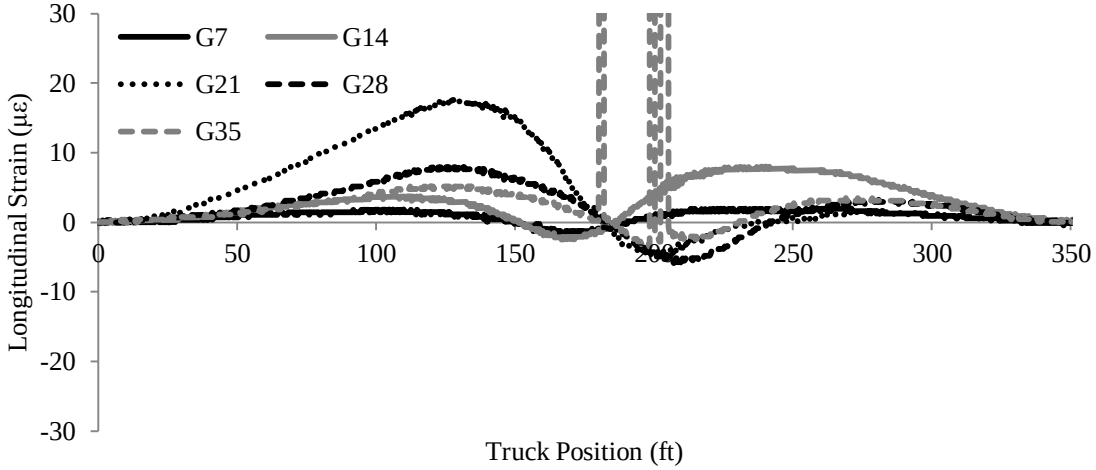

Typical longitudinal strains variation of deck gauges away from the truck axle (LC1)

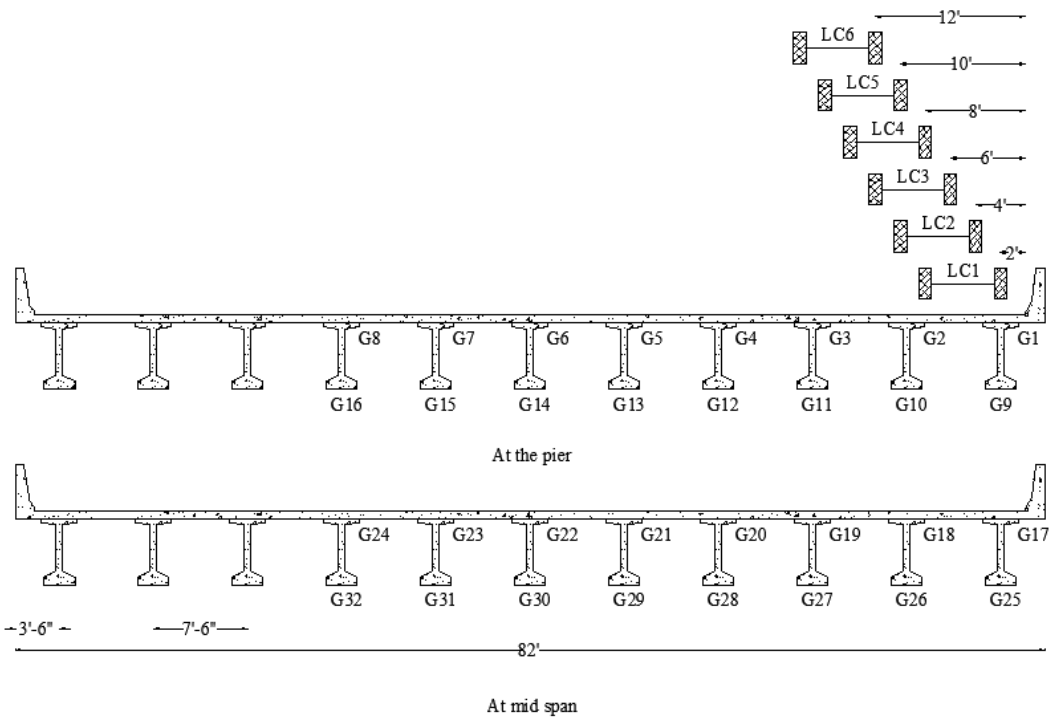

Bridge 2; Instrument plan of girder gauges

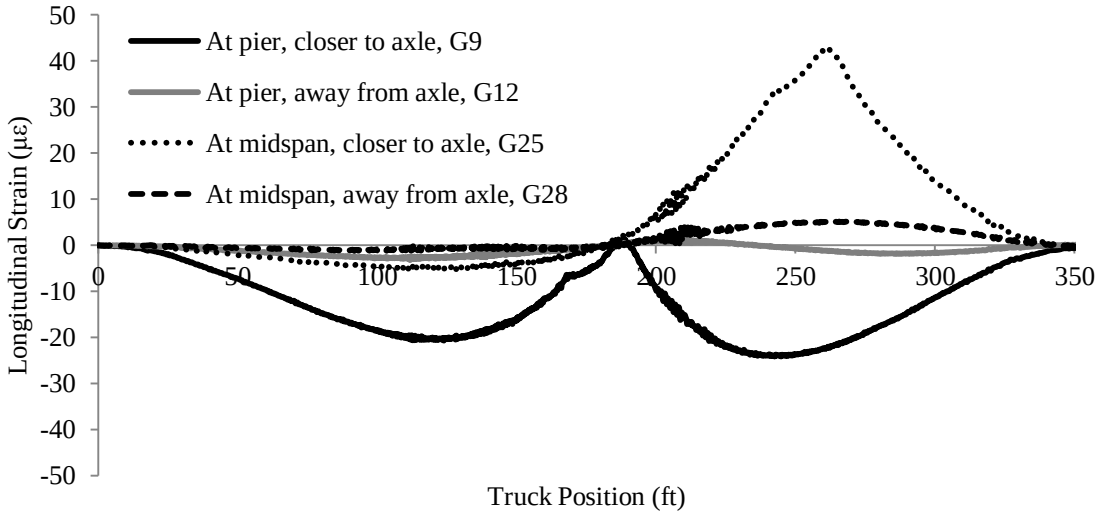

Typical strain variation of girder gauges of Bridge 2 (LC1)

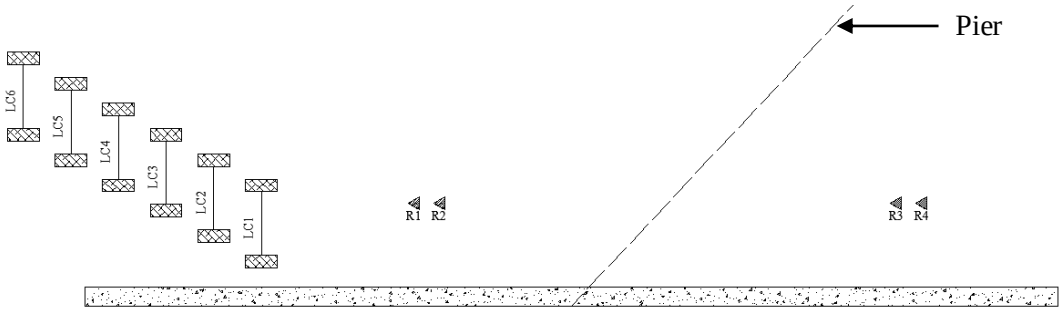

Bridge 2; Instrumentation plan of the rosettes

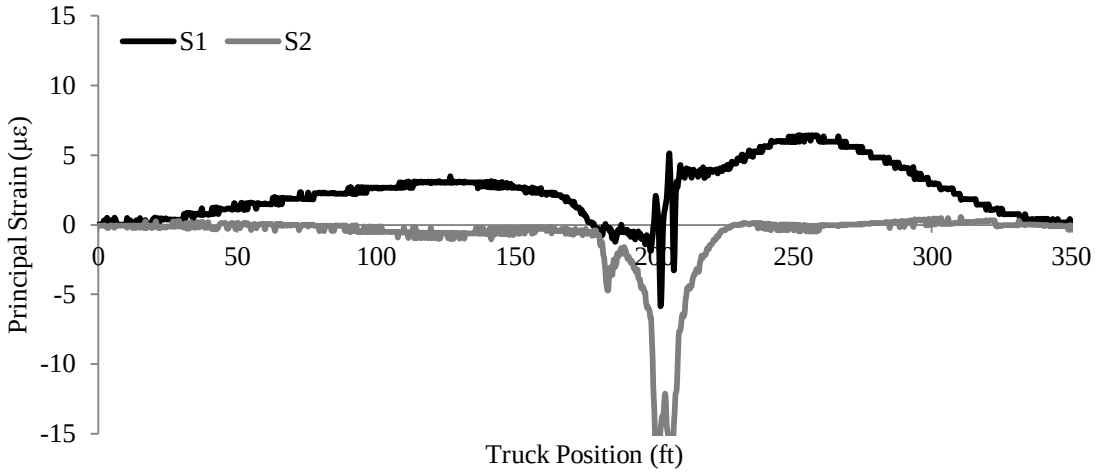

Typical variation of principal strains of rosettes (R4); closer to truck axle (LC1)

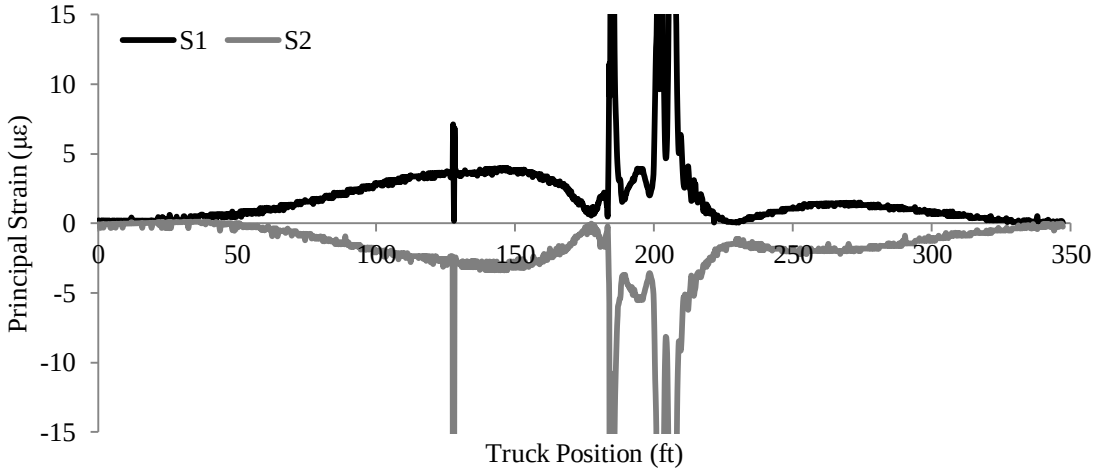

Typical variation of principal strains of rosettes (R4); away from truck axle (LC6)

Bridge 3; On Meredith Drive, Over I35/80

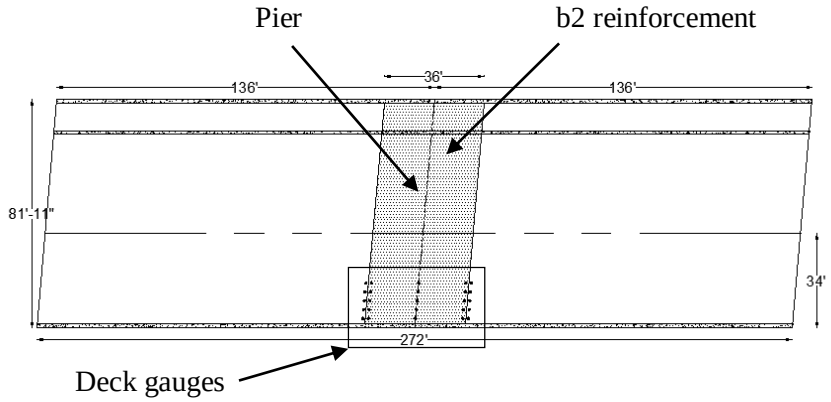

Plan view of the Bridge 3

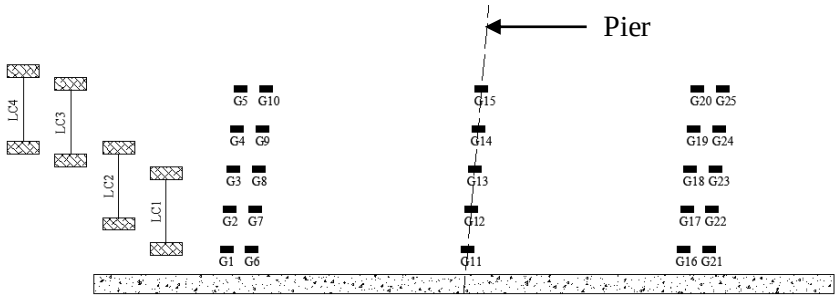

Bridge 3; Instrumentation plan of deck gauges

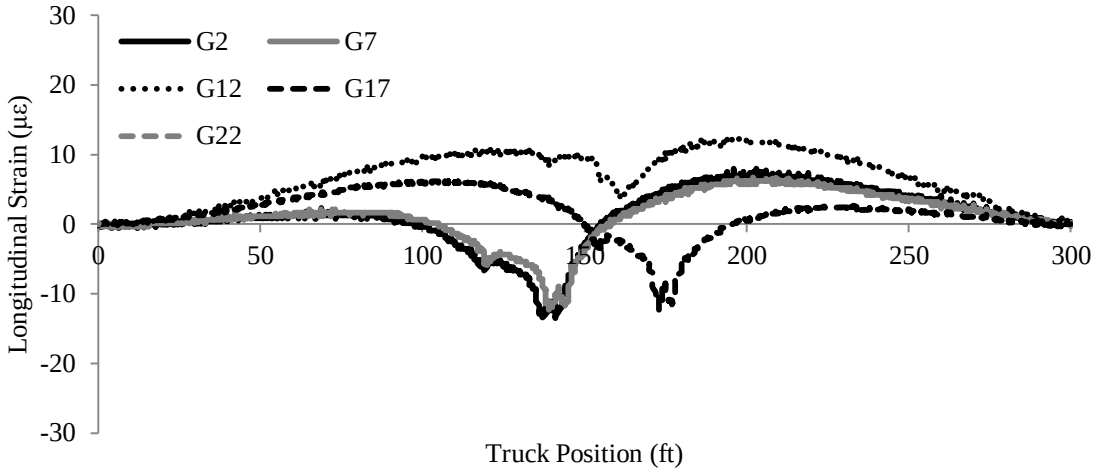

Typical longitudinal strains variation of deck gauges closer to the truck axle (LC1)

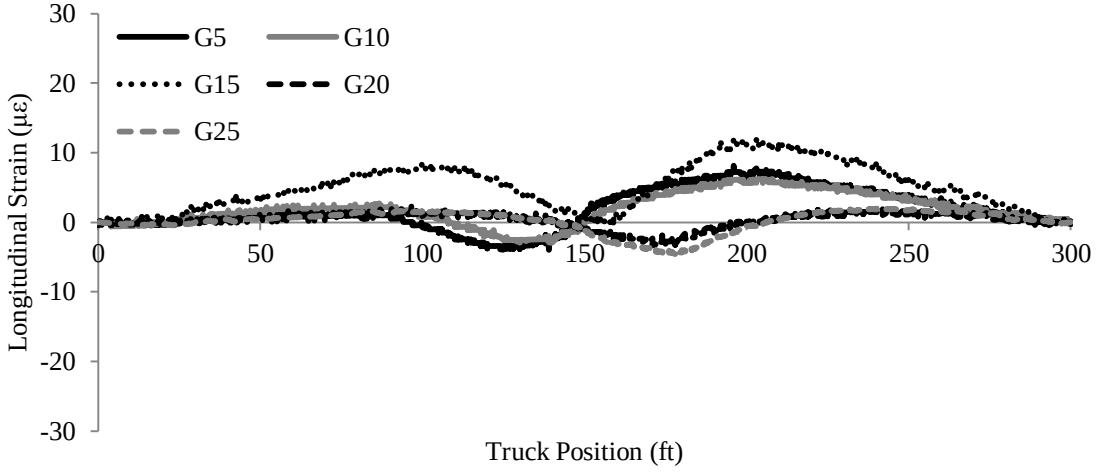

Typical longitudinal strains variation of deck gauges away from the truck axle (LC1)

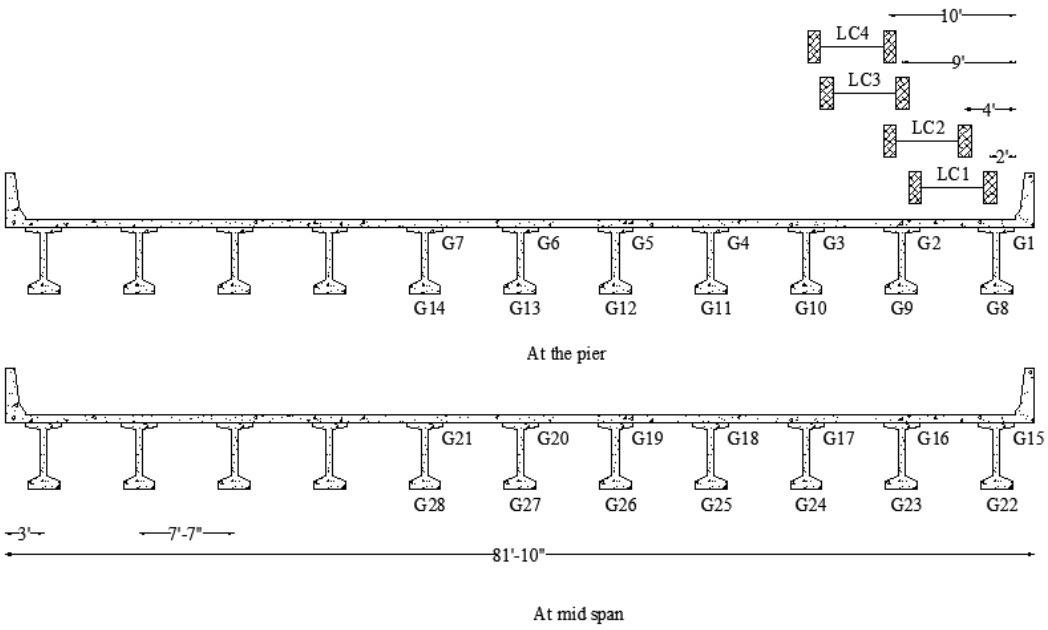

Bridge 3; Instrument plan of girder gauges

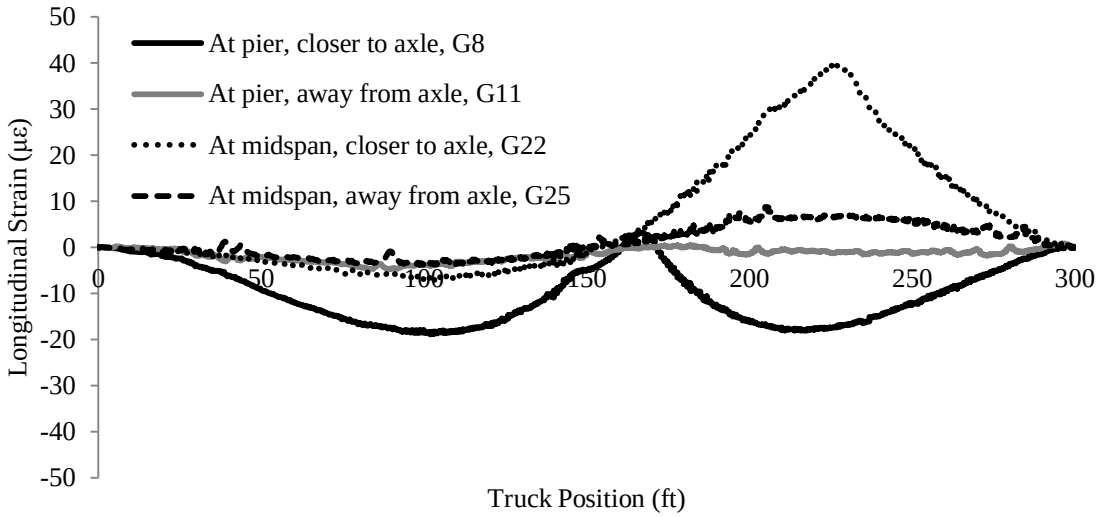

Typical strain variation of girder gauges of Bridge 3 (LC1)

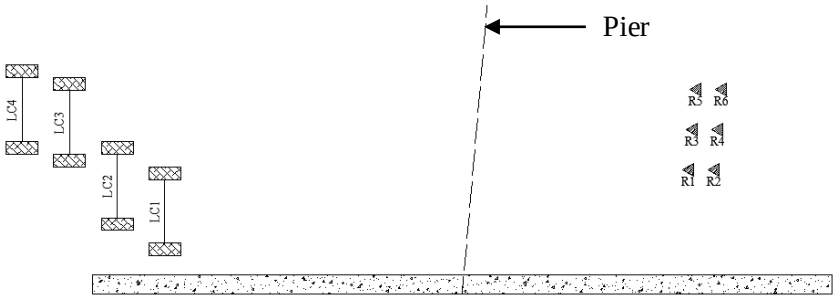

Bridge 3; Instrumentation plan of the rosettes

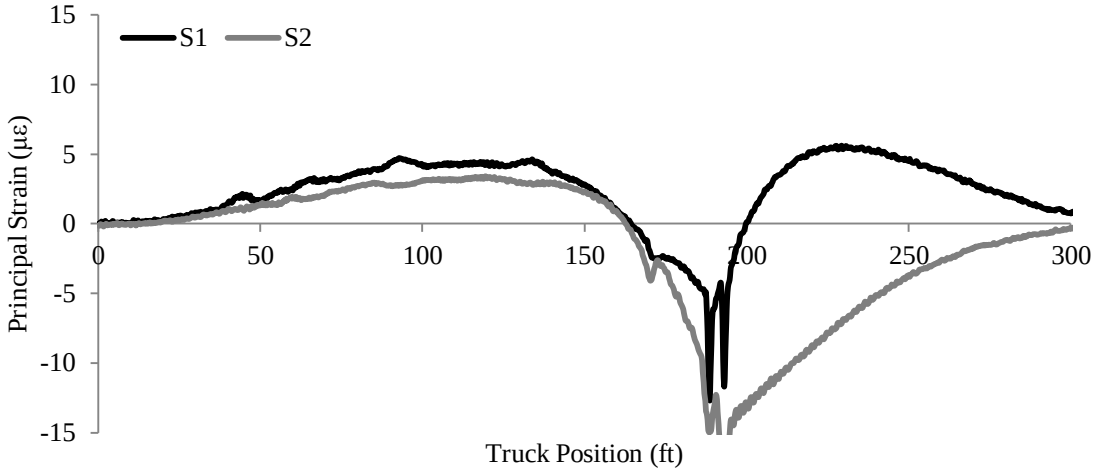

Typical variation of principal strains of rosettes (R6); closer to truck axle (LC4)

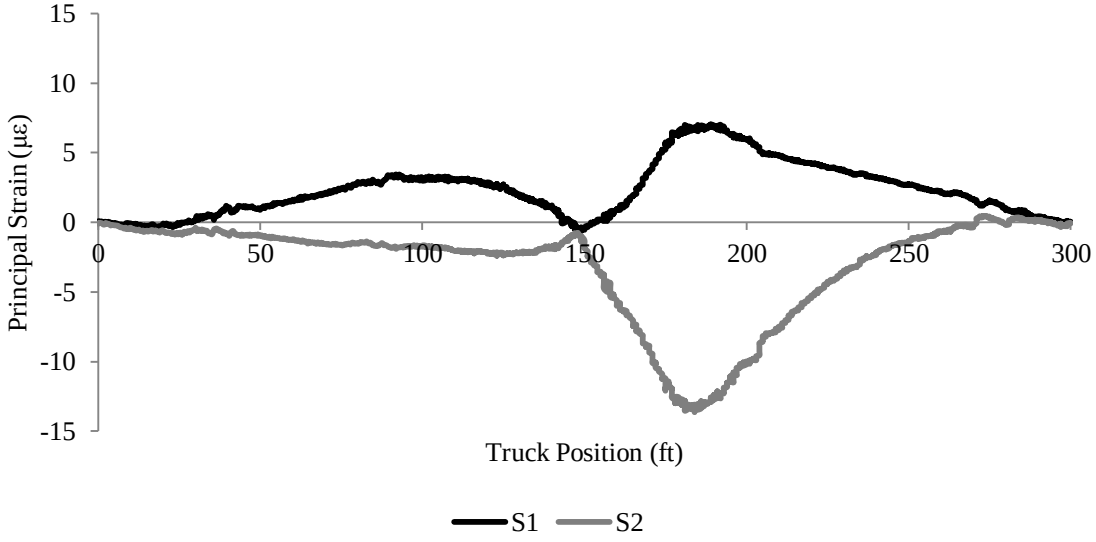

Typical variation of principal strains of rosettes (R6); away from truck axle (LC1)

Bridge 4; On Mt Pleasant bypass, Over Big Creek

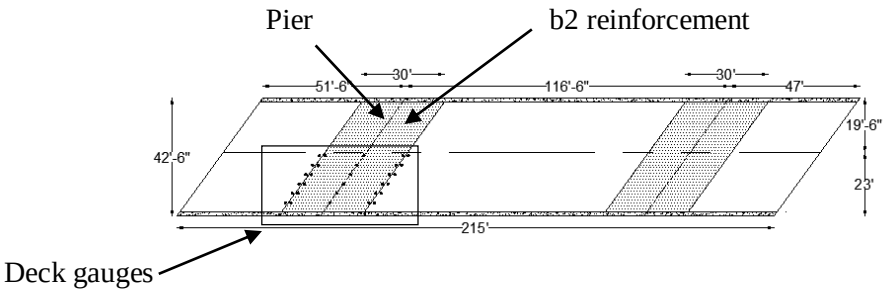

Plan view of the Bridge 4

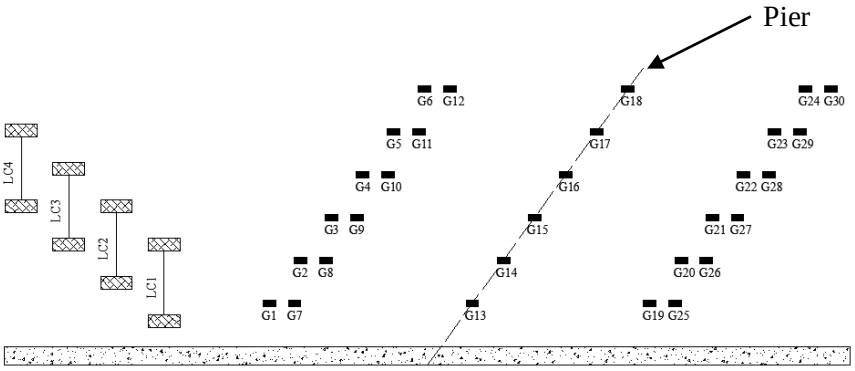

Bridge 4; Instrumentation plan of deck gauges

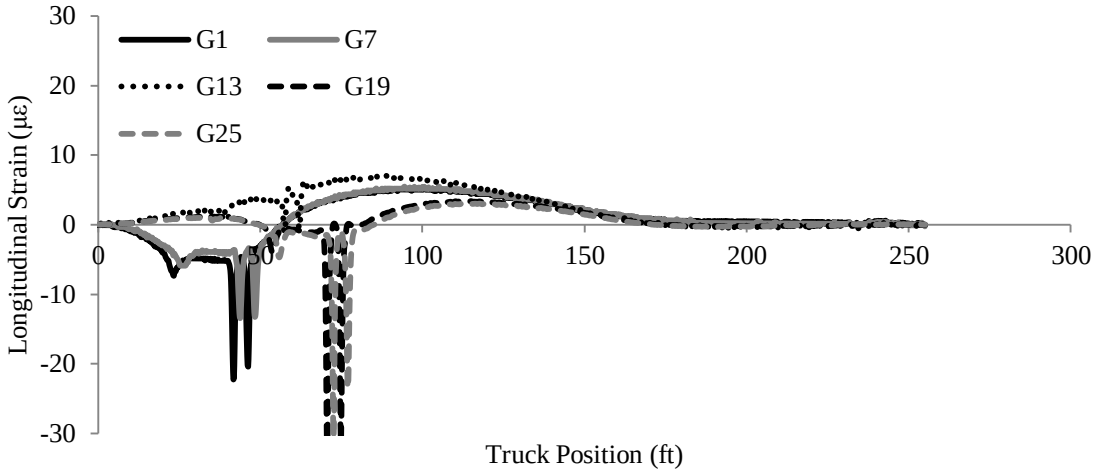

Typical longitudinal strains variation of deck gauges closer to the truck axle (LC1)

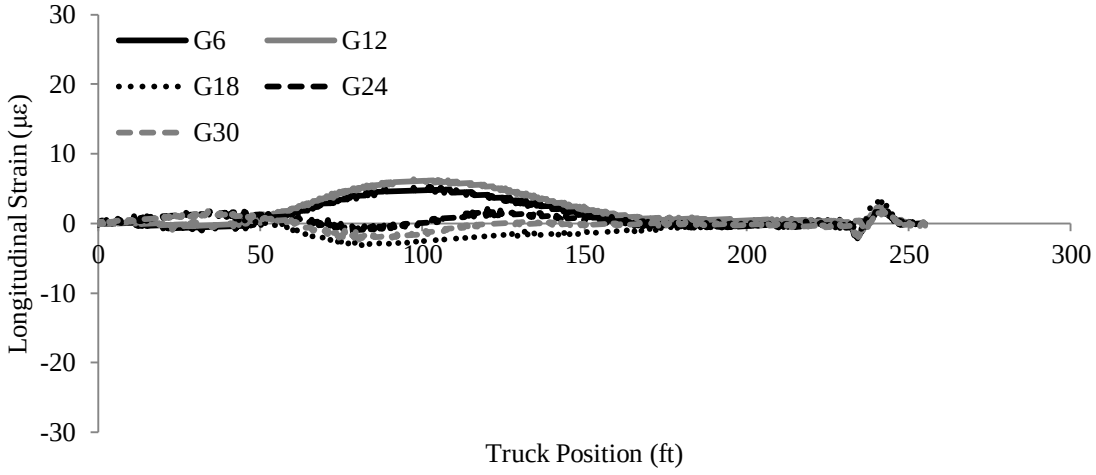

Typical longitudinal strains variation of deck gauges away from the truck axle (LC1)

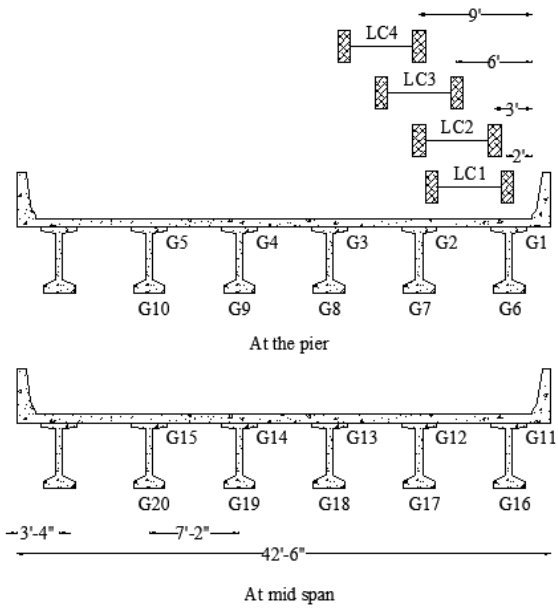

Bridge 4; Instrument plan of girder gauges

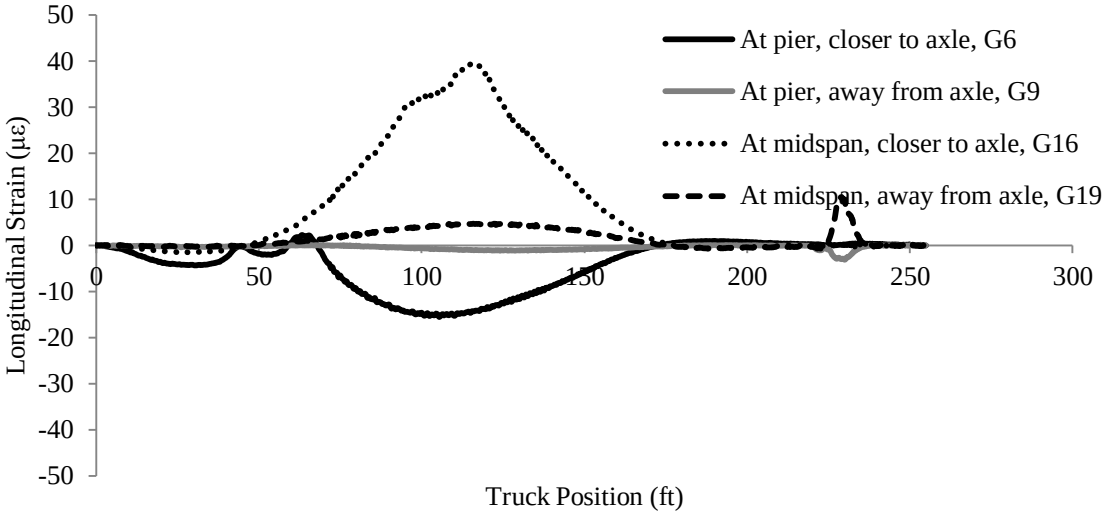

Typical strain variation of girder gauges of Bridge 4 (LC1)

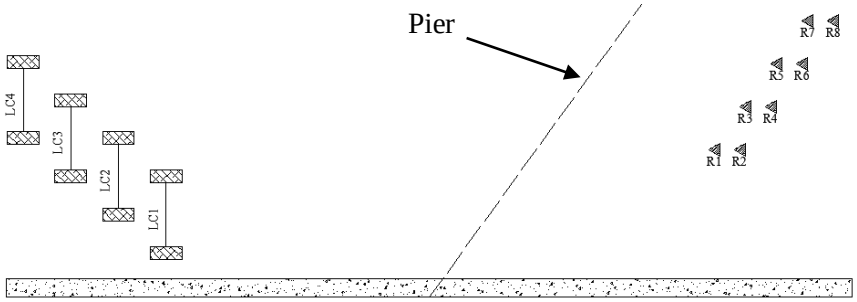

Bridge 4; Instrumentation plan of the rosettes

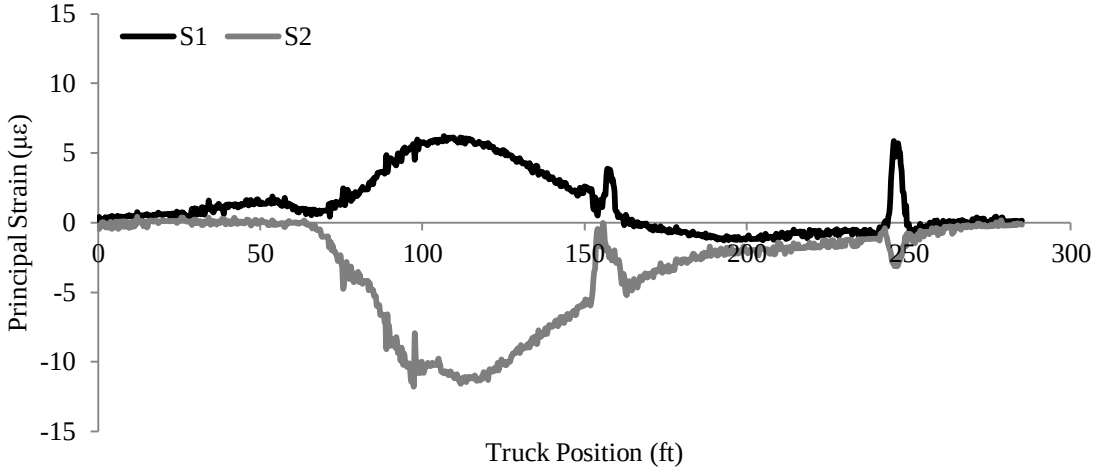

Typical variation of principal strains of rosettes (R6); closer to truck axle (LC4)

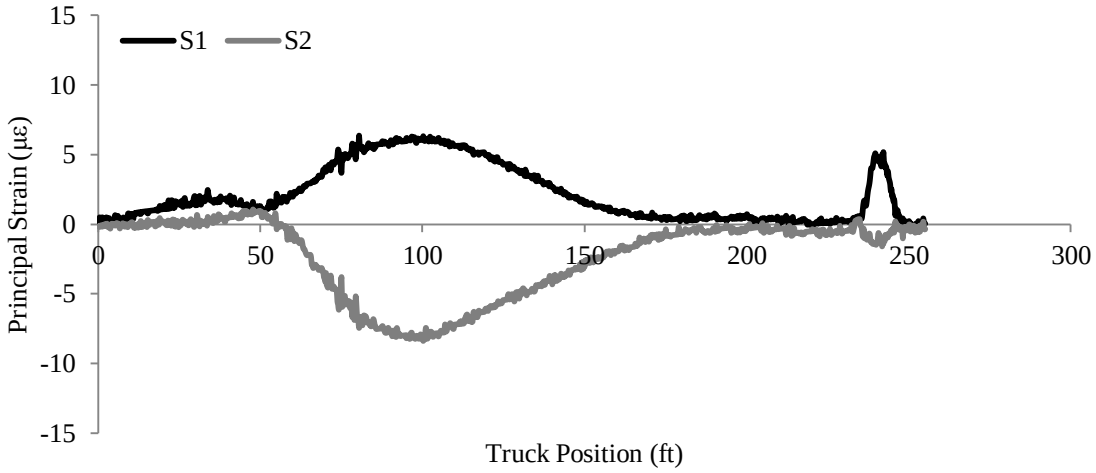

Typical variation of principal strains of rosettes (R8); away from truck axle (LC1)

Bridge 5; On US20, Over Big Whiskey Creek

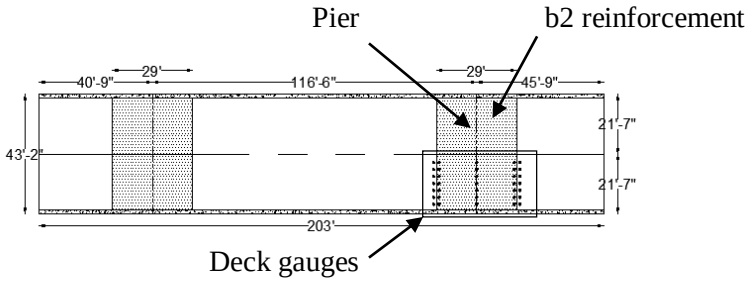

Plan view of the Bridge 5

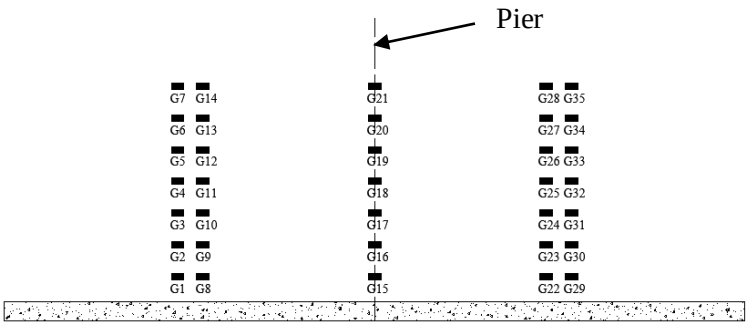

Bridge 5; Instrumentation plan of deck gauges

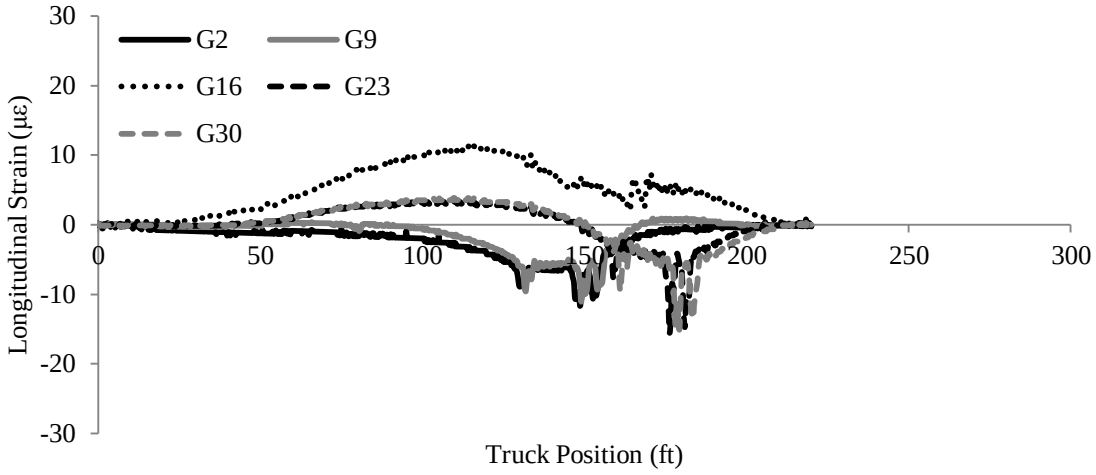

Typical longitudinal strains variation of deck gauges closer to the truck axle (LC1)

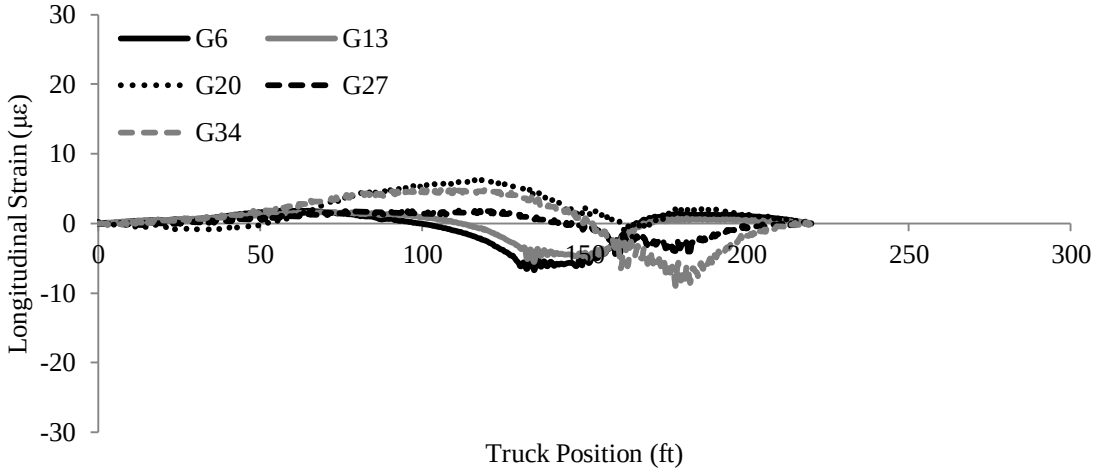

Typical longitudinal strains variation of deck gauges away from the truck axle (LC1)

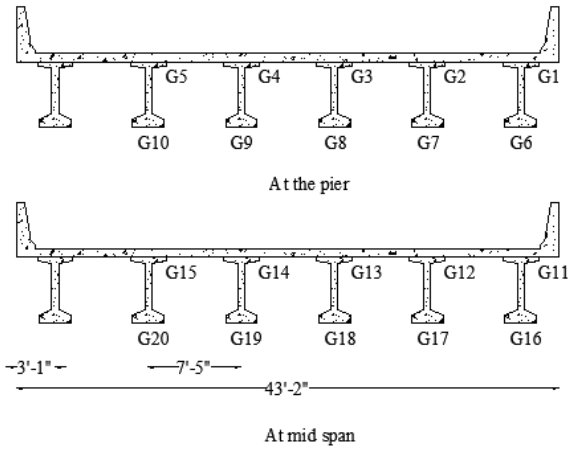

Bridge 5; Instrument plan of girder gauges

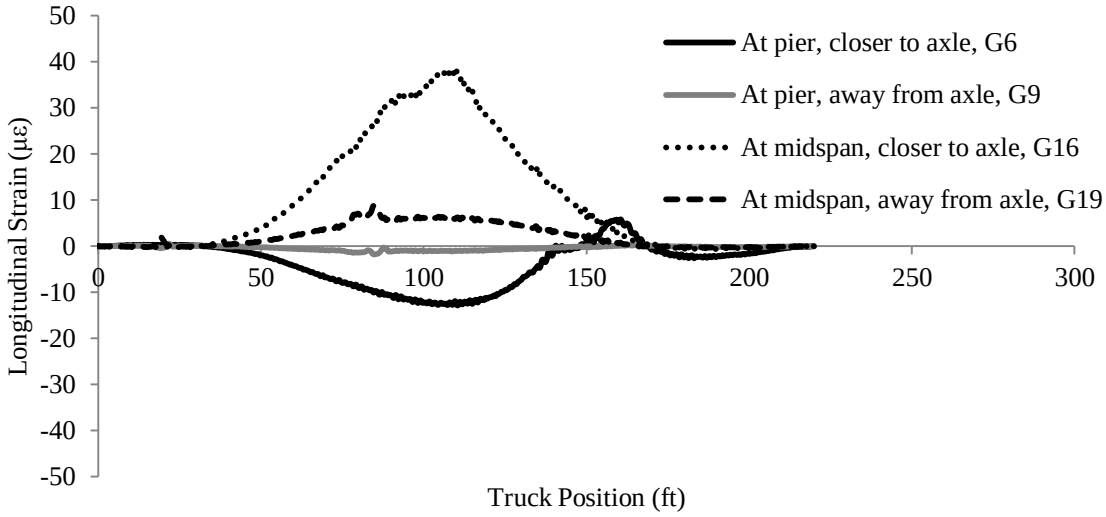

Typical strain variation of girder gauges of Bridge 5 (LC1)

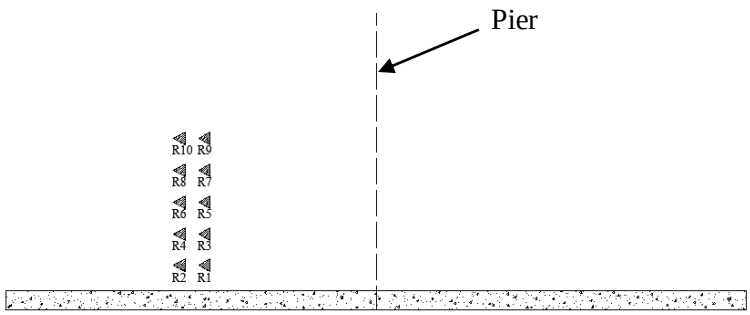

Bridge 5; Instrumentation plan of the rosettes

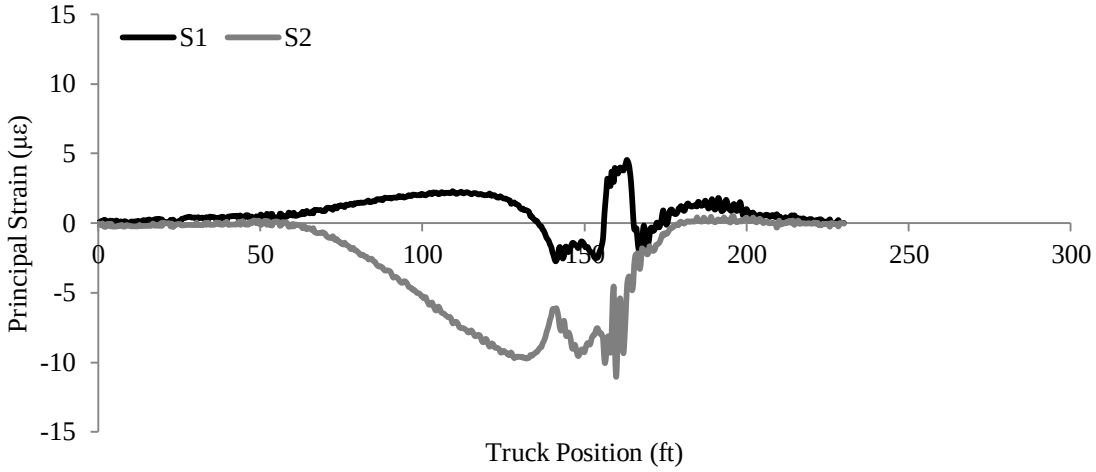

Typical variation of principal strains of rosettes (R9); closer to truck axle (LC4)

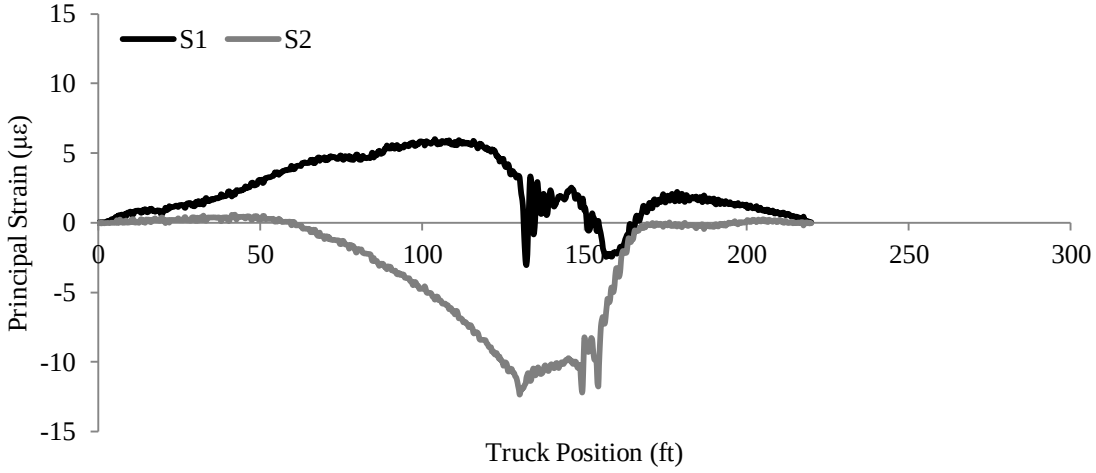

Typical variation of principal strains of rosettes (R9); away from truck axle (LC1)

REFERENCES

[1] R. Hadidi and M. Saadeghvaziri, "Transverse Cracking of Concrete Bridge Decks: State-of-the-Art," *Journal of Bridge Engineering,* vol. 10, no. 5, p. 503–510, 2005.

[2] K. Babaei and R. and Purvis, "Prevention of cracks in concrete bridge decks," Pennsylvania Department of Transportation, Harrisburg, PA, 1994.

[3] C. French, L. Eppers, Q. Le and J. F. Hajjar, "Transverse Cracking in Concrete Bridge Decks," *Transportation Research Record: Journal of the Transportation Research Board,* vol. Volume 1688, no. 1999 Various Bridge Design Issues, pp. 21-29, 2007.

[4] T. R. Schmitt and D. and Darwin, "Cracking in concrete bridge decks," Kansas Department of Transportation, Topeka, Kan., 1995.

[5] P. D. Krauss and E. A. and Rogalla, "Transverse cracking in newly constructed bridge decks," Transportation Research Board, National Research Council, Washington, D.C., 1996.

[6] M. Issa, "Investigation of Cracking in Concrete Bridge Decks at Early Ages," *Journal of Bridge Engineering,* vol. 4, no. 2, pp. 116-124, 1999.

[7] T. T. Cheng and D. W. Johnson, "Incidence assessment of transverse cracking in bridge decks: Construction and material consideration," Federal Highway Administration, Washington, D.C., 1985.

[8] T. Kochanski, J. Parry, D. Pruess, L. Schuchardt and J. Ziehr, "Premature cracking of concrete bridge decks study," Wisconsin Department of Transportation, Madison, Wis., 1990.

[9] G. Ramey, A. Wolff and R. Wright, "Structural Design Actions to Mitigate Bridge Deck Cracking," *Practice Periodical on Structural Design and Construction,* vol. 2, no. 3, p. 118–124, 1997.

[10] R. J. Frosch, R. D. Radabaugh and D. T. Blackman, "Investigation of transverse deck cracking," in *Proceedings Structures Congress, ASCE*, Reston, Va, 2002.

[11] W. T. McKeel, "Evaluation of deck durability on continuous beam highway bridges," Virginia Highway and Transportation Research Council, Charlottesville, Va., 1985.

[12] M. M. D and H. K. B, "Resolving restraint moments: Designing for continuity in precast prestressed concrete girder bridges," *PCI journal,* vol. 48, no. 4, pp. 104-119, 2003.

[13] C. F. Freyermuth, "Design of Continuous Highway Bridges with Precast, Prestressed Concrete Girders," *Journal of the Prestressed Concrete Institute,* vol. 14, no. 2, 1969.

[14] R. G. Oesterle, A. B. Mehrabi, H. Tabatabai, A. Scanlon and C. A. Ligozio, "Continuity Considerations in Prestressed Concrete Jointless Bridges," in *Structures 2004: Building on the Past, Securing the Future*, Nashville, Tennessee, United States, 2004.

[15] A. M. R. M. R. S. a. R. C. Makarand Hastak, "State of Practice for Positive Moment Connections in Prestressed Concrete Girders Made Continuous," *Journal of Bridge Engineering,* vol. 8, no. 5, p. 267–272, 2003.

[16] C. D. Newhouse, "Design and Behavior of Precast, Prestressed Girders Made Continuous - An Analytical and Experimental Study, Doctor of Philosophy Dissertation," Department of Civil and Environmental Engineering, Virginia Polytechnic Institute and State University, Blacksburg, Virginia, 2005.

[17] V. S. M. Chebole, "Long-Term Continuity Moment Assessment in Pre-stressed Concrete Girder Bridges, Master of Science Thesis," The Department of Civil and Environmental Engineering, Louisiana State University, Baton Rouge, LA, 2011.

[18] H.-G. Kwak and Y.-J. Seo, "Numerical analysis of time-dependent behavior of pre-cast pre-stressed concrete girder bridges," *Construction and Building Materials,* vol. 16, no. 1, p. 49–63, 2002.

[19] W. G. Wassef, C. Smith, C. M. Clancy and M. J. Smith, "Comperhensive design example for prestressed concrete (PSC) girder superstructure bridge with commentary," Modjeski and Masters, Inc, Harrisburg, PA, 2003.

[20] G. Vishay Precision, "Strain gauge rosettes: Selection, Application and Data reduction," Vishay Precision Group, Micro-Measurements, Wendell, NC, 2010.

[21] I. ANSYS, "ANSYS APDL V14 Documentation Manual," ANSYS, Inc, Canonsburg, PA, 2011.

[22] C. L. Freyermuth, "Design of Continuous Highway Bridges with Precast, Prestressed Concrete Girders," Portland Cement Association, 1969.

[23] A. Saber and W. Alaywan, "Full-Scale Test of Continuity Diaphragms in Skewed Concrete Bridge Girders," *Journal of Bridge Engineering*, vol. 16, no. 1, pp. 21-28, 2011.

[24] C. S. Cai, M. Shahawy and R. J. Peterman, "Effect of Diaphragms on Load Distribution of Prestressed Concrete Bridges," *Transportation Research Record: Journal of the Transportation Research Board*, vol. 1814, no. Design of Structures 2002, pp. 47-54, 2007.

[25] P. J. Barr, M. O. Eberhard and J. F. Stanton, "Live-Load Distribution Factors in Prestressed Concrete Girder Bridges," *Journal of Bridge Engineering*, vol. 6, no. 5, pp. 298-306, 2001.

[26] A. Saber, R. Freddy, W. Alaywan and T. Joseph, "Effectiveness of Continuity Diaphragm for Skewed Continuous Prestressed Concrete Girder Bridges," *PCI journal*, vol. 52, no. 2, pp. 108-114, 2007.

[27] A. Saber, J. Toups, L. Guice and A. Tayebi, "Continuity Diaphragm for Skewed Continuous Span Precast Prestressed Concrete Girder Bridges," Civil Engineering Department, Louisiana Tech University, Ruston, LA, 2004.

[28] F. M. Russo, "ABC concrete bridges continuity considerations," Michael Baker Jr Inc, Philadelphia, PA.

[29] O. Ralph and A. F. Elremaily, "Guidelines for Design and Construction of Decked Precast, Prestressed Concrete Girder Bridges," Construction Technology Laboratories, Inc, Skokie, IL, 2009.

[30] W. Chunga and E. D. Sotelinob, "Three-dimensional finite element modeling of composite girder bridges," *Engineering Structures*, vol. 28, no. 1, p. 63–71, 2006.

[31] AASHTO, "LRFD bridge design specifications," Washington, D.C., 2004.